Stimulation cérébrale multi-sites : modèles dynamiques et applications aux crises d'épilepsie

Marouan Arrais

UNIVERSITÉ DE RENNES 1

THESE DE DOCTORAT DE

L'UNIVERSITE DE RENNES 1

ECOLE DOCTORALE N° 601
Mathématiques et Sciences et Technologies de l'Information et de la Communication
Spécialité : AST – Signal, image et vision

Par
Marouan ARRAIS

Stimulation cérébrale multi-sites : Modèles dynamiques et applications aux crises d'épilepsie.

Thèse présentée et soutenue à Rennes, le 15 Décembre 2020

Unité de recherche : LTSI – INSERM UMR_S 1099

Université de Rennes 1 – Laboratoire Traitement du Signal et de l'image

Rapporteurs avant soutenance :

Jonathan TOUBOUL	Professeur Associé, Brandeis University, USA
Frédéric ALEXANDRE	Directeur de Recherche, INRIA, Université de Bordeaux

Composition du Jury :

Président :	Lotfi SENHADJI	Professeur – Université Rennes 1
Rapporteur :	Jonathan TOUBOUL	Professeur Associé, Brandeis University, USA
Rapporteur :	Frédéric ALEXANDRE	Directeur de Recherche, INRIA, Université de Bordeaux
Examinateur :	Laure BUHRY	Enseignant-Chercheur, Université de Lorraine
Dir. de thèse :	Fabrice WENDLING	Directeur de Recherche, INSERM, Université Rennes 1
Co-dir. de thèse :	Julien MODOLO	Chargé de Recherche, INSERM, Université Rennes 1

Résumé en français

L'épilepsie est l'un des troubles neurologiques les plus répandus, qui touche plus de soixante-dix millions de personnes dans le monde (environ 1 % de la population mondiale) (Katchanov and Birbeck, 2012; Ngugi et al., 2011). Elle se caractérise par des crises récurrentes (Kwan and Brodie, 2000) qui nuisent considérablement à la qualité de vie des patients. Les crises sont principalement liées à des décharges neurales excessives et synchronisées dans une ou plusieurs structures du cerveau (Badawy et al., 2012). La thérapie la plus immédiate pour traiter et contrôler l'épilepsie est l'utilisation de médicaments, ou éventuellement une combinaison de médicaments (Sankaraneni and Lachhwani, 2015). Cependant, un tiers des patients épileptiques ne répond pas à la thérapie médicamenteuse (Kobau et al., 2008). La chirurgie peut représenter une option pour ces patients, cependant, une grande partie des patients (60-70%) n'est pas éligible en raison d'un rapport bénéfice/risque défavorable. Par conséquent, il existe un besoin urgent de thérapies alternatives qui pourraient réduire de manière significative la fréquence des crises. Parmi les approches candidates, la stimulation cérébrale fait l'objet d'une attention croissante de la part de la communauté scientifique.

En effet, il a été démontré il y a plusieurs décennies (Upton and Cooper, 1976) que la stimulation électrique du cerveau peut impacter l'activité épileptiforme, ce qui a motivé les efforts de recherche visant à identifier ses mécanismes d'action et à optimiser ses effets thérapeutiques. De plus, des études expérimentales ont identifié un lien entre l'amélioration de l'efficacité de la stimulation cérébrale pour mettre fin aux crises d'épilepsie, et le choix des sites de stimulation quand une stimulation multi-site est appliquée (Sobayo and Mogul, 2016). Cependant, l'utilisation clinique de la stimulation cérébrale dans le contexte de l'épilepsie est encore limitée et largement basée sur une approche par essai-erreur (Hoang et al., 2017). En outre, les études axées sur les paramètres (intensité, fréquence, forme d'onde, ...) sont encore peu nombreuses, essentiellement empiriques et basées sur des évaluations qualitatives. Ce problème est dû au fait que la caractérisation précise de la réponse à la stimulation au chevet du patient ne peut pas être réalisée, car cela nécessiterait des séances

prolongées qui ne sont pas compatibles avec le temps et la tolérance limités des patients. Une autre approche consiste à réaliser des expériences *in vivo* et *in vitro* sur des animaux pour identifier les paramètres les plus efficaces, ce qui n'est pas une approche optimale car l'espace total des paramètres de stimulation est trop grand pour être pratique à explorer.

Dans ce contexte, une possibilité d'identifier les paramètres de stimulation optimaux, tout en évitant ces longues séances de test irréalistes des paramètres de stimulation, consiste à utiliser des modèles bio-informatiques neuro-inspirés. Au cours des dernières décennies, de tels modèles ont été développés pour simuler l'activité cérébrale à différentes échelles spatiotemporelles. Les modèles microscopiques (Hodgkin and Huxley, 1952) décrivent l'activité d'un seul neurone, tandis que les modèles mésoscopiques, tels que les modèles de masse neurale (NMM) (Jansen and Rit, 1995; Wendling et al., 2002a) ou les modèles dits de champs neuraux (Spiegler and Jirsa, 2013) décrivent l'activité moyenne de populations de neurones. Dans le domaine de l'épilepsie, les modèles bio-informatiques sont de mieux en mieux acceptés et sont maintenant reconnus comme une approche efficace pour obtenir des informations sur les mécanismes physiopathologiques qui sous-tendent l'activité épileptiforme (F. Wendling et al., 2016). Parmi ces modèles, le choix des NMM pour modéliser l'activité épileptiforme est motivé par leur facilité d'utilisation (petit nombre de paramètres par rapport aux modèles microscopiques), tout en conservant les principales propriétés neuro-anatomiques et neurophysiologiques. En outre, les NMM permettent de simuler des signaux à la même échelle que les signaux électrophysiologiques enregistrés en clinique, à partir de signaux de scalp (EEG) ou intracérébraux (EEG de profondeur, SEEG ou ECoG). L'un des modèles pionniers des NMM est le modèle de Jansen et Rit (Jansen and Rit, 1995), initialement développé pour étudier les potentiels évoqués visuels, puis adapté pour générer des activités épileptiformes avec des valeurs appropriées de paramètres liés à l'excitation et à l'inhibition (Wendling et al., 2000).

En utilisant les NMM et des techniques mathématiques dérivées de la théorie des systèmes dynamiques, nous avons tenté identifier les mécanismes conduisant à l'initiation, la propagation et la terminaison des crises. La stimulation électrique cérébrale a été incluse dans les NMM sur la base de connaissances physiologiques et

biophysiques. Par conséquent, la réponse en fréquence d'une population de neurones épileptiques à une perturbation électrique externe a été étudiée, et une conception plus rationnelle des protocoles de stimulation cérébrale a été suggérée. En plus d'étudier les effets de la stimulation d'une seule région, nous avons abordé la question de la stimulation multi-sites, qui est une technique émergente consistant à stimuler plusieurs sites cérébraux simultanément pour obtenir un effet neuromodulateur. Nous avons étudié l'efficacité de la stimulation multi-sites par rapport à la stimulation d'un seul site, ainsi que le choix des cibles et du moment de la stimulation. Cette recherche nous a conduit à proposer une méthode pour concevoir des méthodes optimales de stimulation multi-site visant à faire avorter l'activité épileptiforme.

Dynamique des populations neuronales locales dans des conditions spontanées (sans stimulation)

La dynamique des masses neurales est étroitement liée aux gains synaptiques. Chaque état d'excitabilité (résultant de la combinaison des gains synaptiques) d'une sous-population neuronale a été associé à un schéma d'activité neuronale. Un tel mode de représentation a permis d'identifier les sous-populations neuronales impliquées dans la génération de types d'activité spécifiques. Les résultats établissent un lien entre l'apparition d'oscillations de haute fréquence et de faible amplitude (dite *fast onset activity*), qui caractérisent l'apparition rapide de l'épilepsie, et une activité accrue d'interneurones projetant vers le soma (interneurones inhibiteurs rapides). Cette activité accrue est représentée par une augmentation du gain synaptique correspondant. De plus, l'activité de fond est liée à des niveaux élevés d'activité d'interneurones lents projetant vers les dendrites. Cette sous-population neuronale inhibe à la fois les interneurones inhibiteurs projetant vers le soma et les cellules pyramidales. Par conséquent, elle entraîne la suppression des oscillations épileptiques et diminue les oscillations de grande amplitude générées par les neurones excitateurs en influençant les cellules pyramidales.

Dynamique de populations neuronales locales dans des conditions de stimulation

Comprendre comment la variation des paramètres de stimulation affecte la dynamique d'une région neuronale est essentiel pour la conception d'un protocole de stimulation rationnel, et fournir de tels diagrammes de bifurcation pour un modèle réaliste de l'activité neuronale sous stimulation électrique est un pas dans cette direction. Ces diagrammes ont fourni des résultats cohérents avec les travaux précédents relatifs à l'identification de paramètres de stimulation efficaces capables d'interrompre les crises d'épilepsie (Beurrier et al., 2001; Filali et al., 2004; Shen et al., 2003). Les résultats ont également confirmé que l'utilisation de hautes fréquences (plus de 90 Hz) associées à une amplitude spécifique (2 mV dans le modèle) a le potentiel de supprimer l'activité épileptiforme à basse fréquence. Des travaux futurs permettront de valider cette prédiction *in vivo*.

Conception d'une stimulation multi-sites capable d'arrêter les crises d'épilepsie au niveau réseau

Les recherches menées au niveau d'une seule population neuronale ont été étendues pour optimiser la neurostimulation multi-sites et générer des hypothèses expérimentalement vérifiables. La perspective d'effectuer une stimulation multi-sites dans l'épilepsie est en partie motivée par les effets rapportés de la stimulation multi-sites chez l'homme, par exemple dans l'amélioration de la mémoire de travail (Alagapan et al., 2019). Dans notre étude, nous avons développé un modèle décrivant un réseau neuronal épileptogène et étudié l'impact de la stimulation multi-sites sur les régions neuronales connectées générant des décharges intericales; une activité reconnue comme un marqueur électrophysiologique des systèmes neuronaux épileptogènes (Wendling et al., 2002). Nos résultats ont confirmé l'efficacité de la stimulation multi-sites pour réduire la fréquence des décharges épileptiques, et ont montré qu'il est possible d'orienter le choix des cibles de stimulation en se basant sur une métrique de la théorie des graphes (à savoir la centralité de vecteur propre). Nous montrons ainsi que l'efficacité de la stimulation multi-sites est directement liée à la structure du circuit et à la connectivité. Ainsi, nous avons présenté une méthode de sélection et de limitation du nombre de régions cibles basée sur les potentiels de champs locaux (LFP) "enregistrés", qui devrait être réalisable expérimentalement sur

la base des LFP enregistrés. Ces « hubs » de connectivité choisis sont caractérisés par une connectivité élevée, et leur stimulation a un impact important sur la dynamique du réseau, contrairement à la stimulation d'autres nœuds moins centraux. En outre, il convient de mentionner que la stimulation multi-sites de quelques régions a été identifiée comme optimale, et a surpassé la stimulation du réseau entier ou d'une seule région du réseau.

Acknowledgments

I was fortunate to have two thesis supervisors who were remarkable not only for their scientific but also for their human qualities. It is therefore with immense gratitude that I would love to thank Messrs. Fabrice Wendling and Julien Modolo, to who I am heavily indebted and who have expertly guided me during these last three years. Thank you for your trust, your support, your encouragement and your help that have been invaluable. I would also like to thank Professor Lotfi Senhadji for welcoming me in his research laboratory.

Of course, I would love to thank all the jury members for accepting to participate to my thesis examination. I would also like to thank Maxime Yochum and Elif Koksal Ersoz, with who I enjoyed discussing, for their helpful advice and support whenever needed. My appreciation also extends to my colleagues and laboratory staff for their support and company over the past few years.

Undoubtedly, I am indebted to my family, whose value to me only grows with age. Thank you for being always by my side.

Table of contents

Introduction

Epilepsy is one of the most prevalent neurological disorders, affecting more than seventy million people worldwide (approx. 1% of the world population) (Katchanov and Birbeck, 2012; Ngugi et al., 2011). It is characterized by recurrent seizures (Kwan and Brodie, 2000) that dramatically impair patient's quality of life. Seizures are primarily related to excessive and synchronized neural discharges in one or several brain structures (Badawy et al., 2012). The most immediate therapy for treating and controlling epilepsy is the use of antiepileptic drugs (AED), or possibly a combination of drugs (Sankaraneni and Lachhwani, 2015). However, one third of epileptic patients do not respond to drug therapy and are classified as patients with drug-resistant epilepsy (DRE) (Kobau et al., 2008). DRE is defined by the International League Against Epilepsy as the failure of adequate trials of 2 tolerated, appropriately chosen, and used AED schedules, whether as monotherapies or in combination to achieve sustained seizure freedom for 12 months, or 3 times the inter-seizure interval before the treatment started (Kwan et al., 2010). Surgery can be an option for those drug-refractory patients, however, a large fraction of patients (60-70%) is not eligible due to several factors, including the location of the epileptogenic zone. Regions involved in key functions cannot be resected since their removal may result in a highly unfavorable benefit/risk ratio. Hence, there is a pressing need for alternative therapies that could decrease seizure frequency, or even preventing them completely. Among the therapies that could represent an alternative to drugs for those patients, brain stimulation has

been receiving increasing attention by the biomedical engineering and clinical communities.

Brain stimulation has been proved as an effective method to modulate neural activity (Davis et al., 1982; Upton and Cooper, 1976; Wright and Weller, 1983). Consequently, studies have been conducted to identify its mechanisms of action and optimize its therapeutic effects, which are still not fully understood today. Stimulation parameters such as amplitude, frequency, waveform, timing and anatomical target play a critical role in neural tissue response and potential seizure abortion. Depending on the combination of those parameters, the net effect has been reported to be either null, able to abort seizures, or even induce seizures. Therefore, a major clinical challenge is identifying the optimal set of parameters among all the possibilities that would result in seizure abortion. An additional challenge is the considerable variation, between patients, of the underlying etiology, location and extent of epilepsy.

Due to this difficulty to rationally provide efficient sets of parameters for epilepsy (i.e., with therapeutic effects), the clinical use of brain stimulation in the field of DRE has remained limited. Accurate characterization of the stimulation response at the bedside cannot be achieved, since this would require extensive testing sessions which are not compatible with patients' and clinicians' limited time and tolerance. An alternative approach is to perform animal *in vivo* and *in vitro* experiments to identify the most effective parameters, however exploring the entire stimulation parameter space is still a major roadblock. *In this context, one possibility to identify optimal stimulation parameters, while avoiding such unrealistic extended testing sessions of stimulation parameters, consists in using computational models taking into account the physiological characteristics of brain tissue.*

Over the past decades, different types of models, either neuro-inspired of purely mathematical, have been developed to simulate brain activity at different spatiotemporal scales. Microscopic models (Hodgkin and Huxley, 1952) describe single neuron dynamics; while mesoscopic models, such as neural mass models (NMMs) (Jansen and Rit, 1995; Wendling et al., 2002b) or neural field models (Spiegler and Jirsa, 2013) describe the averaged activity of neuronal assemblies. In the field of epilepsy, computational models have gained acceptance and are now recognized as an efficient approach to get insights into the pathophysiological mechanisms

underlying epileptiform activity (Fabrice Wendling et al., 2016). In the present thesis, the choice of NMMs to model epileptiform activity has been motivated by their ease of use (small number of parameters as compared to microscopic models), while retaining key neuroanatomical and neurophysiological properties. Furthermore, NMMs simulate signals at the same spatial scale than the electrophysiological signals typically recorded in clinics, from the scalp level using electroencephalography (EEG), or intracerebral using stereo-electroencephalography (SEEG).

Using NMMs and mathematical techniques derived from dynamical systems theory, we have attempted to elucidate the mechanisms underlying the mechanisms leading to seizure initiation, propagation and termination. Brain electrical stimulation was included in NMMs based on physiological and biophysical knowledge. Therefore, the frequency response of an epileptic neuronal population to an external electrical perturbation was studied, and a more rational design for brain stimulation protocols was determined. In addition to investigating the stimulation effects of a single region, we tackled the issue of multi-site stimulation, which is an emerging technique consisting in stimulating several brain sites simultaneously to achieve a neuromodulatory effect. We investigated the effectiveness of multi-site stimulation as compared to single-site stimulation, and the choice of stimulation targets and timing. This investigation led us to propose a method to design optimal multi-site stimulation methods aiming at aborting epileptiform activity.

This thesis is organized as follows:

- Chapter 1: We provide a state-of-the-art regarding electrophysiological activity, the experimental techniques used for measuring neuronal activity, epileptic syndromes and the classification of epilepsy seizures. Then, we present an overview of neurostimulation, along with the computational models and mathematical techniques used to study the brain activity. We also introduce the main research question tackled in this thesis, and present the gap of knowledge limiting the therapeutic effects of brain stimulation. An outline of the proposed approach is provided.

- Chapter 2: We introduce the mathematical models used for simulating the electrical activity of a single neuronal population in the absence or presence of electrical stimulation. The means of coupling neuronal populations and constructing a large neuronal network and including stimulation within the model are presented.

- Chapter 3: First, we present the dynamics of a single neuronal population under spontaneous and stimulation conditions. Neuronal dynamics are linked to the activity and role of specific neuronal types. Furthermore, we present qualitative changes in dynamics while applying electrical stimulation, and identify optimal settings to replace pathological activity with a more physiological activity. Second, we attempt at deriving a transfer function for a non-linear system, with the objective to provide a fast and accurate identification of candidate stimulation frequencies that could effectively abort the generation of epileptiform activity.

- Chapter 4: In this chapter, we focus on networks of coupled neuronal populations. The dynamics of these networks are studied to determine a rational design for efficient (i.e., able to abort epileptiform activity) stimulation protocols. The previous investigation (Chapter 3) is then extended to optimize multi-site neurostimulation by taking into account additional factors such as network effects. Experimentally testable hypotheses are also proposed.

Finally, we conclude this thesis by discussing our results in the context of the existing literature, and provide future perspectives and challenges along our lines of research.

Chapter 1

Literature review and problem statement

1.1 Electrophysiological activity

The brain is the organ located in the cranium enabling perception, thoughts, emotions, consciousness, and sustaining key vital functions. The brain is composed of two main types of cells: neurons (involved in information processing, propagation and storage) and glial cells (mainly involved in regulating metabolic processes and synapses). Neurons communicate by sending and receiving electrical and chemical signals, and are composed of four main parts: dendrites, cell body (soma), axon and synapses, as shown in Figure 1.1. Dendrites are appendages responsible for the reception of information from other cells, and are organized as a tree-like structure that receives inputs from other neurons. The soma supports and maintains the functioning of the neuron, since it produces necessary proteins to the function of dendrites and axons (Marieb and Hoehn, 2010). When the sum of inputs exceeds a threshold within a limited temporal window, the neuron will trigger an action potential that will be conducted through the axon until reaching the neuron ending and releasing at the synaptic level neurotransmitters (chemical messengers) that will bind on post-synaptic receptors (Lovinger, 2008).

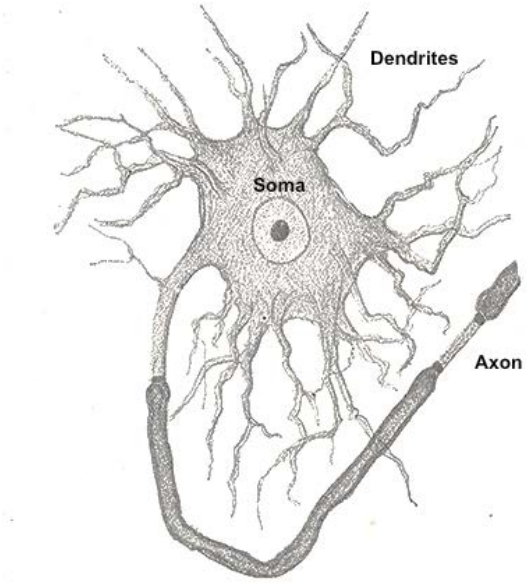

Figure 1.1. Main components of a neuron (adapted from Santiago Ramón y Cajal).

Action potentials play a fundamental role in neuronal communication. This transient phenomenon is characterized by a drastic and short (millisecond scale) depolarization of the membrane. Once the total incoming postsynaptic potentials exceeds the so-called firing threshold, typically around -55 mV, an action potential is triggered. The generation of action potentials is possible thanks to ionic currents that have different kinetics. The ionic channels present on the dendrites' membrane regulate extra/intracellular concentrations of specific ions such as sodium Na^+, potassium K^+ and chloride Cl^-. The opening of channels induces positive ions flow into the cell, particularly the entering of sodium, which depolarizes the membrane. Once the firing threshold is exceeded, a rapid depolarization occurs driven by the rapid opening of voltage-gated Na^+ channels, leading further influx of sodium ions within the cell, contributing to increase the depolarization. This reversal causes the membrane potential to approach the Na^+ equilibrium potential at approximately +50 mV. This peak is followed by a slower repolarization, caused by a current of K^+ ions from the intra-cellular space to the extra-cellular space. The conductance of K^+ ionic channels evolves more slowly than sodium channels, and remains high after that the membrane potential has returned to its resting state (typically -55 mV), resulting in a membrane potential that is transiently more negative than the resting potential, which is called *hyperpolarization*. It is worth mentioning that intra-cellular and extra-cellular ions concentrations do not change significantly during an action potential: only a small

fraction of ions move across neuron membrane (Chrysafides et al., 2020; Lodish et al., 2000). The action potential then propagates through the axon until reaching the synapse, where neurotransmitters are released and bind on the post-synaptic receptors of afferent neurons, potentially inducing action potentials in those target neurons. Figure 1.2 presents the time course of an action potential along with the aforementioned terminology regarding variations of the membrane potential.

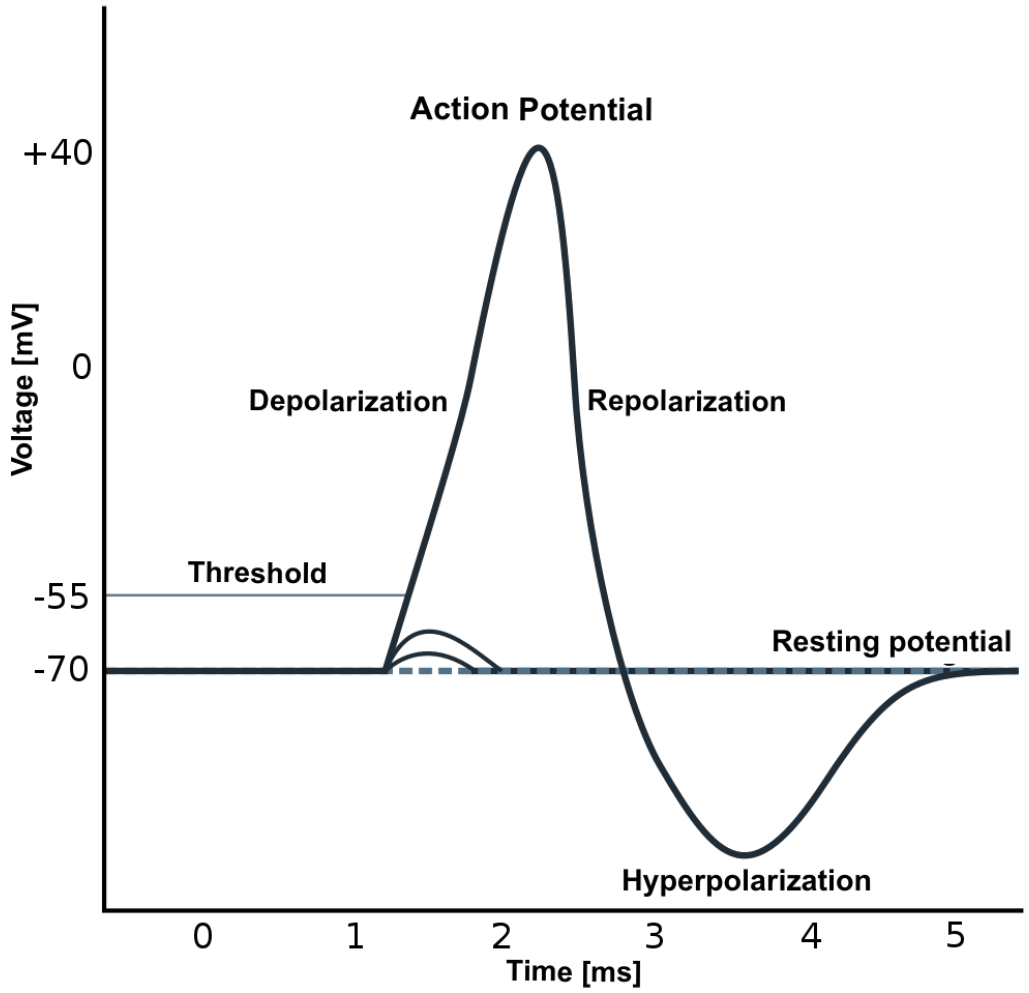

Figure 1.2. Action potential time course (adapted from Wikipedia/Action_potential). Once the firing rate threshold is exceeded, following a rapid summation of inputs, a rapid depolarization occurs, followed by repolarization and hyperpolarization phase of the membrane potential.

The electrical activity of an assembly of neurons, and the summation of their post-synaptic potentials, originate the brain rhythms that can be experimentally

recorded in brain tissue. The different electrophysiological patterns generated by neuronal activity can be recorded using several techniques that have various degrees of invasiveness. For non-invasive recordings, the most common modality is electroencephalography (EEG), which consists in measuring neuronal activity from cortical sources using scalp electrodes, as presented in Figure 1.3. Although it offers a poor spatial resolution (on the order of the square centimeter), it has an excellent temporal resolution and no serious safety restrictions; as opposed to invasive modalities such as stereo-electroencephalography (SEEG, involving recordings through intracranial electrodes). Given the distance between cortical regions and scalp electrodes, EEG measures the synchronized oscillations of a neuronal population, instead of individual action potentials (Nunez and Srinivasan, 2006). These rhythms are classically classified according to their dominant frequency (Buzsáki and Silva, 2012; Nunez and Cutillo, 1995).

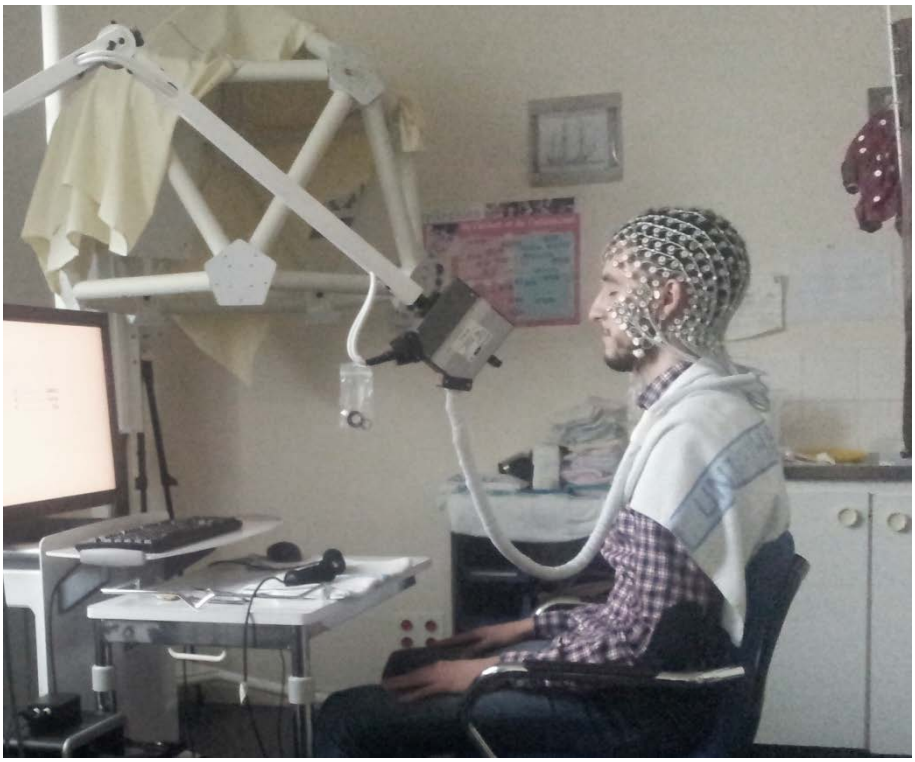

Figure 1.3 Example of a typical recording session of EEG signals (here, a high-resolution EEG cap with 256 electrodes).

Brain rhythms refer to the oscillatory activity patterns that can be recorded for example with EEG or SEEG. Five main oscillatory patterns can be associated with specific behaviors, excitability levels and consciousness states (Mackay, 1997). 1)

Delta corresponds to oscillations of frequency lower than 4 Hz with a high amplitude, are typically generated by thalamo-cortical circuits (Dossi et al., 1992), and are involved in sleep states (Steriade et al., 1993). 2) Theta corresponds to oscillation of a frequency between 4 and 7 Hz, and can be observed in the hippocampus and frontal cortex (Buzsáki, 2002; Cavanagh and Frank, 2014). Moreover, theta activity participates in the process of short-term storage of information also known as working memory (Lega et al., 2012), and in the regulation of emotions (Ertl et al., 2013). 3) Alpha oscillations are between 8 and 12 Hz, and are the first rhythm that has been observed by Hans Berger in 1929, due to its significant amplitude. Alpha oscillations are typically observed in posterior regions. Those oscillations have been related, among others, to awareness and visual attention (*Niedermeyer's Electroencephalography*, 2005; "The Brain's Alpha Rhythms and the Mind - 1st Edition," 2003). 4) Beta oscillations cover the 13-30 Hz frequency band, and are present during normal, waking consciousness for example. 5) Gamma oscillations (>30 Hz) are associated with cognitive processes such as learning and perception (Kucewicz et al., 2014). Those main rhythms are represented below in Figure 1.4.

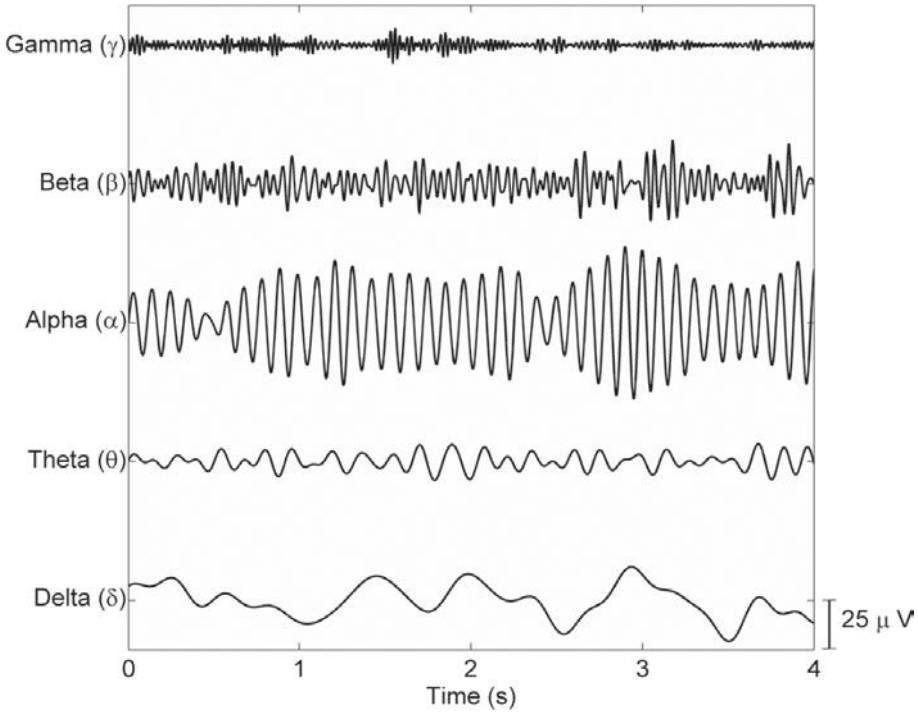

Figure 1.4. Illustration of the five main human EEG rhythms (Campisi et al., 2012).

1.2 Epileptic syndromes

According to the International League Against Epilepsy (ILAE), a seizure can be defined as a “transient occurrence of signs and/or symptoms due to abnormal excessive or synchronous neural activity in the brain” (Fisher et al., 2005). The occurrence of at least two unprovoked or reflex seizures within more than 24 hours leads to the diagnosis of the individual as suffering from epilepsy (Fisher et al., 2014). This chronic neurological disorder can affect people of all ages, and can result in social, behavioral, health and economic consequences to patients and their families.

The symptoms associated with epileptic seizures differ depending on the affected region(s). Common seizure symptoms include temporary confusion, loss of consciousness or awareness, jerking movements and muscle contractions (Pack, 2019). Epileptogenic neuronal regions responsible for this paroxysmal alteration of neurologic function can be observed and detected using several techniques. Computed tomography (CT) and magnetic resonance imaging (MRI) enables detecting epileptic foci caused by morphological abnormalities. In the absence of morphological changes, functional and electrophysiological data are required. Magneto-encephalography (MEG) enables the identification epileptic foci with a good spatial resolution by detecting the (extremely small) magnetic fields generated by neuronal activity, however this neuroimaging modality is sensitive to radial sources and is limited by its high cost and low penetration (Ebersole and Ebersole, 2010). Electroencephalography (EEG) is a commonly used neuroimaging modality proving a good temporal resolution but a relatively poor spatial resolution, unlike intracranial EEG (sEEG) which is an invasive method that has a much improved spatial resolution since electrode contacts are directly at the contact of brain tissue. A combination of EEG and MRI may assist neurologists further for the diagnosis of specific epilepsy syndromes (Pohlmann-Eden and Newton, 2008).

Although the predictive value of interictal spikes has been debated, these brief paroxysmal discharges that occur between seizures have been considered as a biomarker of epileptogenicity (Roehri et al., 2018). Another marker of epileptogenicity is high-frequency oscillations (HFOs) (Jacobs et al., 2009, 2008), for which several studies have related better postsurgical outcomes to the resection of neuronal areas

with higher rates of HFOs (Fedele et al., 2016; Höller et al., 2015; Jacobs et al., 2010, 2008). However, the difficulty to differentiate between physiological and pathological HFOs limits their clinical use as a unique biomarker of epileptogenic tissue (Jacobs et al., 2012; Jefferys et al., 2012; Roehri et al., 2018).

EEG/SEEG signals exhibit typical patterns during seizures, such as spike-waves events, fast onset activity and after seizure slow waves (Worrell et al., 2008). In Figure 1.5, SEEG signals recorded during epileptic seizures in human and mice are presented.

a)

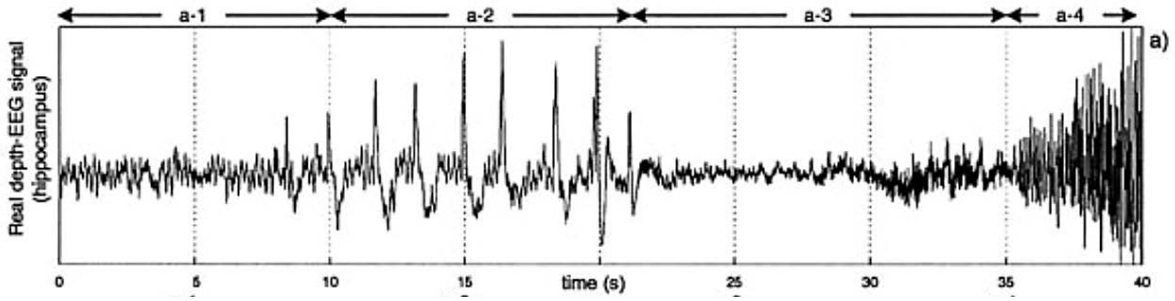

b)

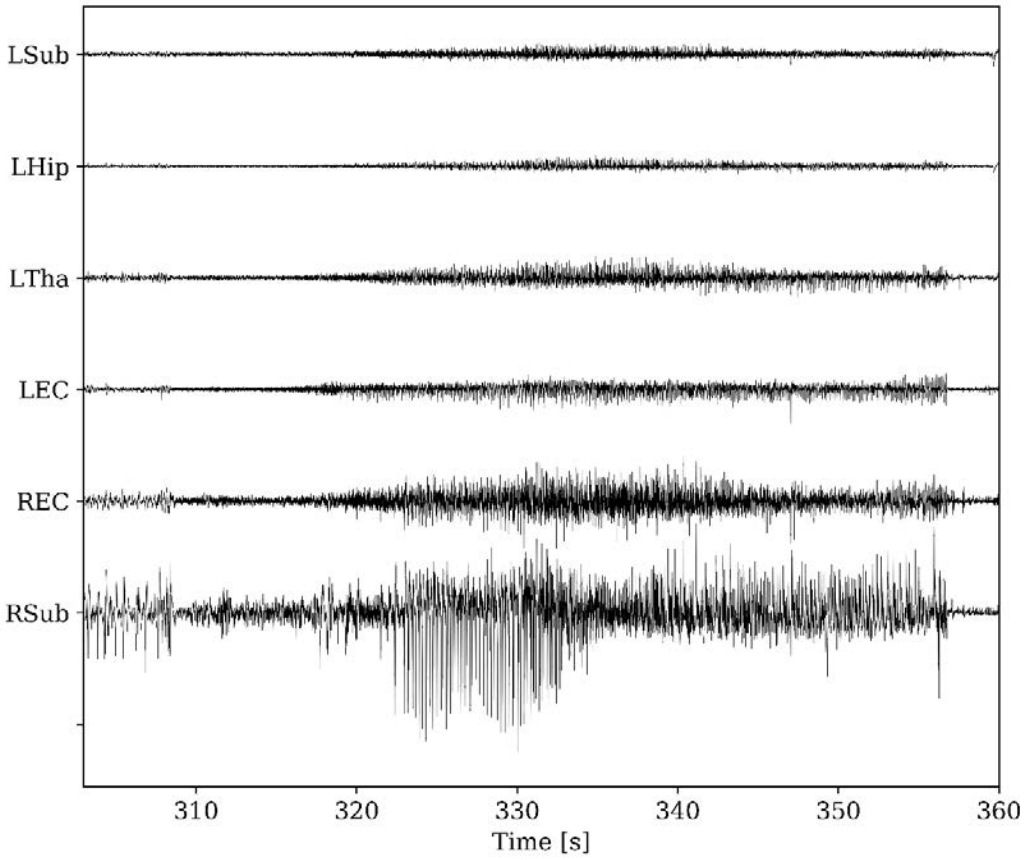

Figure 1.5 a) SEEG signals recorded in human hippocampus at the onset of a temporal lobe seizure. During interval a-1, no epileptiform activity is present, while in a-2 spikes are detected followed by fast onset activity in a-3, and finally slow waves during a-4. b) SEEG signals recorded from different mice brain regions at the beginning of a seizure (left subiculum (LSub), left hippocampus (LHip), left thalamus (LTha), left enthorinal cortex (LEC), right enthorinal cortex (REC), right subiculum (RSub)).

Epileptic seizures are described as either partial or generalized (Pack, 2019). Partial seizures involve one of multiple brain foci belonging to the same hemisphere, and fall into two categories; with and without loss of consciousness. Conversely, generalized seizures involve the entire brain, they can be classified into 6 types; 1) absence seizures causing a brief loss of awareness, 2) tonic seizures causing a stiffening of the muscles, 3) atonic seizures causing a loss of muscle control, 4) clonic seizures associated to repeated or rhythmic, jerking muscle movements, 5) myoclonic seizures, and 6) tonic-clonic seizures that are the most dramatic and can cause an abrupt loss of consciousness and loss of bladder control.

Epileptic syndromes are defined as the group of clinical characteristics that consistently occur together (Scheffer et al., 2017). This cluster of features incorporates seizures types, age at which seizures begin, EEG characteristics, imaging findings, triggering factors, and response to anti-epileptic drugs (AEDs) among others. Those features provide information regarding etiology and the type of drug that could efficiently reduce seizures. Syndromes can vary greatly: some are called ‘benign’, as reference to seizure- and drug-free after a certain age; while other syndromes are severe and difficult to control. The most common syndromes, based on their frequency, are benign rolandic epilepsy, childhood absence epilepsy and temporal lobe epilepsy (Boyer, 2016; Cendes, 2004; Guerrini and Pellacani, 2012). Benign rolandic epilepsy (BRE) is one of the most common types of epilepsy, accounting more than one-third of all epilepsy cases. Symptoms appear during childhood between the ages of 3 and 10, and cause partial seizures during sleep, accompanied of tingling feeling in the mouth and an inability to speak. Anti-epileptic drugs are recommended as a treatment for patients suffering from BRE, but are not necessary. Most children suffering from this syndrome become seizure-free by the age of 16. Childhood absence epilepsy (CAE) is characterized by a brief loss of consciousness and affects children between

3 and 6 years. Seizures are often controlled and the patients can regain their normal life with anti-epileptic drugs. Up to 90% of children with CAE become seizure-free by the age of 12.

One of the most classic syndromes that is of interest in the context of this thesis is temporal lobe epilepsy (TLE), which is common in adults (Tatum, 2012). In TLE, the epileptogenic zone is found in temporal structures such as hippocampus or amygdala. Seizures begin in late childhood and adolescence and are mostly focal, although some TLE patients have generalized seizures. One feature of this type of epilepsy is their resistance to antiepileptic drugs, which might require resective surgery (Bernhardt et al., 2013; Thom et al., 2010) if the candidate satisfies certain factors. However, a large fraction of TLE patients (60-70%) is not eligible to resective surgery due to 1) multiple seizure foci involving one or both cerebral hemispheres, and/or 2) unfavorable benefit/risk ratio. Thus, there is a pressing need to develop and adopt alternative therapies that could significantly relieve seizures. Among the candidate approaches, brain stimulation has been receiving increasing attention in the last decade, which is reviewed in the next section.

1.3 Neurostimulation

Neurostimulation refers to the modulation of neuronal activity through electric, magnetic, or pharmacologic means. In this thesis, we focused on the use of electric stimulation in particular, which consists in delivering an electric current and associated electric field in brain tissue to induce a modulation of neuronal activity. This therapeutic technique has provided promising results in drug-refractory patients suffering from epilepsy in whom surgery would have an unfavorable benefit/risk ratio, and also other neurological diseases such as Parkinson's disease (Deuschl et al., 2006; Weaver et al., 2009), and chronic pain (Kumar et al., 2008, 2005) for example. Moreover, it has been used even for memory enhancement, relieve depression and eating disorders (Akhtar et al., 2016; Dalton et al., 2018; Meisenhelter and Jobst, 2018).

The ability of electrical stimulation to alter neuronal activity has been documented since the mid-20th century (Bailey and Bremer, 1938). Since then, significant research efforts have been conducted to determine its mechanisms, effects,

potential applications and optimal parameters. The effects of an induced electric field are categorized as 1) sub-threshold changes in ongoing neural activity (Bikson et al., 2004); delivering of a weak electric current assuring and preserving the main properties of neuronal function (Lundstrom et al., 2017), or 2) supra-threshold stimulation that directly triggers action potentials (Lopez et al., 1991) by depolarizing the neuron membrane (Ranck, 1975; Rattay, 1989), and thus activating voltage sensitive ion channels responsible for action potential generation (Hodgkin and Huxley, 1952).

Neurostimulation can be delivered through a variety of modalities differing by their invasiveness, targeted neuronal structures and adaptability of its parameters, as reviewed below.

Invasive versus non-invasive

Neurostimulation can either be invasive (targeting deep structures), or non-invasive (targeting the cortex, i.e. brain surface). Invasive neurostimulation modalities require surgical interventions and include deep brain stimulation (DBS), responsive neurostimulation (RNS), vagal nerve stimulation and chronic sub-threshold cortical stimulation. Non-invasive approaches include transcranial magnetic or electrical stimulation. By applying these techniques, the induced currents spread through a large portion of neuronal tissue (Miranda et al., 2006), as compared to the focal stimulation reached using invasive methods as DBS (Butson et al., 2006). However, non-invasive methods are safer, since they do not require a surgical procedure that can induce a number of complications such as hemorrhages (Zewdie et al., 2020).

Closed-loop *versus* Open-loop paradigms

Most neurostimulation devices are open-loop, i.e. stimulation is delivered according to a predefined pattern regardless of underlying electrophysiological activity. Stimulation parameters are then fixed based on patients' response and seizure frequency. In contrast, other devices use are based on a closed-loop approach, such as the RNS® device (Neuropace, USA) that analyzes in real–time electrophysiological

patterns and delivers stimulation only when epileptiform patterns are detected (Heck et al., 2014; Jobst et al., 2017; Skarpaas et al., 2019).

Transcranial magnetic stimulation (TMS)

TMS refers to the application of a magnetic field which, in turn, causes electric currents to flow in brain tissue according to Maxwell-Faraday's law. In order to induce the magnetic field, high-level pulses of electric current are delivered to a coil placed on the patient's head. TMS is a form of supra-threshold stimulation, since neurons are forced to trigger action potentials. TMS is used to treat drug-refractory depression (Reddy and Vijay, 2017; Rizvi and Khan, 2019) and chronic pain (Hamid et al., 2019), and is explored for a wide range of potential applications.

Transcranial electrical stimulation (TES)

TES is a non-invasive neurostimulation technique, and depicts a direct application of electric current *via* electrodes placed on the scalp, in correspondence of a specific cortical region. TES covers different techniques, which include transcranial direct current stimulation (tDCS), transcranial alternative current stimulation (tACS) and random noise stimulation (tRNS). As opposed to TMS, TES techniques uses a low-intensity current unable to elicit an action potential, thereby only affecting cortical excitability (Radman et al., 2009).

Vagal nerve stimulation (VNS)

Unlike TMS and TES, VNS is an invasive neurostimulation consisting in the implantation of a pulse generator called stimulator in the thoracic chest that supplies electrodes threaded around the vague nerve. Used in humans for the first time in 1990 (Penry and Dean, 1990), VNS is recognized as an effective neurostimulation techniques for treating epilepsy (Ben- Menachem et al., 1994; Handforth et al., 1998).

Deep brain stimulation (DBS)

DBS involves the insertion of intracranial electrodes to stimulate deep, specific brain structures. The implantation of intracranial electrodes to record electrical brain activity and stimulation was first introduced by Delgado (Delgado et al., 1952). Since then, clinical studies were conducted to explore neurostimulation targets to provide relief and alter pathological activity. Although that the mechanisms of DBS are not well

understood, it is proven as an effective therapeutic neurostimulation technique to treat several neurological disorders, notably Parkinson's disease (Benabid et al., 1987; Cooper et al., 1980). DBS is also being actively explored as a possible therapy for epilepsy (Laxpati et al., 2014; Zangiabadi et al., 2019).

Responsive neurostimulation (RNS)

The RNS system is an invasive, closed-loop neuromodulation approach involving implantation of the stimulator in the skull connected to leads placed in up to two seizure onset areas. Brain activity is monitored and stimulation is delivered as response to the detection of precursor epileptic biomarkers (Morrell and Halpern, 2016; Sun et al., 2008). Unlike open-loop approaches which do not include a feedback loop, this is an adaptive approach takes into account changes and fluctuations in ongoing electrophysiological activity by employing recording sensors.

Chronic sub-threshold cortical stimulation (CSCS)

CSCS represents another type of invasive stimulation that is still under investigation and not widely available. It is an experimental form of stimulation that delivers continuous, low-level stimulation at the level of seizure onset zones (Lundstrom et al., 2016).

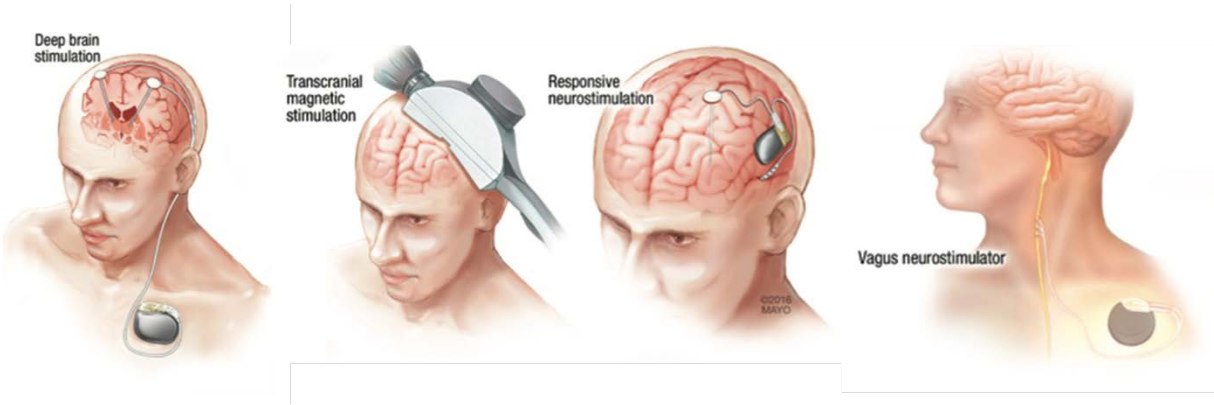

Figure 1.6. Neurostimulation techniques for the treatment of neurological disorders. Illustrations present examples of stimulation targets and devices used. (Figure adapted from (Edwards et al., 2017)).

1.4 Gap of Knowledge

Significant advances related to recording techniques, molecular and computational investigations have enriched our understanding about brain functioning in physiological and pathological states. However, several questions remain unanswered. Knowledge about the mechanisms of action at the level of neural networks, the bridging between neural network and a single neuron, and the factors impacting therapeutic effects of a neurostimulation is still limited. In this section, we expose the present gaps of knowledge regarding electrical brain stimulation in epilepsy.

Causes of epilepsy

Clinical and molecular biochemistry, electrophysiological and neuroimaging exploration techniques such as EEG, computed tomography, and (functional) magnetic resonance imaging have contributed in identifying abnormal tissue (Shorvon, 1994) and mechanisms of many inherited and acquired disorders. Below, we present several possible epilepsy etiologies.

- Structural etiology: this refers to abnormalities visible on structural neuroimaging. Neuroimaging techniques as CT and MRI enable the detection of structural abnormalities such as malformations, stroke and trauma. For instance, temporal lobe epilepsy is associated to hippocampal sclerosis, which is a severe cell loss that can be detected using MRI. The association of epileptiform activity with a structural etiology can inform potential surgical interventions.

- Genetic etiology: this refers to genetic mutation involved in the development of epilepsy. Molecular genetics can identify these pathogenic mutation, nevertheless, in the most cases the underlying genes are unknown. This etiology can be suggested based on family history and patients' age, and is more detected in neonatal, childhood and juvenile epilepsies.

- Infectious etiology: this is the most common cause of epilepsy (Vezzani et al., 2016). Infections such as cerebral malaria, viral encephalitis, tuberculosis and cerebral toxoplasmosis can lead to triggering epileptic seizures.

- Metabolic etiology: here, epilepsy results from biochemical changes occurring throughout the body such as porphyria, uremia and aminoacidopathies. The identification of specific metabolic causes allows the suggestion of efficient therapies, note that antiepileptic drugs are ineffective against metabolic epilepsy.

- Immune etiology: the increasing interest to antibody tests has led to the recognition of several immune epilepsies both in adults and children (McKnight et al., 2005; Peltola et al., 2000). This etiology is associated with central nervous system inflammation that increases the risk of causing epilepsy.

Let us mention that the unicity of etiology is not guaranteed, and that the identified etiology can be caused by another etiology. For instance, metabolic disorders or structural abnormalities can be caused by a genetic defect. Moreover, one third of adult epilepsy patients are of unknown etiology (Ramanathan et al., 2014). This lack of knowledge impairs treatment efficacy since patients' condition remain refractory to conventional medications. Recent studies assume that up to 20% of these epilepsies could be explained by autoimmune encephalitis (Dubey et al., 2017).

Electrical brain stimulation

Despite the widespread use of electrical brain stimulation, either invasive or non-invasive, a knowledge gap persists regarding its mechanisms of action, potential targets and stimulation parameters, which we briefly review below.

Mechanisms: Electrical brain stimulation induces neurochemical and neurophysiological changes at the membrane and synaptic levels, thereby affecting activity changes at the network level via the structural connectome. The mechanisms underlying these alterations are still poorly understood. However, the therapeutic

effects of brain stimulation are generally linked to either a release of inhibitory transmitters (Dostrovsky and Lozano, 2002), or an inactivation of neurons through depolarization blockade (Pollo and Villemure, 2007).

Stimulation targets: Among the factors influencing stimulation efficacy, stimulation targets and parameters are crucial. Stimulation can be either applied directly to the identified seizure onset zone (SOZ), or indirectly by stimulating a neuronal structure indirectly connected to the so-called epileptogenic network. Direct stimulation of the SOZ alters tissue excitability and neuronal synchronization, and can exert inhibitory effects (Jobst et al., 2010). Conversely, indirect stimulation aims to suppress neuronal structures that favor seizure emergence by perturbing neuronal networks. Moreover, electrical stimulation can be single-site, i.e. focusing on one brain region; or multi-site, i.e. targeting multiple neuronal regions. In the case of seizures involving multiple seizure onset zones, multi-site stimulation could be more adequate and efficient than single-site stimulation. Multiple targets have been evaluated regarding DBS, including the anterior nucleus of the thalamus (ANT), which is one of the most targeted structures for the treatment of drug refractory epilepsy (Fisher et al., 2010), but also hippocampus, subthalamic nucleus (STN) and centromedian thalamic nucleus (CMTN) (Rahman et al., 2010). Typical stimulation settings are: frequency ≥ 100 Hz and voltage between 1 and 10 V for ANT stimulation; frequency ≥ 130 Hz and voltage between 1 and 5 V for hippocampal and STN stimulation; high-frequency stimulation (~100 - 250 Hz) at voltage between 1 and 10 V for CMTN (Li and Cook, 2018). Nevertheless, the chosen stimulation parameters are empirically fixed during post-operative sessions while optimal values remain unknown. Furthermore, there is still a lack of clinical randomized control trials comparing these different paradigms.

1.5 Challenges

Electrical brain stimulation is recognized as a promising therapeutic technique to relieve patients suffering from neurological diseases such as epilepsy. The increasing attention paid to this neuromodulation strategy has led to the development of various stimulation approaches. As aforementioned, the main factors differentiating these protocols are the degree of invasiveness, number and type of stimulation targets

and stimulation properties including intensity, frequency and waveforms. In addition, stimulation can be either single-site or multi-site, invasive targeting deep neuronal structures, or non-invasive applied on the scalp and targeting cortical regions. Due to this significant diversity in stimulation protocols (Li and Cook, 2018), their comparison is especially challenging.

Only the delivered electrical field can be directly comparable between those techniques, but the impact on neuronal tissue and thus the responses to this external perturbation are varied and unpredictable. For example, while applying a tDCS, although the delivered electrical currents are identical, variables such as the neuronal networks involved and the orientation of neurons with respect to the injected electric field influence the effects of stimulation and challenge the comparison between clinical trials. Various factors, including biological variation, measurement reproducibility and the ongoing activity of the stimulated neuronal tissue, which can be affected by factors such as past and present neurological activity, influence the response to a specific electrical brain stimulation protocol. Those factors limit the identification of optimal strategies tailored for specific diseases and patients.

During the last decades, several computational models have been developed and gained acceptance thanks to their ability to 1) simulate brain activity at different scales, and 2) reproduce a large range of neuronal rhythms and patterns. Neuro-inspired models provide access to variables that are difficult or impossible to record clinically such as firing rates (FRs) or post-synaptic potentials (PSPs). The monitoring of these quantities enables testing hypotheses about the underlying mechanisms, and elucidate the general understanding about the function of those neural circuits and their modulation by electrical stimulation. In addition, it becomes possible to perform extensive exploration of the stimulation parameters space in a relatively short time. In the following, the main modeling approaches to simulate brain electrical activity in both physiological and pathological states are presented.

1.6 Computational models of brain activity

Computational models have been developed with the objective to understand, simulate and predict brain activity at various spatial scales, from the change of ions' gradient along the membrane to electrical oscillations observed on scalp recordings. These mathematical formulations can integrate detailed knowledge coming from neurobiological research to explain experimental findings, to generate experimentally testable hypotheses about possible interaction mechanisms, and analyze overall dynamics such as the stability with respect to oscillations / perturbations in the case of epileptic systems.

Microscopic approach

Over the past decades, several models have been constructed at the individual neuronal level, and involve a large number of individual neurons interacting through synaptic projections. The dynamics of each neuron can be described by models with biological relevance such as Hodgkin-Huxley or Morris-Lecar models, or more phenomenological representations such as FitzHugh-Nagumo and Hindmarsh-Rose models. In the field of epilepsy, these models have advanced our understanding of how hyperexcitability develops, how hypersynchronization leads to paroxysmal activity and how seizure-like events emerges (van Drongelen et al., 2007).

Hodgkin-Huxley model

The Hodgkin-Huxley model is a conductance-based model that reproduces accurately the generation of action potentials (Hodgkin and Huxley, 1952). This biophysical model describes the evolution of the different ionic channels underlying the generation and propagation of action potentials in the axon using a set of differential equations describing membrane potential dynamics. The relatively slow dynamics across the neuron's membrane is assumed to be explicitly dependent from sodium Na^+ and potassium K^+ channels that govern the flow of those ions through the cell membrane, and from the leakage current, primarily related to chloride Cl^-. The Hodgkin-Huxley model can be expressed as:

$$
\begin{aligned}
C\dot{V} &= I - g_{Na}m^3h(V - E_{Na}) - g_K n^4(V - E_K) - g_{CL}(V - E_{CL}) \\
\tau_m \dot{m} &= (m_\infty(V) - m) \\
\tau_n \dot{n} &= (n_\infty(V) - n) \\
\tau_h \dot{h} &= (h_\infty(V) - h)
\end{aligned}
\tag{1.1}
$$

The constants $E_i, g_i,\ i \in \{Na, K, CL\}$ represent the reversal potentials and conductance, respectively. The variables m, n and h represent the probability that a channel is activated, while the constants $\tau_i,\ i \in \{m, n, h\}$ correspond to time constants. $m_\infty, n_\infty, h_\infty$ represent values at equilibrium. C denotes the membrane's capacity, and I is the externally applied current.

FitzHugh-Nagumo model

As opposed to the Hodgkin-Huxley model, the FitzHugh-Nagumo model (FitzHugh, 1961) is a phenomenological model. It is written under an analytical form allowing the simulation of the neurons membrane potential without distinguishing the contributions of different ion channels. It is represented by the following equations:

$$
\begin{aligned}
\dot{V} &= \tau\left(I + V - \frac{V^3}{3} + W\right) \\
\dot{W} &= -\frac{1}{\tau}(V - a + bW)
\end{aligned}
\tag{1.2}
$$

where V represents the neurons' membrane potential, W is a recovery variable and I is the external input denoting the magnitude of the stimulus current that may come from other neurons. a and b are constant parameters usually fixed at 0.7 and 0.8. In the case of $a = b = 0$, the FitzHugh-Nagumo model becomes the Van der Pol oscillator (B Van der Pol, 1927).

Hindmarsh-Rose model

The Hindmarsh model extends the FitzHugh-Nagumo model by adding a third dimension. The system representing this model is given by:

$$\begin{aligned}\dot{X} &= Y - aX^3 + bX^2 - Z + I \\ \dot{Y} &= c - dX^2 - Y \\ \dot{Z} &= r[s(X - X_R) - Z]\end{aligned} \tag{1.3}$$

where X, Y, Z denote the membrane potential, the fast and slow ion channels dynamics, respectively. I represents the external input, similarly to the FitzHugh-Nagumo model. The variation of model parameters leads to a large variety of dynamics (Barrio and Shilnikov, 2011; Lainscsek et al., 2013). This model is known for its chaotic nature, since it is able to generate different spiking patterns while starting from the same initial conditions and having the same afferences (Freeman, 2000). Moreover, it enables the simulation of neuronal bursting.

Morris-Lecar model

The Morris-Lecar model (Morris and Lecar, 1981) is a spiking model compromising between the biophysically detailed Hodgkin-Huxley and phenomenological FitzHugh-Nagumo or Hindmarsh-Rose models. The difference of voltage V depends on the conductance of ionic channels and reversal potential of different ions; however, the probabilities of activation or deactivation of ions channels are replaced by hyperbolic approximations. The model is given by:

$$\begin{aligned}C\dot{V} &= I - g_{CL}(V - V_{CL}) - g_{Ca}m_\infty(V - V_{Ca}) - g_K n(V - V_K) \\ \dot{n} &= (n_\infty - n)/\tau_n\end{aligned} \tag{1.4}$$

Where

$$m_\infty = \frac{1}{2}\left(1 + \tanh\left(\frac{V - V_1}{V_2}\right)\right)$$

$$n_\infty = \frac{1}{2}\left(1 + \tanh\left(\frac{V - V_3}{V_4}\right)\right)$$

$$\tau_n = \frac{1}{\varphi \cosh\left(\frac{V - V_3}{2V_4}\right)}$$

V represents the membrane potential, and n recovery variable, i.e. the probability that potassium channel is open. I is the external current, and C depicts the membrane capacitance. $V_i, g_i,\ i \in \{CL, Ca, K\}$ are conductance and equilibrium potential of chloride, calcium and potassium. Other parameters are constants.

Macroscopic approach

Although neuronal network models constructed at the level of a single neuron offer the advantage of investigating ongoing mechanisms both at the cellular and network levels, they include a large amount of variables and are computationally expensive and time consuming. To overcome this issue, mesoscopic models have been developed, representing neurons in terms of populations without describing explicitly cellular-level mechanisms and considering instead averaged, mean field dynamics. Electrophysiological signals that can be experimentally recorded, such as the EEG, can be generated and result from interactions between interconnected neuronal subpopulations. Neural field models and neural mass models constitute two classes of mesoscopic models describing how a quantity characterizing neural activity evolves in a spatiotemporal space and only temporal space, respectively.

Epileptor

Epileptor is a phenomenological model developed to reproduce brain electrical activity recorded at seizure onset and offset, such as the abrupt transition to fast spiking, and pre-ictal spikes before seizure (Jirsa et al., 2014). It comprises one subsystem responsible for generating fast discharges and another responsible for generating sharp-wave events. Its mathematical formulation is given by:

$$\begin{aligned}
\dot{x}_1 &= y_1 - f_1(x_1, x_2) - z + I_{ext_1} \\
\dot{y}_1 &= c_1 - d_1 x_1^2 - y_1 \\
\dot{x}_2 &= -y_2 + x_2 - x_2^3 + I_{ext_2} + 0.002g - 0.3(z - 3.5) \\
\dot{y}_2 &= \frac{\left(-y_2 + f_2(x_2)\right)}{r_2} \\
\dot{z} &= \begin{cases} r(s(x_1 - x_0) - z - 0.1z^7) & if\ z < 0 \\ r(s(x_1 - x_0) - z) & if\ z \geq 0 \end{cases}
\end{aligned} \tag{1.5}$$

Where

$$f_1(x_1, x_2) = \begin{cases} ax_1^3 - bx_1^2 & if\ x_1 < 0 \\ -(m - x_2 + 0.6(z-4)^2)x_1 & if\ x_1 \geq 0 \end{cases}$$

$$f_2(x_2) = \begin{cases} 0 & if\ x_2 < -0.25 \\ a_2(x_2 + 0.25) & if\ x_2 \geq -0.25 \end{cases}$$

$$g(x_1) = \int_{t_0}^{t} e^{-\gamma(t-\tau)} x_1(\tau) d\tau$$

The variables x_1 and y_1 represent the subsystem responsible for the generation of fast discharges, while x_2 and y_2 represent the system generating spike-wave events. The variable z represents a slow adaptation variable that drive the system to and out of a seizure. All other parameters are constants.

Z^6 model

The Z^6 model is an analytical model that does not represent directly a physiological reality, however, its parameters can be interpreted as realistic variables such as overall excitability of the neuronal population and the balance between excitation and inhibition. It is described by a second-order nonlinear ordinary differential equation:

$$\begin{aligned} \frac{dZ}{dt} &= -\frac{\delta U(Z, \bar{Z})}{\delta \bar{Z}} + \eta(t) \\ U(Z, \bar{Z}) &= -\frac{1}{3}a|Z|^6 - \frac{1}{2}b|Z|^4 - c|Z|^2 - i\omega|Z|^2 \end{aligned} \tag{1.6}$$

where *a, b* and *c* are real parameters and represent the refractory and shunting properties regulating the occurrence of activation rates, the overall excitability of the neuronal population and the control parameter, respectively. The variable $\eta(t)$ represents an additive noise following a normal distribution of mean of 1 and standard deviation of 0.2. This model features a bistability, i.e. it can change state from the initial

steady state to the limit cycle state describing a seizure-like activity following a perturbation.

This model has been used to investigate the impact of an external random noise and study the transition between steady-state and limit-cycle state (Koppert et al., 2016). This model includes only a few parameters, and its dynamics is similar to physiological models. However, this model does not allow distinguishing between contributions of specific physiological properties. The results show the possibility to abort ongoing seizures using random noise.

Wilson-Cowan model

Wilson and Cowan (Wilson and Cowan, 1973) have considered the excitatory and inhibitory properties of a neural mass as two distinct neuronal populations that were connected to each other. These excitatory and inhibitory populations are represented by two differential equations comprising nonlinear function to couple them and mimic an average synaptic effect. This model is written under the following form:

$$\begin{aligned}\frac{dp_E}{dt} &= -\frac{p_E}{\tau_E} + C_{EE}F_E p_E + C_{IE}F_I p_I \\ \frac{dp_I}{dt} &= -\frac{p_I}{\tau_I} + C_{II}F_I p_I + C_{EI}F_E p_E\end{aligned} \tag{1.7}$$

where τ is the population dynamics time constant, p is the population activity, C_{ab} is the coupling strength from population a to b, and F is a sigmoid function representing the population average rate

$$F(p) = \frac{1}{1 + \exp\big(-\gamma(p - \sigma)\big)} \tag{1.8}$$

with σ and γ representing the threshold and slope, respectively.

This model had then been extended and used to investigate the mechanisms that influence the success of single-pulse stimulation in noise-induced spike-wave

(SW) seizures characterizing generalized absence seizures. The model represents the thalamo-cortical neural population, and was fixed on the bi-stable region in the parameter space. Results predicted that SW can be aborted through the application of single-pulse stimulation. Moreover, this study pointed at the influence of the direction of the stimulus in state space, in addition to the amplitude and phase of (SW), on the success of response to stimuli (Taylor et al., 2014).

In this thesis, our main focus is temporal lobe epilepsy, which is different from general absence epilepsy studied by Taylor BN and colleagues, where thalamo-cortical loops play the major role. We will use bio-inspired neural mass models, which include knowledge from neuroanatomy and neurophysiology. These models have the capacity to produce EEG-like signals, while most variable represent a precise physiological quantity. Our aim is to advance our understanding about the mechanisms leading to the generation, propagation and abortion of epileptogenic activity in brain tissue. Mathematical techniques will be used to relate seizure dynamics to the activity of specific neuronal types and properties. Moreover, stimulation protocols beyond from single-pulse stimulation will be explored, and the variables influencing the efficiency of external perturbation to decrease / abort epileptogenic activity will be discussed and studied. Those models are presented in details in the next Chapter (Neural mass models of epilepsy: extension to stimulation-like perturbations).

1.7 Mathematical methods for analysis of brain models

The variation of model parameters can lead to sudden changes in neuronal dynamics. To describe these qualitative changes in system dynamics in response to quantitative changes of model parameters, a mathematical method derived from the theory of dynamical systems, and known as bifurcation analysis, is used. This technique enables a complete visualization of the dynamical repertoire under the variation of a parameter, and highlights bifurcation points. Therefore, such bifurcation diagrams provide insights regarding physiological factors responsible for these alterations, and formulating hypotheses regarding the mechanisms underlying neuronal dynamics.

The dynamics of neuronal populations can be described by non-linear systems of equations. Since these systems are challenging to solve analytically, they are often approximated by linear systems near equilibrium points. For instance, a non-linear dynamical system, $\dot{X} = f(X)$, with $X(t) \in \mathbb{R}^n$ and $f: \mathbb{R}^n \rightarrow \mathbb{R}^n$ is a non-linear function, at an equilibrium point P (ensuring $f(P) = 0$), can be approximated and studied through the approximated linear system at this point, written as $\dot{X} = MX$. The state portrait and stability are then investigated based on the eigenvalues and eigenvectors of the Jacobian matrix M.

A bifurcation is defined as the point where the system undergoes a transition from one dynamic mode into another non-topologically equivalent mode under the change of one or more parameters. This is closely related to the equilibria of the dynamical system and the qualitative change of its eigenvalues at those equilibria. In contrast, stability is related to the signs of the real part of the eigenvalues of the linearized system. An equilibrium is stable if all eigenvalues have a negative real part (Kuznetsov, 1998), otherwise the equilibrium is unstable. This notion of stability includes other closed trajectories, known as limit cycles, which appear when the imaginary part of eigenvalues is nonzero. These limit cycles denote oscillations in brain models. Furthermore, the eigenvalues position in the complex plane classify the equilibrium point. Equilibrium can be:

- *Stable nodes* attract neighboring points. They occur when all eigenvalues are negative and real.

- *Unstable nodes* repel neighboring points. They occur when all eigenvalues are positive and real.

- *Stable focuses* attract neighboring points by spiraling inward. They occur when eigenvalues are complex conjugate with negative real parts.

- *Unstable focuses* attract neighboring points by spiraling outward. They occur when eigenvalues are complex conjugate with positive real parts.

- *Saddles* attract along two directions and repel along two directions. They occur when eigenvalues are real with an opposite sign.

A bifurcation occurs when the stability or number of equilibrium points changes.

Below, we present the most important types of bifurcations on which we will focus in this manuscript.

- *Saddle-node bifurcation*: depicts the collision and disappearance or sudden creation of two equilibria (one stable and one unstable). It is also known as “fold” or “limit point bifurcation”.

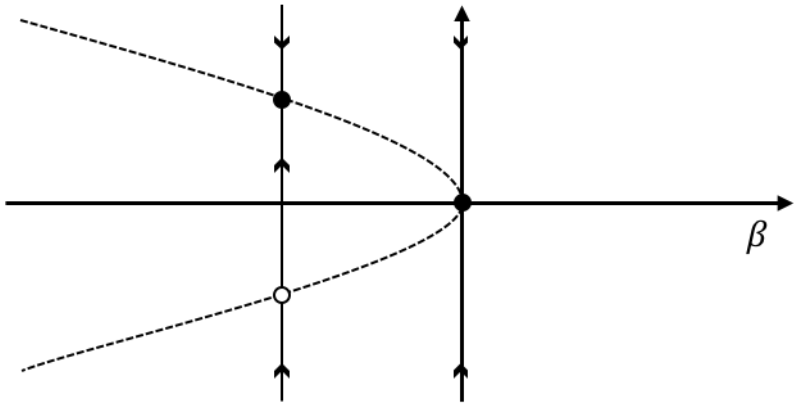

Figure 1.7. Saddle node bifurcation. While variable β is increasing, one stable equilibrium points denoted by black dot approaches an unstable equilibrium point denoted by a white dot. For $\beta = 0$, the two equilibrium point collide and then disappear.

- *Hopf bifurcation*: This is an important point when analyzing the dynamics of a neuronal model, since it marks the transition from rest to periodic states; appearance or disappearance of oscillations. A Hopf bifurcation occurs when an equilibrium point changes stability via a pair of imaginary eigenvalues. Furthermore, it can be either *supercritical* (a stable equilibrium becomes unstable and a stable limit cycle appears), or *subcritical* (resulting in an unstable limit cycle).

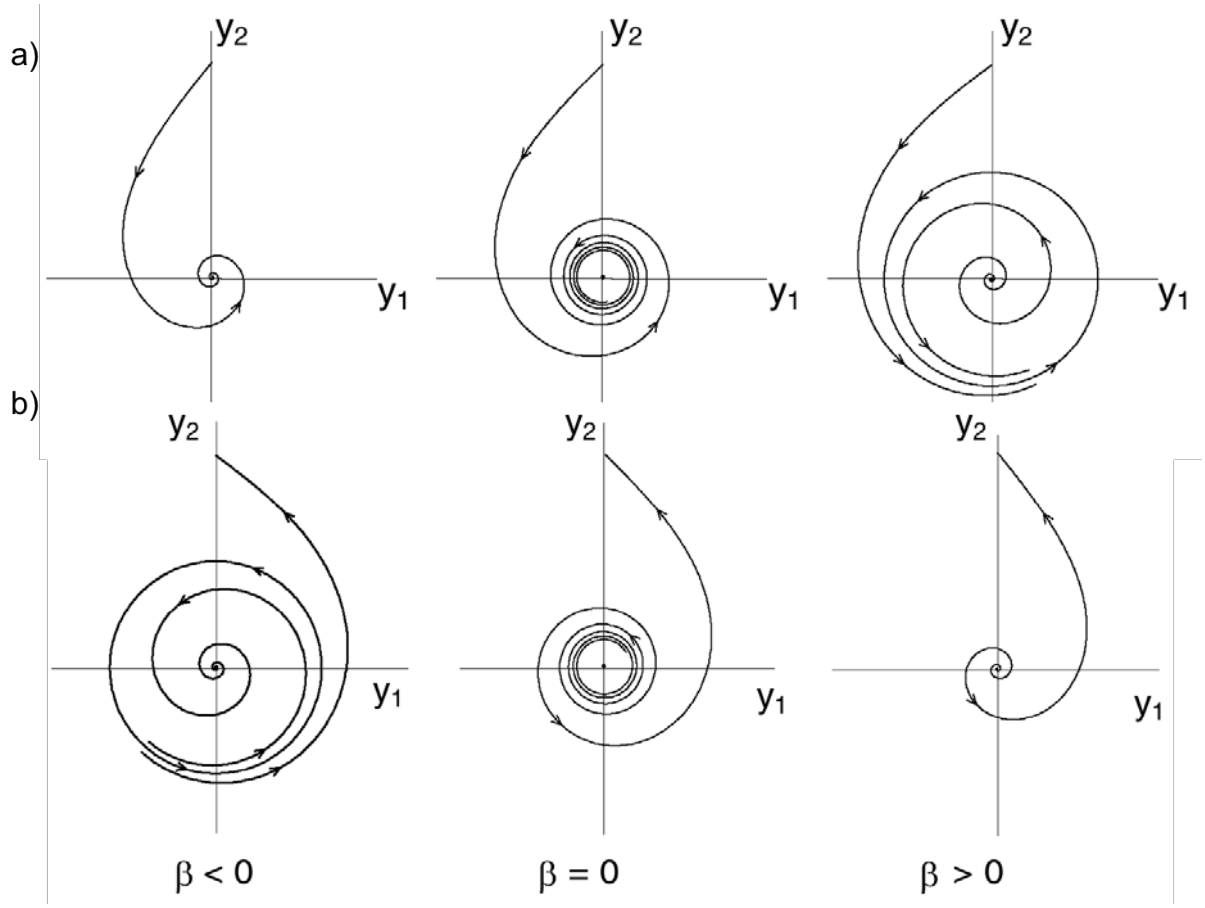

Figure 1.8. a) Super- and b) sub-critical Hopf bifurcation. Regarding the supercritical Hopf bifurcation, a stable equilibrium point becomes unstable while a stable limit cycle emerges. Conversely, during subcritical Hopf bifurcation, an unstable limit cycle emerges or disappears, depending on the variation of the control variable represented in the figure by β. (Figure adapted from Kuznetsov YA)

- *Period doubling*: denotes a point involving the appearance or disappearance of a periodic oscillation with twice the period of the original period. A new limit cycle emerges from an existing one, while the period is doubled.

- *Torus* or *Neimark-sacker* bifurcation: This bifurcation denotes the appearance of an invariant closed curve from an equilibrium point. It can be detected near limit-Hopf bifurcation.

Other bifurcations can be detected, such as *saddle-node on a limit cycle*, or more generally *saddle-homoclinic bifurcation*. These bifurcations represent another type

from which oscillations can emerge from a fixed point. Saddle node on a limit cycle, also called *saddle node on invariant circle*, (SNIC) depict the collision and disappearance of stable and unstable equilibrium points on a limit cycle, and should not be confused with saddle-node of limit cycles, representing the collision and disappearance of limit cycles. Nevertheless, saddle-homoclinic bifurcations denote the collision of a limit point with a limit cycle.

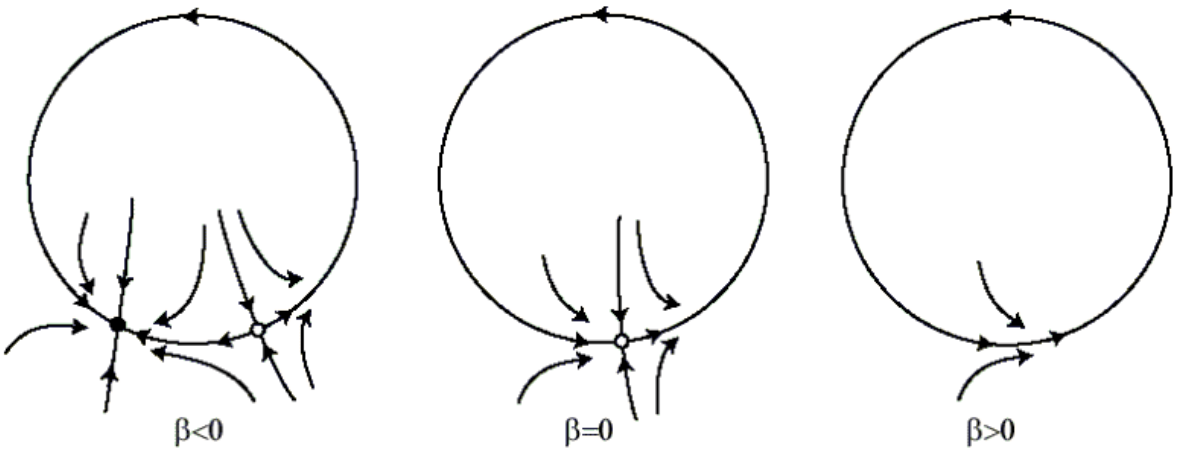

Figure 1.9. Saddle node bifurcation occurring on a limit cycle (SNIC). The stable equilibrium point denoted by a black dot, and the unstable equilibrium point denoted by a white dot, collide and annihilate with each other. (Figure by Eugene Izhikevich, distributed under a CC BY-NC-SA 3.0 License)

Several tools are available to perform numerical bifurcation analysis, such as MATCONT (Dhooge et al., 2003), XPPAUT (Ermentrout, 2002) and AUTO (Doedel et al., 1997). For a dynamical system $\dot{X} = f(X, K)$, the numerical bifurcation analysis involves solving a series of problems of the form $\dot{X} = f(X, K = k_i), \forall i \in \{1, \dots, n\}$ where k_i is a fixed value of the parameter K.

Problem statement

We have provided an overview regarding the physiological properties of brain tissue, how increased excitability leads to the generation of epileptiform activity, and the challenges of using electrical brain stimulation as a symptomatic treatment for this neurological disease. Thus, ***the main problem that will be addressed in this thesis is the design of optimal electrical stimulation protocols able to suppress epileptiform activity and restore physiological patterns of activity.***

The problem statement is threefold:

- **Dynamics of neuronal regions according to intrinsic or synaptic properties.**

  Problem: The dynamics of a neuronal region depending on intrinsic properties, such as subpopulation synaptic gain, or influence of neighboring regions is not yet fully revealed. For example, how alterations of excitability or afferent activity leads to the emergence or disappearance of specific activity patterns remain to be elucidated.

  Proposed Solution: We propose to perform a bifurcation analysis of biologically-inspired mesoscopic models. This mathematical method can provide a complete characterization of a non-linear dynamical system in terms of stability and topological alterations, depending on physiological quantities such as neuronal connectivity and excitability parameters.

- **The impact of electrical stimulation on a brain region and main underlying mechanisms.**

  Problem: Electrical brain stimulation is recognized as promising technique for the treatment of epilepsy. However, it must be designed with care, since its impact can either be positive or negative depending on the chosen parameters. Indeed, although stimulation can lead to the abortion or prevention of epileptic seizures, the choice of inappropriate parameters could exacerbate epileptiform activity. Nowadays, stimulation parameters are still chosen empirically based on trial-and-error approach.

Proposed Solution: We propose to integrate external stimulation into a neuro-inspired model of epileptic activity. Then, we analyze the impact of stimulation according to its parameters (intensity/amplitude, frequency, waveform, stimulation timing) and target. The number of parameters influencing brain tissue response and the associated high-dimensional parameter-space are among the main factors limiting clinical studies. This procedure will enable analyzing the parametric effects of perturbations on a non-linear stochastic dynamical system, and gain information about the mechanisms leading to seizure abortion.

- **Design of network-level optimal stimulations**

Problem: Neuronal dynamics at the single-region level depends on the activity of other regions within the associated network. The emergence of epileptic activity in a region can be caused by afferences from other connected regions. Therefore, stimulation of this epileptic region might not be optimal, even if the set of stimulation parameters is effective in the case of single, separated neuronal region. Additional factors should be taken into account when designing a brain stimulation protocol able to suppress epileptiform activity at the large-scale network level. Stimulation targets identification (which and how many regions to stimulate) is crucial.

Proposed Solution: Using graph theory to evaluate the influence of brain regions belonging to an epileptogenic network. The identification of the main regions driving epileptiform activity will guide the design of optimal stimulation.

Chapter 2

Neural mass models of epilepsy

In the following, we use a modelling approach known as the neural mass model (NMM) approach, which has been developed to simulate the averaged activity of neurons assemblies at a mesoscopic scale. NMM are based on the description of excitatory and inhibitory interactions between populations of neurons. The fundamental properties of NMM are their physiological relevance and ease-of-use, since they include a small number of parameters, as compared for example to microscopic models, while retaining key neuro-anatomical and neuro-physiological properties. Furthermore, NMMs enable simulating signals at a comparable scale than electrophysiological signals typically recorded experimentally or clinically, from scalp (EEG) or intracerebral (depth-EEG / SEEG) signals.

2.1 Jansen and Rit neural mass model

One of the pioneering neural mass models is the biologically inspired Jansen and Rit model (Jansen and Rit, 1995). This model was initially developed to study visual evoked potentials, and is used to describe the activity of a neuronal population composed of two subsets of neurons: excitatory glutamatergic cells (i.e. pyramidal cells) and inhibitory GABAergic interneurons. Each subset is described by two functions: the first one is the “wave-to-pulse” function, converting incoming post

synaptic potentials into a population firing rate. This static function was proposed by Freeman (Freeman, 1975):

$$Sig(v) = \frac{\vartheta_{max}}{2}\left(1 + tanh\frac{r}{2}(v - \vartheta_0)\right) = \frac{\vartheta_{max}}{1 + exp^{r(\vartheta_0 - v)}} \quad (2.1)$$

where ϑ_{max} is the maximum firing rate, ϑ_0 the value of the average membrane potential acting as a firing threshold, and r the slope of the sigmoid at ϑ_0.

The second one is the "pulse-to-wave" function, $h_e(t)$ or $h_i(t)$, converting the density of pre-synaptic action potentials into an average excitatory (EPSP) or inhibitory (IPSP) post-synaptic potential. This function includes physiological time constants:

$$h_k(t) = A_k a_k t exp^{-a_k t} \quad (2.2)$$

where $A_k,\ k \in \{e, i\}$ represents the average excitatory or inhibitory synaptic gain, and a_k represents the average time constant of the postsynaptic potential, expressed is s^{-1} (or equivalently [Hz]). This operator acts as a linear second order low-pass filter, and can be also described as a linear second-order ordinary differential equation *via* the Laplace transform:

$$\ddot{y} = A_k a_k x - 2a_k \dot{y} - a^2 y \quad (2.3)$$

where x, y are the input and output signals, respectively. This equation can also be written as a system of two first-order differential equations:

$$\dot{y}(t) = z(t)$$
$$\dot{z}(t) = A_k a_k x(t) - 2a_k z(t) - a^2 y(t) \quad (2.4)$$

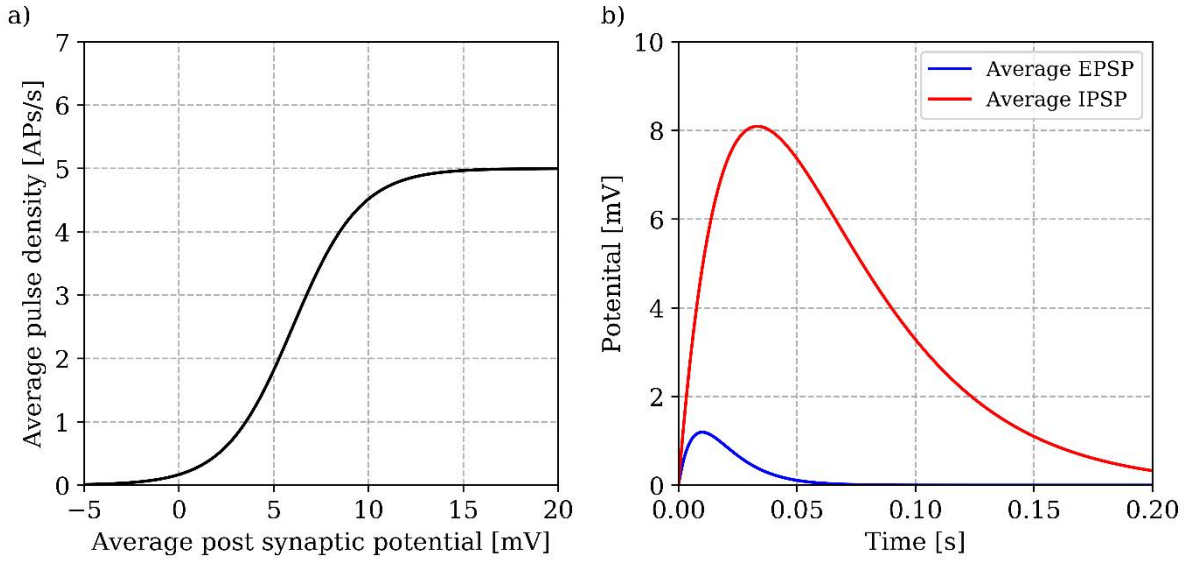

Figure 2.1. a) Sigmoid function: average pulse density (average firing rate as a function of the average post-synaptic potential). b) Average post-synaptic membrane potentials: excitatory and slow inhibitory obtained from impulses at $t = 0$ and expressed as $h_{exc}(t) = A.a.t.e^{-at}$, $h_{inh}(t) = B.b.t.e^{-tb}$ with $t \geq 0$. Corresponding parameters are presented in Table 1.

The afferences of neighboring neural masses are represented by an excitatory input, which is modeled by a white Gaussian noise. The interactions between pyramidal cells and interneurons are represented by four connectivity constants, C_1 to C_4, representing the average number of synaptic contacts. The model is summarized below in Figure 2.2.

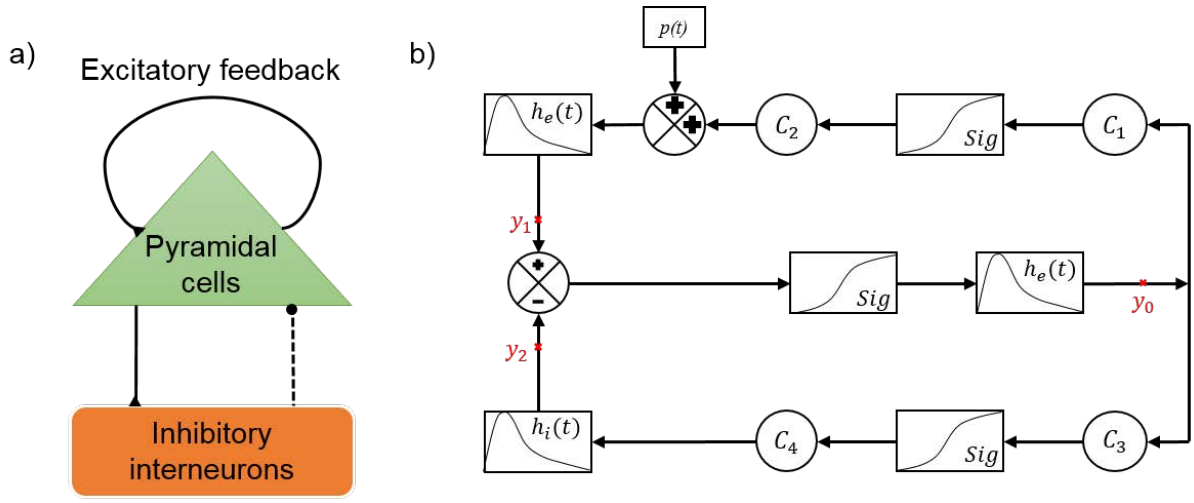

Figure 2.2. a) Structure and b) Block diagram of the Jansen and Rit NMM**.** a) Population of pyramidal cells (green triangle) interacts with an inhibitory population of interneurons (orange rectangle). Solid-lines arrows represent excitatory connections, while dashed-lines represent inhibitory ones. b) $y_i(t), i \in \{0,1,2\}$ correspond to the output of pyramidal cells, excitatory and inhibitory interneurons, respectively. $p(t)$ is a white Gaussian noise representing excitatory inputs from neighboring areas. The $C_i, i \in \{1,2,3,4\}$ coefficients represent the average number of synaptic contacts.

This model can be translated into the following set of differential equations:

$$\begin{aligned}
\dot{y}_0(t) &= y_3(t) \\
\dot{y}_3(t) &= Aa\{p(t) + Sig(y_1(t) - y_2(t))\} - 2ay_3(t) - a^2y_0(t) \\
\dot{y}_1(t) &= y_4(t) \\
\dot{y}_4(t) &= AaC_2Sig(C_1y_0(t)) - 2ay_4(t) - a^2y_1(t) \\
\dot{y}_2(t) &= y_5(t) \\
\dot{y}_5(t) &= BbC_4Sig(C_3y_0(t)) - 2by_5(t) - b^2y_2(t)
\end{aligned} \tag{2.5}$$

The average post-synaptic potential of pyramidal cells $y_1(t) - y_2(t)$ represents the model output, according to the assumption that the summation of post-synaptic potentials onto pyramidal cells constitutes the main contribution of local field potentials (Kandel, 2000). Model parameters, their interpretation and their typical values as evaluated experimentally are provided in Table 1.

Parameter	Description	Value
A, B	Average excitatory and inhibitory synaptic gains, respectively.	$A = 3.25\ mV$ $B = 22\ mV$
a, b	Average time constants of post-synaptic potentials.	$a = 100\ s^{-1}$ $b = 30\ s^{-1}$
$C_i, i \in \{1, 2, 3, 4\}$	Average number of synaptic contacts of excitatory and inhibitory connections.	$C_1 = C$ $C_2 = 0.8 \times C$ $C_3 = 0.25 \times C$ $C_4 = 0.25 \times C$ $C = 135$
$\vartheta_0, \vartheta_{max}, r$	Threshold, maximum output, and slope of the sigmoid function $Sig(v)$.	$\vartheta_0 = 6\ mV$ $\vartheta_{max} = 5\ s^{-1}$ $r = 0.56\ mV^{-1}$

Table 1. Jansen and Rit model parameters and their physiological meaning.

Depending on excitatory and inhibitory synaptic gains (A, B), the model can generate a variety of neuronal rhythms (background activity, sporadic spikes, periodic spikes and alpha-band sinusoidal oscillations), as shown below (Figure 2.3):

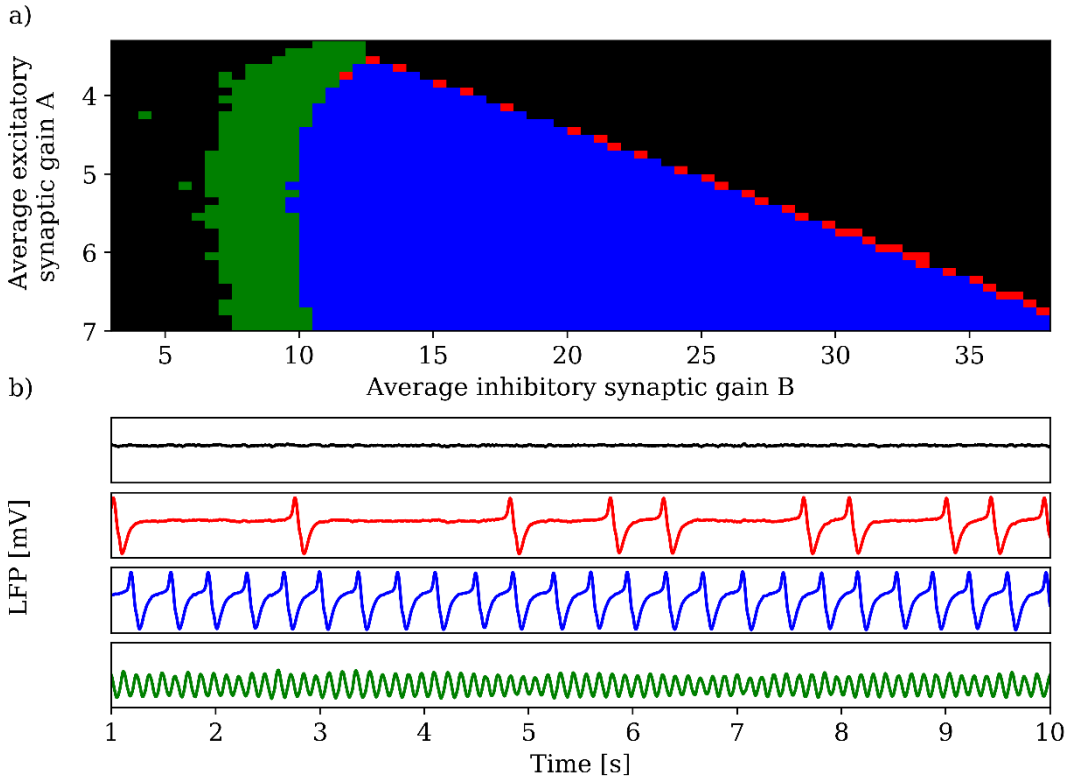

Figure 2.3. a) Activity map in the excitatory / inhibitory synaptic gains space. Black region represents background activity. Red region represents aperiodic spikes. Blue region represents periodic spikes, while green region represents alpha-band sinusoidal oscillations. b) Different model outputs while changing synaptic gains $(A, B) \in \{(4.1, 25.5), (4.4, 20), (5.2, 23.5), (5.5, 9)$. Color codes for activities are respected.

The different patterns presented in Figure 2.3-b have been classified either based on a combination of signal properties such as the frequency domain and the peaks detection, or using a sequential machine learning model for which the inputs is the frequency domain and the outputs are the different neuronal activities that the system able to generate. The accuracy of this model for detecting background activity, periodic spikes and alpha-band sinusoidal oscillations was higher than 95%, and equal to 79.56% for aperiodic spikes.

Regarding numerical calculations, all stochastic simulations were performed with a linear additive Gaussian white noise, and using the Euler-Maruyama method (Maruyama, 1955). Deterministic simulations are performed using the Runge-Kutta 4 method.

2.2 Wendling's neural mass model

Although the Jansen and Rit model can produce a large variety of EEG-like waveforms and rhythms, this model cannot generate the high-frequency activity that characterize the onset of epilepsy seizures (Allen et al., 1992) and guide the identification of epileptogenic regions. This so-called *fast onset activity* is hypothesized to originate from increased activity of fast inhibitory interneurons, thereby modulating the membrane potential of pyramidal cells. Therefore, based on the literature (Banks et al., 2000; Jefferys et al., 1996; Whittington et al., 2000), Wendling et al. have extended the Jansen and Rit formulation by introducing a second type of inhibitory interneurons $GABA_{A,fast}$ with faster kinetics. This class of neurons represents fast somatic-projecting inhibitory interneurons, which activate rapidly and contribute to the generation of gamma rhythms (Veit et al., 2017).

The Wendling NMM consists of three different neuronal subpopulations; pyramidal cells, dendritic-projection interneurons with slow synaptic kinetics $GABA_{A,slow}$ and somatic-projecting interneurons with fast synaptic kinetics $GABA_{A,fast}$. Each population is described by the same two functions presented while introducing Jansen and Rit neural mass model. For more details, the reader is referred to (Wendling et al., 2002b). This model can be translated into a set of five second-order differential equations:

$$\begin{aligned}
\ddot{y}_0(t) &= AaSig\big(y_1(t) - y_2(t) - y_3(t)\big) - 2a\dot{y}_0(t) - a^2 y_0(t) \\
\ddot{y}_1(t) &= Aa\big\{p(t) + C_2 Sig\big(C_1 y_0(t)\big)\big\} - 2a\dot{y}_1(t) - a^2 y_1(t) \\
\ddot{y}_2(t) &= BbC_4 Sig\big(C_3 y_0(t)\big) - 2b\dot{y}_2(t) - b^2 y_2(t) \\
\ddot{y}_3(t) &= GgC_7 Sig\big(C_5 y_0(t) - y_4(t)\big) - 2g\dot{y}_3(t) - g^2 y_3(t) \\
\ddot{y}_4(t) &= BbC_6 Sig\big(C_3 y_0(t)\big) - 2b\dot{y}_4(t) - b^2 y_4(t)
\end{aligned} \tag{2.6}$$

The summation $y_1 - y_2 - y_3$ represents the incoming firing rate to the population of pyramidal cells. Moreover, it represents the local field potential of the neuronal region (Kandel, 2000).

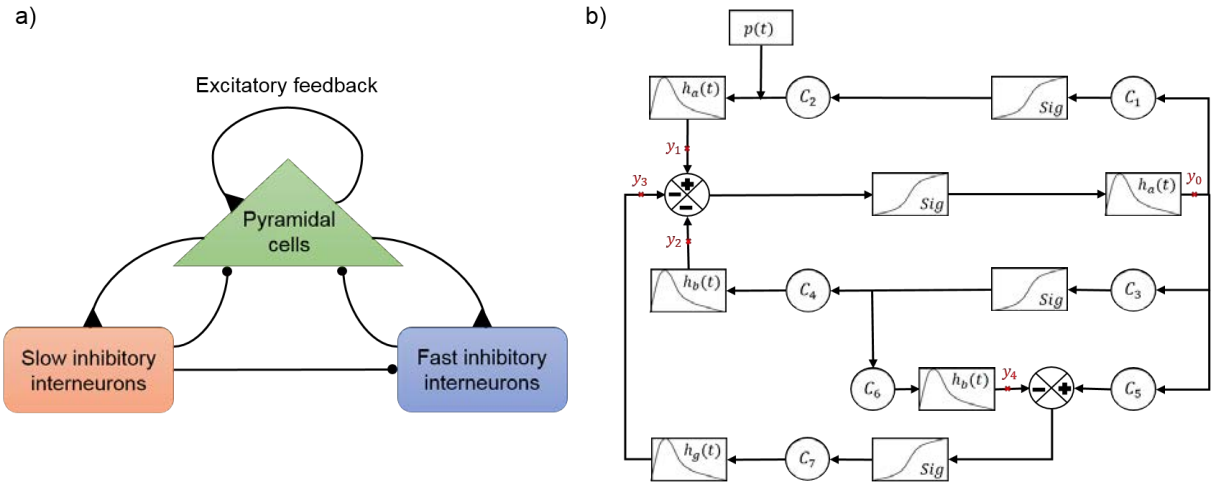

Figure 2.4. a) Schematic and b) Block diagram representation of Wendling's neural mass model. a) The arrows ending with triangles represent excitatory connections, while arrows ending with circles denote inhibitory connections. b) The terms $y_i, i \in \{0, 1, 2, 3, 4\}$ represent the post-synaptic potentials of pyramidal cells, excitatory feedback, and both slow and fast inhibitory interneurons, respectively. Input $p(t)$ represents the influence of neighboring regions and is modelled by a white Gaussian noise. The $C_i, i \in \{1, \dots, 7\}$ coefficients represent the average number of synaptic contacts. The summation of post-synaptic potentials at the level of pyramidal cells constitute the main contribution of LFP (Kandel, 2000). This value is present in the model with the term $y_1(t) - y_2(t) - y_3(t)$.

Parameter	Description	Value
A, B, G	Average excitatory, slow and fast inhibitory synaptic gains, respectively.	$A = 3.25\ mV$ $B = 22\ mV$ $G = 20\ mV$

a, b, g	Average time constants of post synaptic potentials.	$a = 100\ s^{-1}$ $b = 30\ s^{-1}$ $g = 350\ s^{-1}$
$C_i, i \in \{1, \dots, 7\}$	Average number of synaptic contacts of excitatory and inhibitory connections.	$C_1 = C$ $C_2 = 0.8 \times C$ $C_3 = 0.25 \times C$ $C_4 = 0.25 \times C$ $C_5 = 0.3 \times C$ $C_6 = 0.1 \times C$ $C_7 = 0.8 \times C$ $C = 135$
$\vartheta_0, \vartheta_{max}, r$	Threshold, maximum output, and slope of the sigmoid function $Sig(v)$.	$\vartheta_0 = 6\ mV$ $\vartheta_{max} = 5\ s^{-1}$ $r = 0.56\ mV^{-1}$

Table 2. Model parameters and their physiological meaning.

Example of bifurcation analysis of a Wendling's NMM

For a Wendling's NMM, the system of equations is of the form $\frac{dy}{dt} = f(y, K)$, where f is a map from $\mathbb{R}^{10}$ to $\mathbb{R}^{10}$, K is the input, and y is the state space and equal to $(y_0, \dots, y_9)^T$. To study the model response while varying the excitatory synaptic gain A, for example, we first determine equilibrium points. Then, based on eigenvalues of the system Jacobian at each point, we study and identify the various types of bifurcations that the system undergoes.

The equilibrium points are the points for which $\frac{dy}{dt} = f(y, A) = 0$. We obtain:

$$
\begin{aligned}
y_0(t) &= \frac{A}{a} Sig\big(y_1(t) - y_2(t) - y_3(t)\big) \\
y_1(t) &= \frac{A}{a}\{p + C_2 Sig\big(C_1 y_0(t)\big)\} \\
y_2(t) &= \frac{B}{b} C_4 Sig\ \big(C_3 y_0(t)\big) \\
y_3(t) &= \frac{G}{g} C_7 Sig\big(C_5 y_0(t) - y_4(t)\big) \\
y_4(t) &= \frac{B}{b} C_6 Sig\big(C_3 y_0(t)\big) \\
y_5(t) &= y_6(t) = y_7(t) = y_8(t) = y_9(t) = 0
\end{aligned}
\tag{2.7}
$$

This system leads to the equation of the one-parameter family of equilibrium points in the $(A, X = y_1 - y_2 - y_3)$-plane:

$$
\begin{aligned}
X = \frac{A}{a}\left\{p + C_2 Sig\left(C_1 \frac{A}{a} Sig(X)\right)\right\} - \frac{B}{b} C_4 Sig\left(C_3 \frac{A}{a} Sig(X)\right) \\
- \frac{G}{g} C_7 Sig\left(C_5 \frac{A}{a} Sig(X) - \frac{B}{b} C_6 Sig\left(C_3 \frac{A}{a} Sig(X)\right)\right)
\end{aligned}
\tag{2.8}
$$

$X = y_1 - y_2 - y_3$ represents the model output and A is the input. We present the curve defined by the equation (2.8) in Figure 2.3. For a particular value of A, the number of intersections between the curve and the vertical line A correspond to the number of equilibrium points.

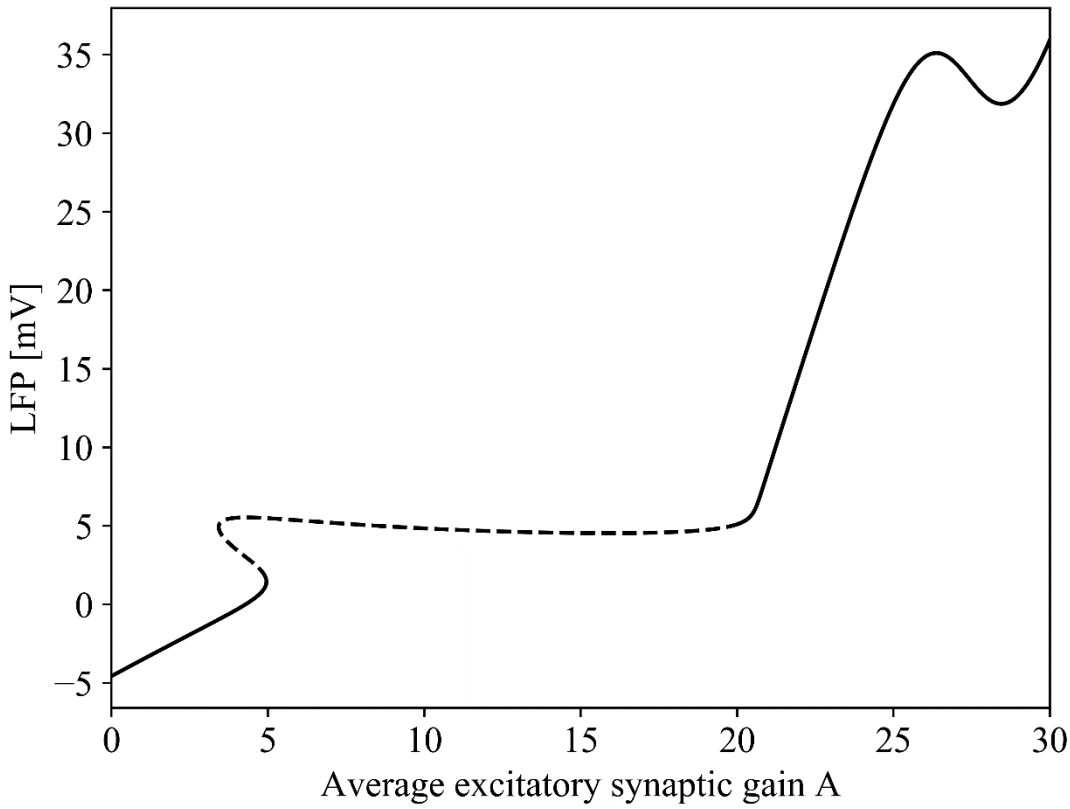

Figure 2.5. Equilibrium points. This curve has been defined by equation (2.8). The solid lines represent stable equilibrium points, while dashed line represents unstable ones.

To describe the system behavior near an equilibrium point, we rely on the Hartman-Grobman theorem (Grobman, 1959; Hartman, 1960) that relates the local behavior of its linearized system around the same point. Then, we calculate the eigenvalues of the Jacobian matrix Jac of the linearized system at this point:

$$Jac = \begin{pmatrix} 0_5 & I_5 \\ A_1 & A_2 \end{pmatrix} \tag{2.9}$$

where I_5 is the identity matrix, 0_5 is a null matrix and A_1 and A_2 are five-dimensional matrices defined as follow:

$$A_1 = \begin{pmatrix} -a^2 & \alpha(X) & -\alpha(X) & -\alpha(X) & 0 \\ \beta(X) & -a^2 & 0 & 0 & 0 \\ \delta(X) & 0 & -b^2 & 0 & 0 \\ \varphi(X) & 0 & 0 & -g^2 & \phi(X) \\ \eta(X) & 0 & 0 & 0 & -b^2 \end{pmatrix}, \tag{2.10}$$

$$A_2 = diag(-2a, -2a, -2b, -2g, -2b)$$

The functions $\alpha, \beta, \delta, \varphi, \eta, \phi$ are defined as follows:

$$\begin{aligned} \alpha(X) &= AaSig'(X), \\ \beta(X) &= AaC_1C_2Sig'\left(C_1\frac{A}{a}Sig(X)\right), \\ \delta(X) &= BbC_3C_4Sig'\left(C_3\frac{A}{a}Sig(X)\right), \\ \varphi(X) &= GgC_5C_7Sig'\left(C_5\frac{A}{a}Sig(X) - \frac{B}{b}C_6Sig\left(C_3\left(\frac{A}{a}Sig(X)\right)\right)\right), \\ \eta(X) &= BbC_6C_3Sig'\left(C_3\frac{A}{a}Sig(X)\right), \\ \phi(X) &= -GgC_7Sig'\left(C_5\frac{A}{a}Sig(X) - \frac{B}{b}C_6Sig\left(C_3\frac{A}{a}Sig(X)\right)\right) \end{aligned} \tag{2.11}$$

where Sig' is the derivative of the sigmoid function.

The eigenvalues of the Jacobian matrix determine the stability of equilibrium points and detect bifurcations, as reviewed previously. As a reminder, on the one hand, stability is related to the sign of eigenvalues' real part. If all eigenvalues have a negative real part, the equilibrium point is stable; otherwise, this point is considered as unstable. On the other hand, bifurcations are linked to the eigenvalues position in the complex plane. For example, when two complex conjugate eigenvalues cross the imaginary axis, the system undergoes a Hopf bifurcation. The detection of this point is crucial, since it highlights the appearance or disappearance of limit cycles; i.e. periodic

oscillations. As another example, when a real eigenvalue crosses the imaginary axis and there are no other eigenvalues on this axis, a fold bifurcation occurs. For more details, the reader is referred to (Kuznetsov, 1998; Perko, 2001).

In the following, we present the detected bifurcation points while increasing the average excitatory synaptic gain A:

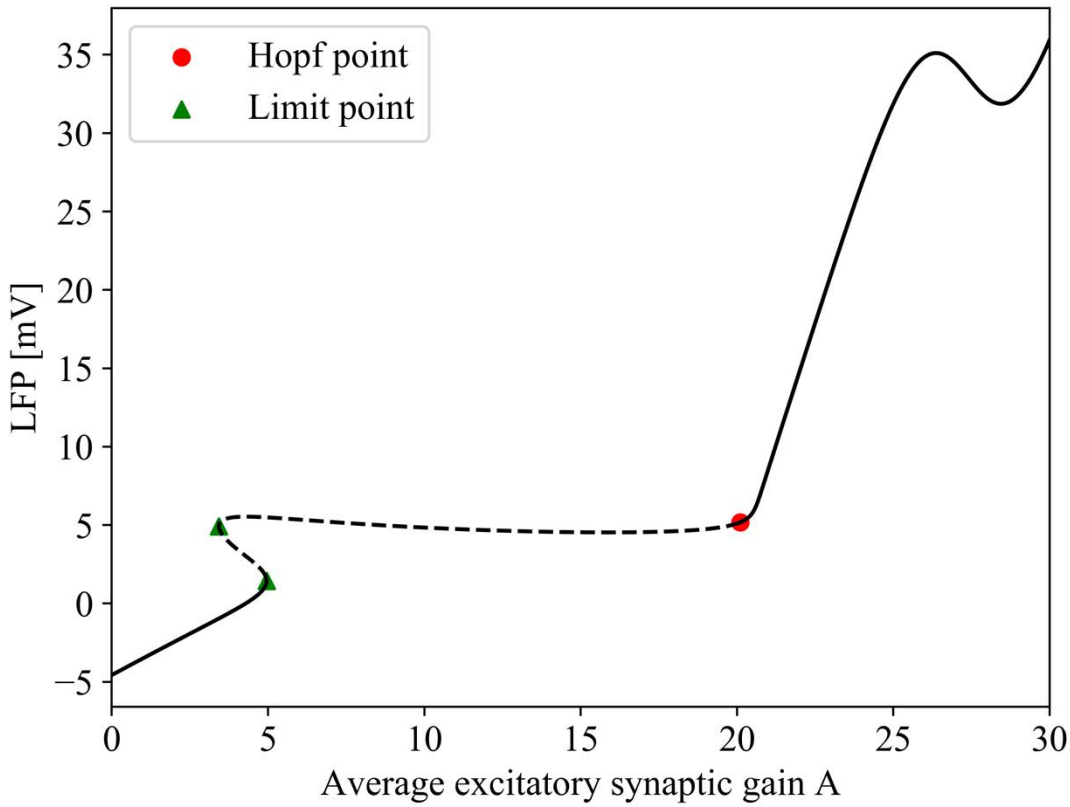

Figure 2.6. Equilibrium points and detected bifurcation points. The black curve is defined by the equation (2.8). The solid lines represent stable equilibrium points, while the dashed line represents the unstable ones. The system undergoes bifurcations, while changing the value of the average excitatory synaptic gain A. Two limit point denoted by green triangles are detected for $A = 3.42$ mV and $A = 4.95$ mV. A Hopf bifurcation is detected for $A = 20.1$ mV and highlights the emergence or disappearance of periodic oscillations.

Identifying which physiological parameters are key to the dynamics of a single neural mass is key to investigate hypotheses about seizures initiation and termination.

Moreover, this is a pre-requisite before moving on to large-scale models and analyze seizures propagation.

2.3 Coupling of models

Neurons communicate through a combination of chemical and electrical interactions. Information passes electrically through the dendrites, soma and axon. Then, the transmission from one neuron to another at the level of synapses is generally chemical (Lovinger, 2008; Ovsepian, 2017). First, vesicles filled of neurotransmitters are positioned at the axon terminal of the presynaptic neuron. When an action potential reaches the axon and causes the opening of voltage-sensitive calcium channels, this leads to an increase in local intracellular calcium concentration. This increase in concentration causes the release of neurotransmitters into the small synaptic gap between the two neurons. The post-synaptic neuron on the other side of the synaptic cleft senses the released neurotransmitters via various types of receptors (Hyman, 2005) situated on its surface membrane.

Synaptic contacts and functional mechanisms (i.e., causing excitation or inhibition) depend on the type of neurotransmitter receptors on the post-synaptic neuron. These receptors are specific of the chemical neurotransmitter, and modulate the post-synaptic neuron membrane potential by causing either excitation or inhibition, depending on the net current flow across the membrane (Davies, 2007; Kandel, 2000). Although we are using a non-microscopic modelling approach, this information about the transmission mechanism is taken into account when constructing a neuronal network comprising multiple neuronal regions. Figure 2.7 represents the method followed to couple two neural masses.

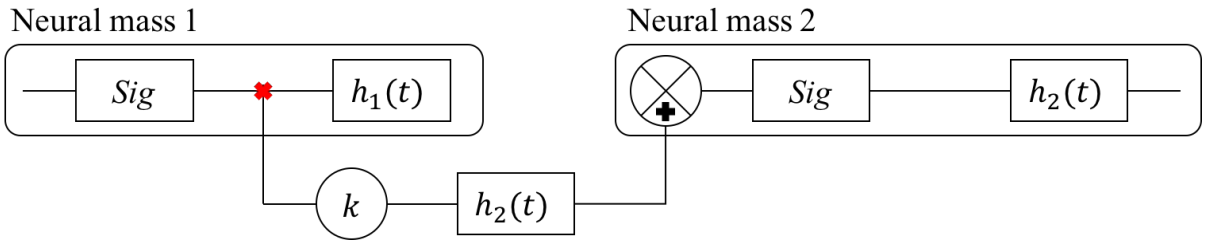

Figure 2.7. Neural mass coupling strategy. The firing rate (red cross) of a subpopulation belonging to neural mass 1 is added to postsynaptic potential entering a population belonging to neural mass 2 after being multiplied by connectivity coefficient k and passing the transfer function of the receiving population.

Network studied in this thesis: Two feed-forward connected Wendling neural mass models

We designed a simple neural mass network including two Wendling models to explore and reveal mechanisms responsible for the onset, spread and termination of epileptiform activity. We constructed the network as presented in equation (2.3). We assumed that only the pyramidal neurons of region 1 projected to region 2. Hence, the firing rate generated by the pyramidal neurons of the region 1 is converted into an excitatory postsynaptic potential at the level of the projected subpopulations. Figure 2.7 illustrates a connection between the pyramidal neurons of region 1 and the subpopulations of region 2. The system describing the two uni-directionally coupled Wendling NMMs is represented by 22 first-order differential equations: ten describing each region as given in (2.6), plus two additional equations representing the synaptic projection, as follows:

Region 1:

$$\dot{y}_0(t) = y_{10}(t)$$
$$\dot{y}_{10}(t) = A_1 a Sig\big(y_1(t)\big) - 2a y_{10}(t) - a^2 y_0(t)$$
$$\dot{y}_1(t) = y_{11}(t) - y_{12}(t) - y_{13}(t)$$
$$\dot{y}_{11}(t) = A_1 a\big\{p(t) + C_2 Sig\big(C_1 y_0(t)\big)\big\} - 2a y_{11}(t) - a^2\big(y_1(t) + y_2(t) + y_3(t)\big)$$
$$\dot{y}_2(t) = y_{12}(t)$$
$$\dot{y}_{12}(t) = B_1 b C_4 Sig\big(C_3 y_0(t)\big) - 2b y_{12}(t) - b^2 y_2(t)$$
$$\dot{y}_3(t) = y_{13}(t)$$
$$\dot{y}_{13}(t) = G_1 g C_7 Sig\big(C_5 y_0(t) - y_4(t)\big) - 2g y_{13}(t) - g^2 y_3(t)$$
$$\dot{y}_4(t) = y_{14}(t)$$
$$\dot{y}_{14}(t) = B_1 b C_6 Sig\big(C_3 y_0(t)\big) - 2b y_{14}(t) - b^2 y_4(t)$$

Region 2:

$$\dot{y}_5(t) = y_{15}(t) \qquad (2.12)$$
$$\dot{y}_{15}(t) = A_2 a Sig(y_6(t) + C_{PP} y_{20}(t)) - 2a y_{15}(t) - a^2 y_5(t)$$
$$\dot{y}_6(t) = y_{16}(t) - y_{17}(t) - y_{18}(t)$$
$$\dot{y}_{16}(t) = A_2 a\big\{p(t) + C_2 Sig\big(C_1 y_5(t)\big)\big\} - 2a y_{16}(t) - a^2\big(y_6(t) + y_7(t) + y_8(t)\big)$$
$$\dot{y}_7(t) = y_{17}(t)$$
$$\dot{y}_{17}(t) = B_2 b C_4 Sig(C_3 y_5(t) + C_{PSI} y_{20}(t)) - 2b y_{17}(t) - b^2 y_7(t)$$
$$\dot{y}_8(t) = y_{18}(t)$$
$$\dot{y}_{18}(t) = G_2 g C_7 Sig(C_5 y_5(t) - y_9(t) + C_{PFI} y_{20}(t)) - 2g y_{18}(t) - g^2 y_8(t)$$
$$\dot{y}_9(t) = y_{19}(t)$$
$$\dot{y}_{19}(t) = B_2 b C_6 Sig(C_3 y_5(t) + C_{PSI} y_{20}(t)) - 2b y_{19}(t) - b^2 y_9(t)$$

Synaptic projection:

$$\dot{y}_{20}(t) = y_{21}(t)$$
$$\dot{y}_{21}(t) = A_2 a Sig\big(y_1(t)\big) - 2a y_{21}(t) - a^2 y_{20}(t)$$

Where variable y_{20} represents the afferent EPSPs, and the variables C_{PP}, C_{PSI}, C_{PFI} are the connectivity strengths between pyramidal neurons of region 1; and pyramidal neurons, slow and fast inhibitory interneurons, respectively. The variable y_{20} represents the afferent from region 1.

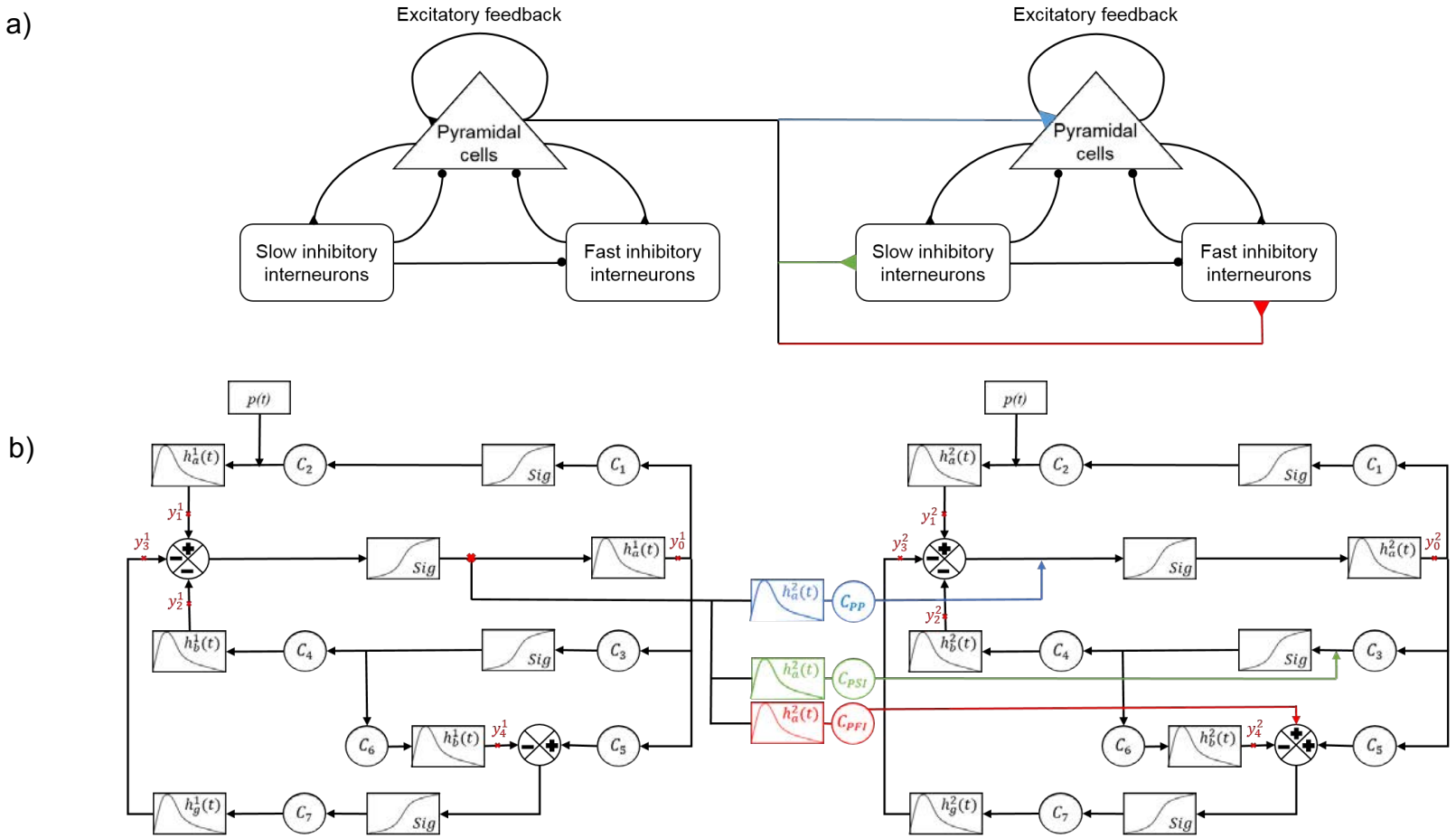

Figure 2.8. Structure of a simple network formed by two uni-directionally coupled Wendling's NMMs. a) Schematic representation, and b) Block diagram. Each region is composed of three neural subpopulations, as shown in Figure 2.4. The firing rate of pyramidal cells of the region 1 is projected at each time step on the subpopulations of region 2 after going through the transfer function of region 2 pyramidal cells and adding a connectivity constant, which represents the synaptic strength of the corresponding synaptic projection.

2.4 How we added the perturbation

In this section, we present how the stimulation protocol is integrated in the computational models presented above.

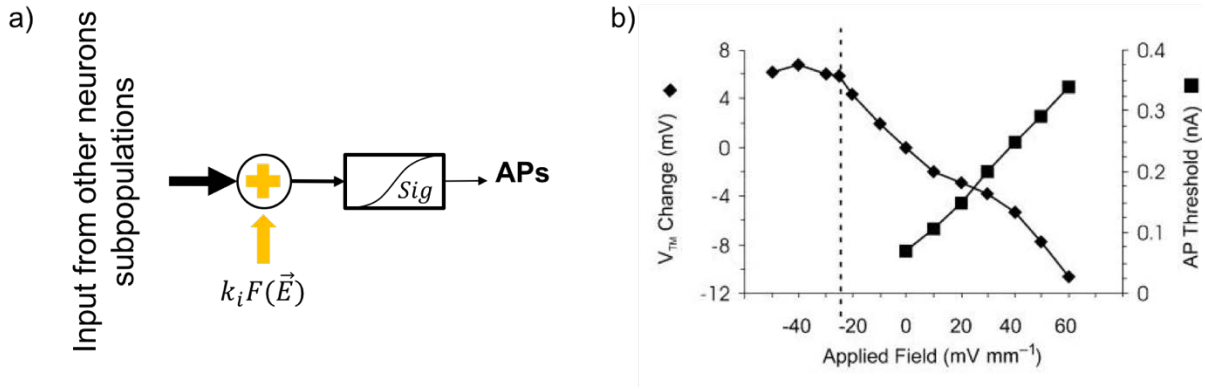

Figure 2.9. Influence of an electric field on a subpopulation of neurons. a) How stimulation applied on specific neuronal subpopulation is added. b) Effect of applied fields on transmembrane potentials and threshold for triggering a single action potential (Figure adapted from M. Bikson et al. 2004)

Neurons are excitable cells that are sensitive to external electric fields $\vec{E}$ (Bikson et al., 2004). More precisely, the variation of the transmembrane potential of neurons (ΔV), therefore the excitability, is assumed to be a linear function of electric field $\Delta V = \lambda . \vec{E}$, where λ is a constant (Miranda et al., 2009). Based on this assumption, the electrical stimulation was added to post-synaptic potentials entering each subpopulation. Therefore, the net effect of the stimulation was to depolarize targeted subpopulations. For example, while modeling a neuronal region using the Wendling's neural mass model, the LFP is the result of the interaction of three neuronal subpopulations, as presented earlier. An applied electrical stimulation impacted each of these neuronal subpopulations, and was added as an input to the sigmoid functions after being multiplied by subpopulation-dependent stimulation coefficient.

We present below the differential equations describing a stimulated Wendling's NMM:

$$
\begin{aligned}
y_0' &= y_5 \\
y_5' &= AaSig(k_P Stim + X) - 2ay_5 - a^2 y_0 \\
X' &= y_6 - y_7 - y_8 \\
y_6' &= Aa\{p + C_2 Sig(k_P Stim + C_1 y_0)\} - 2ay_6 - a^2(X + y_2 + y_3) \\
y_2' &= y_7 \\
y_7' &= BbC_4 Sig(k_{SI} Stim + C_3 y_0) - 2by_7 - b^2 y_2 \\
y_3' &= y_8 \\
y_8' &= GgC_7 Sig(k_{FI} Stim + C_5 y_0 - y_4) - 2gy_8 - g^2 y_3 \\
y_4' &= y_9 \\
y_9' &= BbC_6 Sig(k_{SI} Stim + C_3 y_0) - 2by_9 - b^2 y_4
\end{aligned}
\tag{2.13}
$$

This set of differential equations provides a direct access to the LFP value presented by the variable X. The variables (k_P, k_{SI}, k_{FI}) represent stimulation coefficients upon pyramidal cells and slow and fast inhibitory interneurons, respectively. The variable $Stim$ represent the applied electrical stimulation.

It is now established that epilepsy is a network disease (Berg et al., 2010). An epileptic network consists of cortical and subcortical structures that are anatomically and functionally connected (Spencer, 2002). Thus, afferents from any structures belonging to the epileptic network will affects other structures. Temporal lobe epilepsy, studied in this thesis, involves seizures that originate in hippocampus and other anatomically and functionally connected neuronal brain networks within and beyond the temporal lobe (Bettus et al., 2009; Morgan et al., 2010). These networks include neuronal structures such as thalamus, entorhinal cortex and amygdalae (Norden and Blumenfeld, 2002). This network structure justified and led to the existence of two different stimulation paradigms; direct and indirect stimulation. The first one represents a direct targeting of the neuronal structure implicated in the generation of the pathological activity. The second consists in stimulating a neuronal structure belonging to the epileptogenic network and presenting afferent output to the epileptogenic structure from which the seizure is triggered and propagated. This indirect stimulation alters the pathological activity *via* synaptic activation of neurons, in contrast to direct activation caused by a direct stimulation.

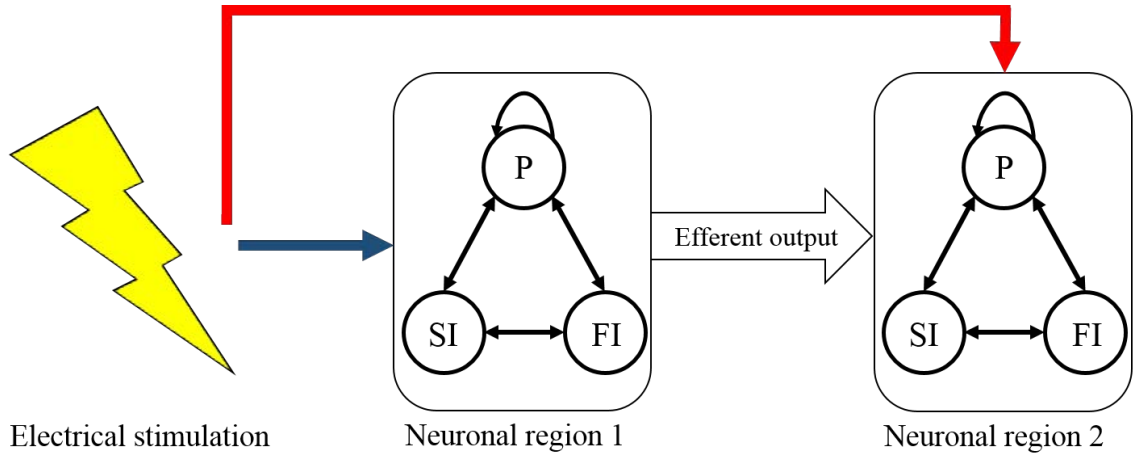

Figure 2.10. Stimulation paradigms. Neuronal region 2 could be either directly stimulated (red arrow) or indirectly stimulation through stimulating neuronal region 1 presenting an afferent output to neuronal region 2. A neuronal region is modeled using Wendling's neural mass model. P, SI and FI represent pyramidal cells, slow and fast inhibitory interneurons, respectively.

Chapter 3

Dynamics of local neuronal populations under spontaneous and stimulated conditions

3.1 Spontaneous condition: Investigation of models parameters

The variation of model parameters, extrinsic input and synaptic gains, can lead to sudden, qualitative changes in neuronal activities. In this section, we perform a bifurcation analysis of the WNMM presented in the previous chapter. We describe below the qualitative changes in dynamics for system (2.3) in response to quantitative input changes (external input p and synaptic gains).

Variation of the external input p

All parameters, except the extrinsic noise p, were kept constant and equal to standard values mentioned in Table 2.

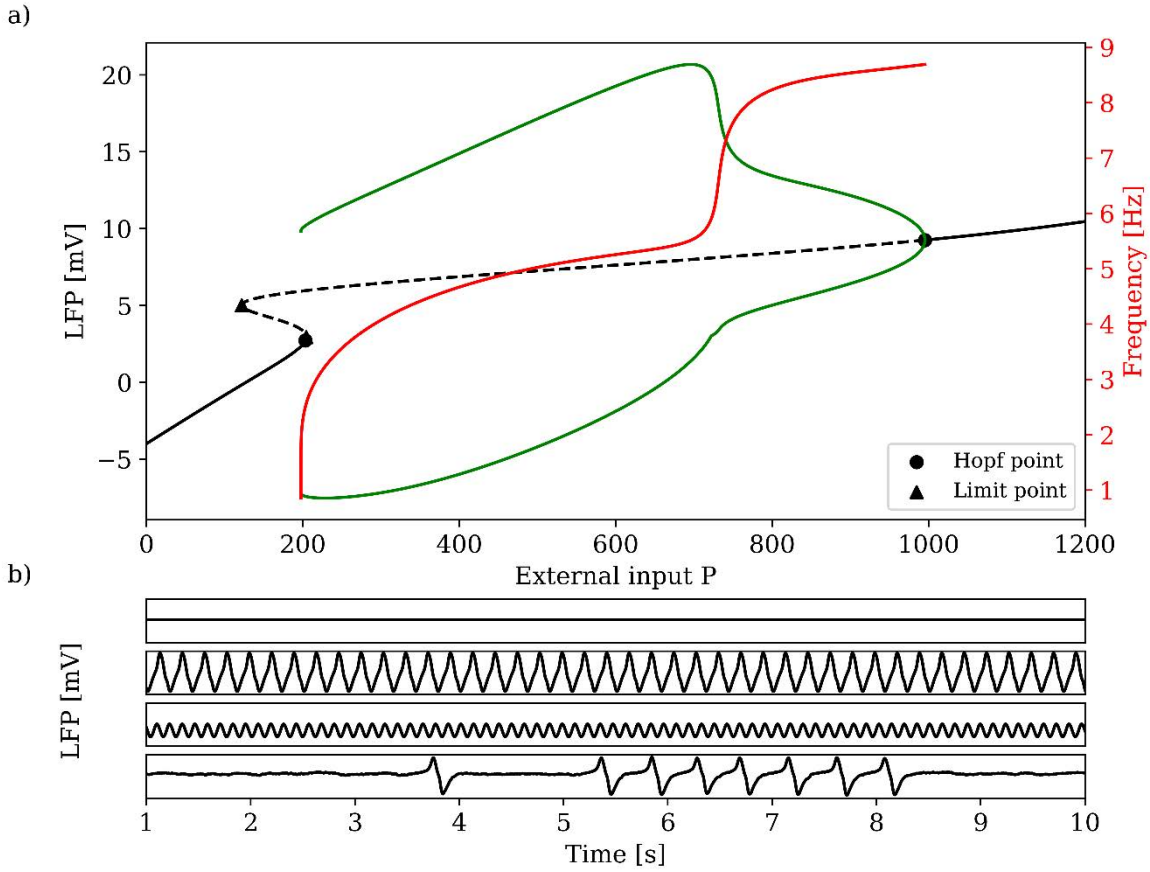

Figure 3.1. a) Bifurcation of the LFP with respect to the input p. The solid and dashed black lines denote stable and unstable equilibrium points, respectively. The green curve corresponds to stable limit cycles. The red curve depicts the frequency of periodic oscillations for $p \in [203.22, 995.41]$. Triangles and circles denote limit and Hopf bifurcation points. b) LFP time-series while $p \in \{180, 400, 800, N(198, 50)\}$, respectively.

The bifurcation diagram (Figure 3.1-a) can be divided into three regions. For $0 \leq p \leq 203.2$, all the eigenvalues of matrix (2.9) have a negative part, and the equilibrium points are stable, corresponding to background activity. Then, a homoclinic limit cycle appears suddenly and generates high amplitude oscillations (Grimbert and Faugeras, 2006). For a Gaussian noise of a mean value near to the point separating the two regions and a non-null standard deviation, spikes are generated. The last time series in Figure 3.1-b illustrates an example, where the mean noise mean value is equal to 198 and the standard deviation is equal to 50, which generates a spiking

activity. For $203.22 \leq p \leq 995.41$, the system exhibits quasi-sinusoidal activities that arise from a branch of stable periodic orbits delimited by a Hopf bifurcation. The oscillations with a large amplitude are related to a rhythmic activity, while those with a relatively small amplitude are related to alpha activity. For values of p greater than 995.41, the system returns to background activity.

Typically, the white Gaussian noise p used has a rate ranging from 60 to 120 pulses per second. This interval belongs to the first region where the system generates background activity. Increasing the noise can induce the onset of spiking activity.

Influence of synaptic gains

Previous studies have shown that electrical stimulation modulates neurotransmitters' concentrations (Das et al., 2016; Tawfik et al., 2010) and thereby neuronal excitability, while the associated mechanisms are still unclear. In the following, we investigate how the variation of synaptic gains controls the type of activity that can be generated.

Variation of the average excitatory synaptic gain A

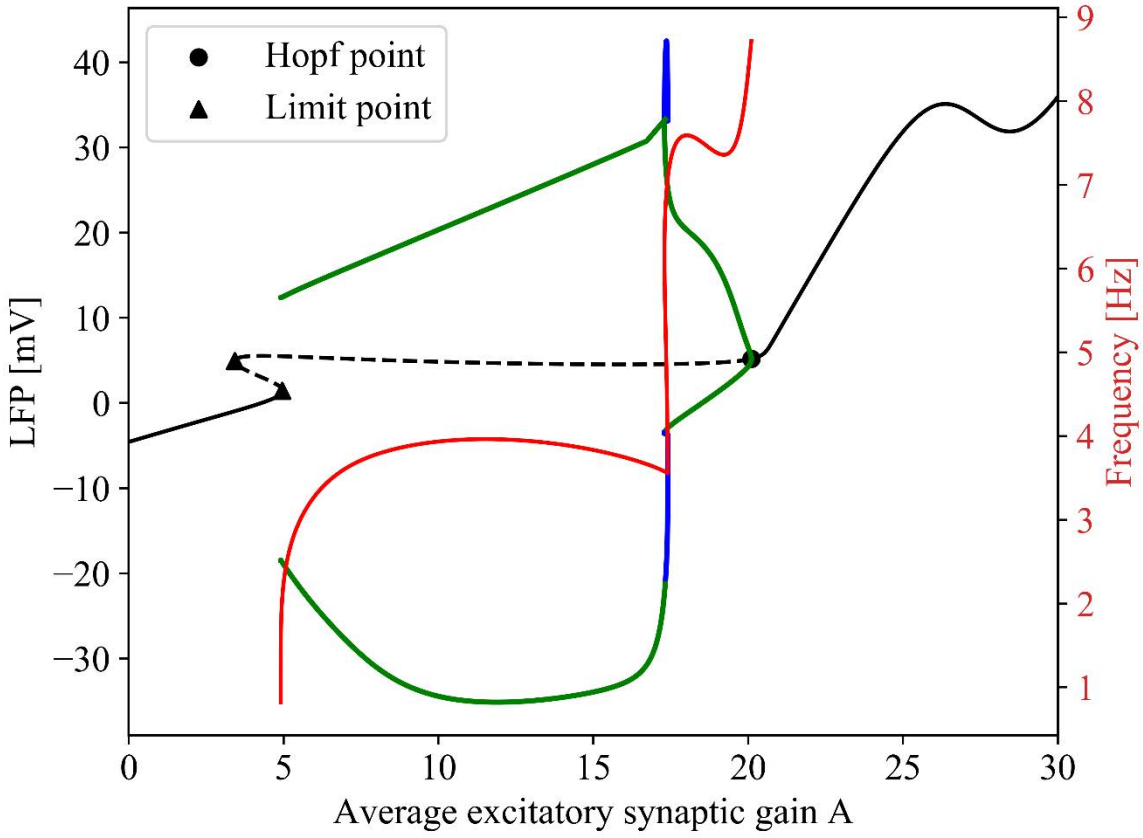

Figure 3.2. LFP as a function of the average excitatory synaptic gain A and frequency of periodic oscillations. The solid and dashed black curves represent stable and unstable equilibrium points, respectively. The green and blue curves correspond to stable and unstable limit cycles, respectively. The red curve depicts the frequency of periodic oscillations for $A \in [4.95, 20.1]$ mV. Triangles and circle denote limit and Hopf bifurcation points.

Figure 3.2 presents all the dynamics that the differential equations system (2.6) can generate while varying the excitatory synaptic gain A. This diagram enables discriminating the A values for which the system oscillates, and those for which the system is attracted by a stable limit point corresponding to either background activity or low-amplitude high-frequency activity in the presence of noise. Therefore, this analysis delivers insights about the required alterations to modify pathological dynamics towards more physiological dynamics.

The bifurcation diagram (Figure 3.2, left y-axis) can be divided into five regions. In the first region where $A \in [0, 3.42)\ mV$, the system possesses a single branch of stable equilibrium points and generates background activity with an increasing LFP mean value. In the second region where $A \in [3.42, 4.95]\ mV$, the equilibrium points lie on a S-shaped curve between two limit point bifurcations at the interval extremities. At $A = 4.95\ mV$, the system undergoes a saddle-node on invariant circle (SNIC) bifurcation where a rhythmic activity appears. This rhythmic activity persists until the supercritical Hopf bifurcation at $A = 20.1\ mV$. The region of periodic oscillations is further divided into two regions (see Figure 3.2, right y-axis). For $A \in (4.95, 17.3]\ mV$, the system generates alpha-band oscillations at a frequency around 8 Hz. The diagram shows the existence of multiple types of alpha rhythms, representing different limit cycles with different amplitude ranges. Finally, for $A \in [20.1, 30)\ mV$, the system has stable equilibrium points.

Variation of the average inhibitory synaptic gains (B, G)

Inhibitory interneurons originate specific oscillatory patterns at different frequencies depending on their type. In particular, GABAergic interneurons have been shown to exhibit different firing patterns in relation to network oscillations (Middleton et al, 2008), indicating that they control oscillations in the brain (Klausberger and Somogyi, 2008; Le Magueresse and Monyer, 2013; Tremblay et al., 2016). For example, it has been experimentally evidenced that these neurons play a critical role in the generation and maintenance of high-frequency activity (Magloire, Mercier et al., 2019). Therefore, linking the oscillations to degree of excitability of these interneurons, and understanding how a lack of slow GABAergic neurons affected by epilepsy (Dudek and Shao, 2003) can impact the generation of epileptiform activity crucial.

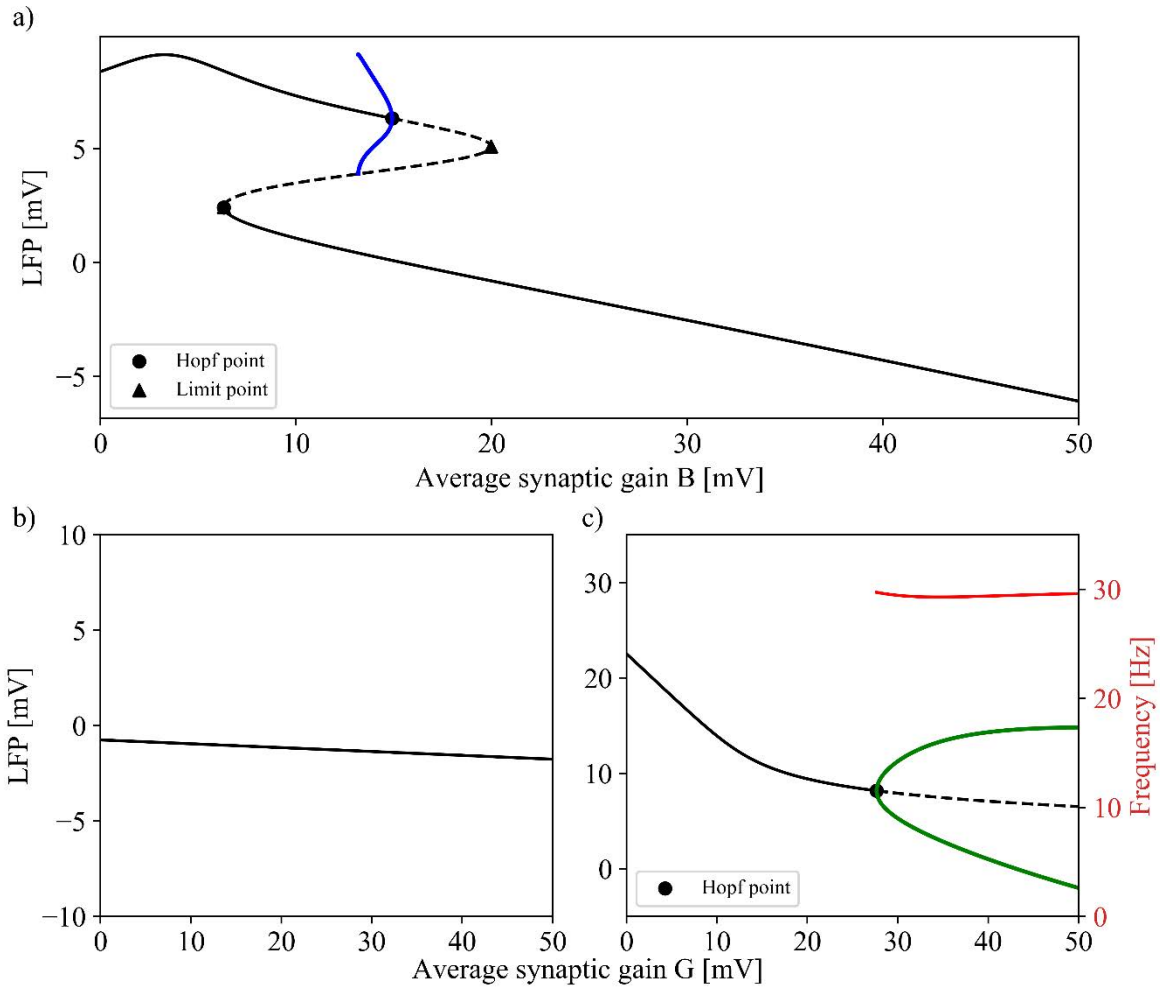

Figure 3.3. LFP as a function of the average inhibitory synaptic gains B (upper panel) and G (lower panels). a,b) All model parameter values except B in a) and G in b) are equal to the values in Table 1. c) The values of slow inhibitory and excitatory synaptic gains A and B were modified to 2 mV and 5 mV, respectively. Stable and unstable equilibria lie on solid and dashed black curves, respectively. Blue and green curves represent the minima and maxima of the unstable and stable limit cycles rising from Hopf bifurcations at $B = 14.9$ mV in a) and $G = 32.2$ mV in c). The red curve represents the frequency of stable limit cycles.

Figure 3.3 presents the solutions of the WNMM (equation (2.6)) as a function of the inhibitory synaptic gains B and G, while other parameters are provided in Table 1. The equilibria (2.8) as a function of B lie on a Z-shaped curve, as can be seen in Figure 3.3-a. The lower branch of the Z-shaped curve corresponds to background activity $(B > 6.29\,mV)$, whereas the upper branch solutions for $0 < B < 14.9\,mV$ can yield ripples with a frequency greater than 8 Hz under noisy input. The system can switch

between these two behaviors in the bi-stable region for $B \in [6.29, 14.9]\, mV$, which is separated by the unstable branch of equilibria (Figure 3.4-a). The upper branch undergoes a Hopf bifurcation at $B = 14.9\, mV$, resulting in a branch of stable limit cycles for $B \in [13.1, 14.9]\, mV$ making a homoclinic connection with a saddle point on the middle branch of the A-shaped curve. Note that the LFP mean value decreases as the parameter B increases, which is equivalent to decreasing the excitation/inhibition ratio (A/B).

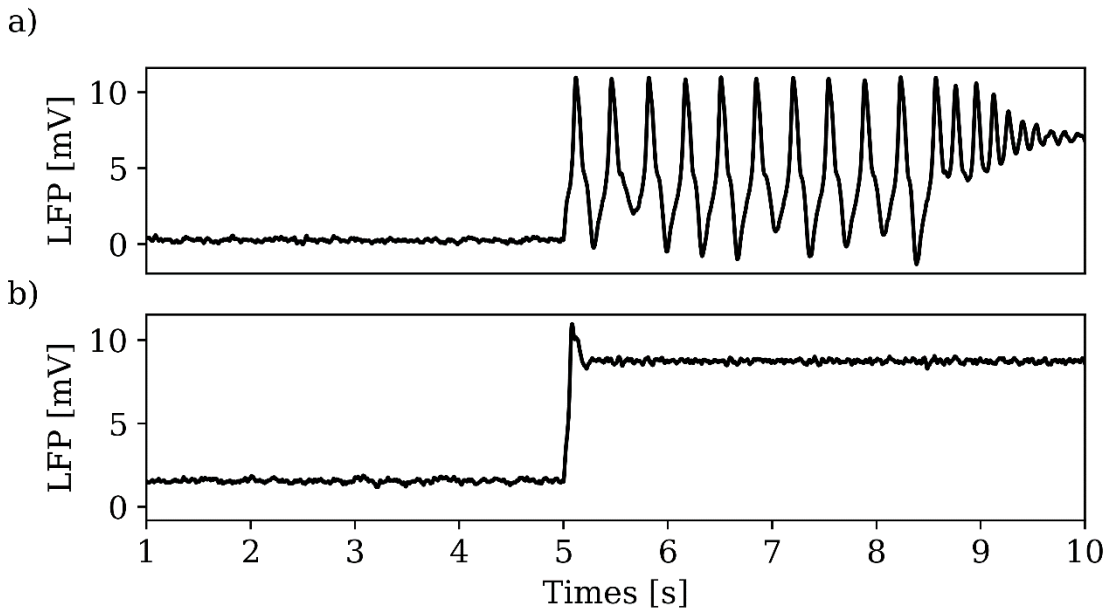

Figure 3.4. LFP signals for slow inhibitory synaptic gains equal to 14 mV in a) and 8 mV in b). The noise mean is equal to 90 until 5 s and is then doubled. The noise standard deviation is kept constant and equal to 30.

$GABA_{A,fast}$ neurons have been shown to be involve in the generation of low amplitude, high-frequency oscillations, namely low-voltage fast onset activity, which is one of the markers of epileptic seizures (Jacobs et al., 2008; Roehri et al., 2018). Wendling et al (Wendling et al., 2002b) have noted that the system can generate low-voltage fast onset when the $GABA_{A,slow}$ interneuron inhibitory impact on the $GABA_{A,fast}$ interneuron population is decreased and the excitation is increased. Indeed, increasing the value of G, while all the other parameters are kept constant and equal to values presented in Table 1, slightly decreases the mean LFP value but does not generate fast onset activity (Figure 3.3-b). Fast activity appears if the slow inhibitory synaptic gain B is decreased and the excitatory one A is increased, as exemplified in Figure

3.3-c. Under such conditions, the system has stable equilibrium points until $G = 32.2\,mV$ where a Hopf bifurcation occurs, and high-frequency, high-amplitude oscillations appear (about 30 Hz). This behavior is preceded by the appearance of low-amplitude, fast-frequency oscillations for values of G closer to 32.2 mV. Let us note that the oscillation amplitude increases with G.

These diagrams enable us formulating hypotheses about the mechanisms leading to the generation or abortion of epileptic seizures. For instance, the excitation of glutamatergic neurons drives the neuronal population to theta- and alpha-band oscillations, as presented in Figure 3.2. However, the same figure also provides an unintuitive prediction: over-excitation of glutamatergic neurons could stop oscillations, through a possible depolarization block. Although further *in vivo* experiments could be performed to test this this computational result, this result could explain seizures termination. Regarding inhibitory processes, excitation of $GABA_{A,slow}$ interneurons weakens the influence of $GABA_{A,fast}$ interneurons, and keeps the system in background activity mode. Conversely, excitation of glutamatergic neurons and $GABA_{A,fast}$ interneurons combined with the inhibition of $GABA_{A,slow}$ interneurons promotes the emergence of high-frequency activity that resembles epileptic seizures (Figure 3.3-c). Such prediction is possible thanks to the WNMM formulation, which considers different GABAergic interneuron subtypes with fast and slow kinetics separately and distinguishes excitatory/inhibitory ratio between them and pyramidal neurons.

In the following, we performed a co-dimension 1 bifurcation analysis of the WNMM by changing one of the gain parameters, while all the other model parameters were kept constant and equal to the values presented in Table 2. Then, we continue our investigation in the parameter space of (A, B, G) for which the system has an oscillatory behavior. In particular, we follow the Hopf and limit points of the bifurcation diagram in Figure 3.3-a, since they are related to sporadic spikes and periodic oscillations.

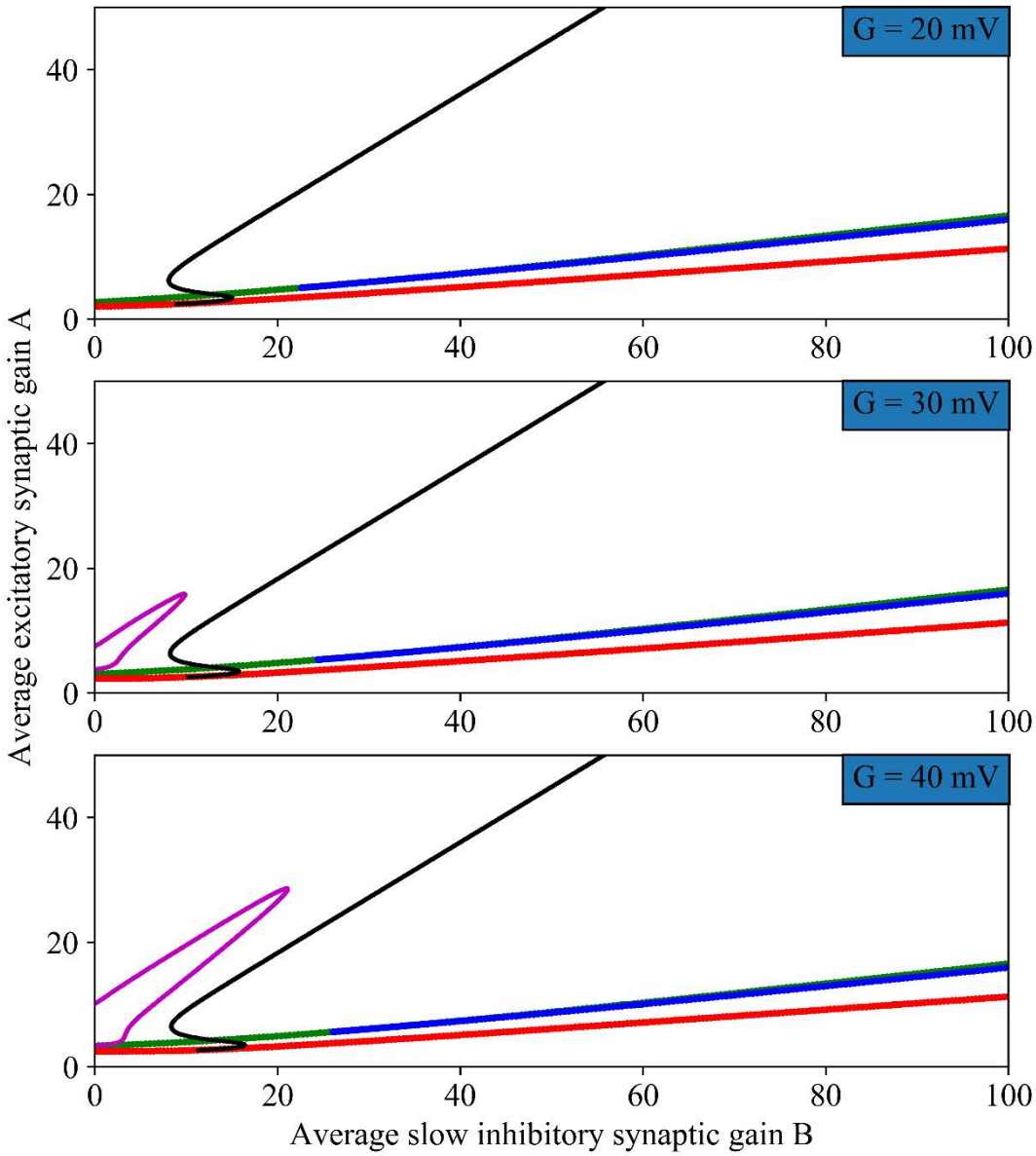

Figure 3.5. Continuation of Hopf and limit point bifurcations in (A, B)-parameter space for different values of G. The green and red curves represent limit points; while blue, black and purple curves represent Hopf points.

Figure 3.5 presents the locations of Hopf and limit point bifurcation points in Figure 3.2 and 3.3 in the (A, B) space for different values of G. Fast oscillations can be introduced by increasing G. For instance, for $G = 40\,mV$ and $A = 10\,mV$, the system undergoes three Hopf bifurcations along the B axis. The system generates a periodic activity of a frequency around 30 Hz between the first two Hopf bifurcations (the purple curve) similar to the one presented in Figure 3.6-a. In the small interval between the

second and the third Hopf Bifurcations, although the system has equilibrium points, fluctuations in the input parameter $p(t)$ yield ripples. The system generates fast onset activity for B values closer to the second Hopf bifurcation. Figure 3.6-b shows a time series of this fast onset activity in the presence of noisy input. The frequency decreases as the B value approaches the third Hopf bifurcation point before switching to alpha oscillations of a frequency around 8 Hz followed by high-amplitude theta-band spiking oscillations. For this example, the system undergoes a SNIC bifurcation for $B > 50\ mV$, where the system switches from a stable periodic behavior to background activity.

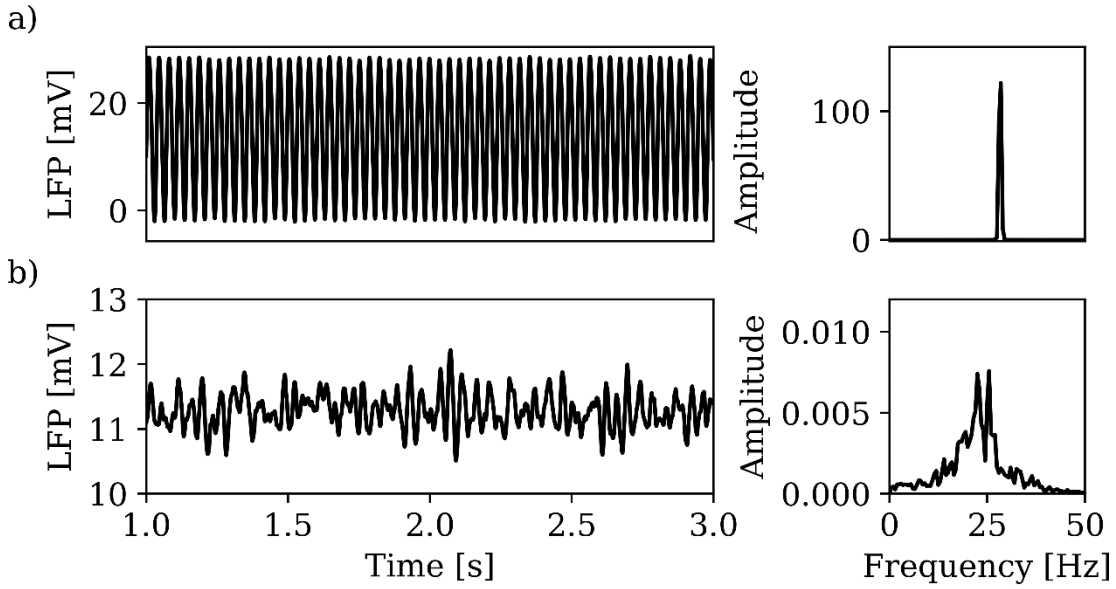

Figure 3.6. LFP and corresponding power spectrum generated by a WNMM for synaptic gains $(A, B, G) \in \{(10, 4, 40)\ mV, (10, 7, 40)\ mV\}$, respectively. A) The fast oscillations (high beta / gamma range) observed in the LFP are due to the activity of fast inhibitory interneurons.

For a better understanding of Figure 3.5, we present a set of co-dimension 1 bifurcation diagrams in Figure 3.7. These diagrams provide three key information on the system's dynamics. First, increasing the excitatory synaptic gain A leads to periodic solutions and expands the range of slow inhibitory synaptic gains for which the system generates periodic oscillations. Second, increasing the fast inhibitory synaptic gain G promotes the appearance of fast oscillations, including low-voltage, fast-onset activity. Third, increasing the slow inhibitory synaptic gain B inhibits the system and leads to

replacing oscillatory activity by background activity. Indeed, the network structure explains this inhibitory impact of $GABA_{A,slow}$ interneurons, which (i) prevent pyramidal cells from excessively firing, thereby modulating the activity of connected subpopulations, and (ii) inhibit $GABA_{A,fast}$ interneurons and prevent them from generating high-frequency oscillations.

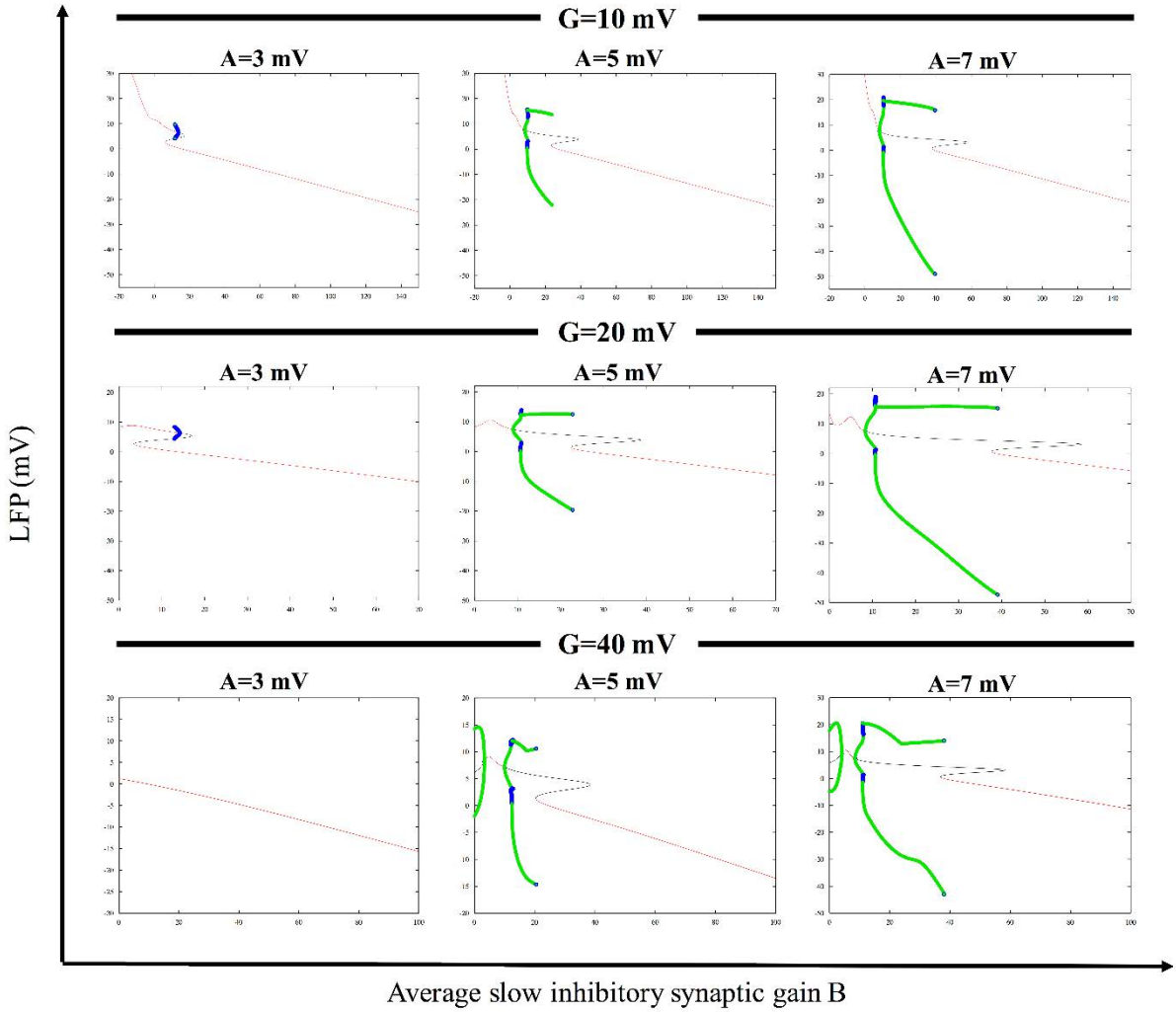

Figure 3.7. Bifurcation diagrams obtained when changing the average slow inhibitory synaptic gain B for several values of excitatory and fast inhibitory synaptic gains (A, G). The red and black curves represent stable and unstable equilibrium points, respectively. The green and blue curves represent stable and unstable limit cycles, respectively.

In a nutshell, we investigated, in this section, how neural masses dynamics change in response to alterations in synaptic gains. Each excitability state (resulting from the combination of synaptic gains) of a neuronal subpopulation was associated with a neuronal activity pattern. Such visualization enabled the identification of the neuronal subpopulations involved in the generation of specific activity patterns. Results link the appearance of high-frequency low-amplitude oscillations, which characterize epileptic fast onset, to an increased activity of somatic-projecting, fast inhibitory interneurons (Figure 3.3-c). This increased activity is represented by an increase in the corresponding synaptic gain. Furthermore, background activity is related to high levels of activity of dendritic-projecting, slow inhibitory interneurons. This neuronal subpopulation inhibits both the somatic projecting inhibitory interneurons and pyramidal cells. Therefore, it leads to the suppression of epileptic oscillations and diminishes high-amplitude oscillations generated by the excitatory neurons through influencing pyramidal cells.

3.2 Stimulated condition: Investigation of stimulation parameters

Bifurcation analysis of a Wendling's neural mass model under stimulation

The main objective of this section is to determine effective stimulation parameters that can effectively abort an epileptic seizure, thereby replacing pathological activity by another activity pattern closer to physiological activity.

In theory, the impact of electrical brain stimulation differs depending on the impacted neuronal types, due to several factors such as the electrical field orientation with respect to the somato-dendritic axis of neurons (Komarov et al., 2019). However, for the sake of simplicity, we assume in the following that the considered neuronal populations were equally impacted by the applied electrical stimulation.

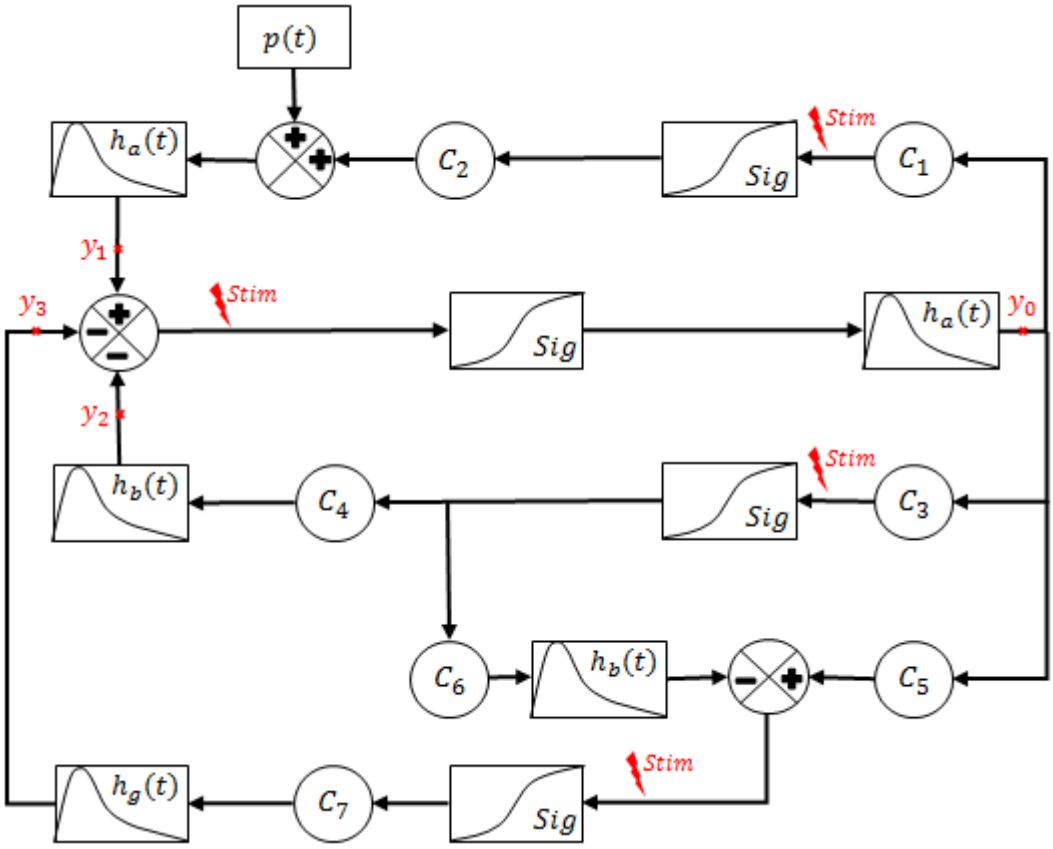

Fig. 3.8. Block diagram of Wendling's neural mass model. The terms $y_i, i \in \{0, \dots, 3\}$ represent post-synaptic potentials of pyramidal cells, excitatory interneurons and both slow and fast inhibitory interneurons, respectively. The h boxes denote the post-synaptic response function of each type, whilst Sig denote the non-linear conversion of the membrane potential into an output firing rate. The constants $C_i, i \in \{1, \dots, 7\}$ account for the strength of the synaptic connections between populations. The red flashes indicate where in the model the stimulation was included.

Wendling's NMM alone is described by 10 first-order differential equations, i.e. two equations for each neural subpopulation. Furthermore, we added two first-order differential equations whose solution consisted in the desired sinusoidal stimulation pattern.

$$
\begin{aligned}
y_0' &= y_6 \\
y_6' &= AaSig(amp{\times}y_5 + X) - 2ay_6 - a^2 y_0 \\
X' &= y_7 - y_8 - y_9 \\
y_7' &= Aa\{p + C_2 Sig(amp{\times}y_5 + C_1 y_0)\} - 2ay_7 - a^2(X + y_2 + y_3) \\
y_2' &= y_8 \\
y_8' &= BbC_4 Sig(amp{\times}y_5 + C_3 y_0) - 2by_8 - b^2 y_2 \\
y_3' &= y_9 \\
y_9' &= GgC_7 Sig(amp{\times}y_5 + C_5 y_0 - y_4) - 2gy_9 - g^2 y_3 \\
y_4' &= y_{10} \\
y_{10}' &= BbC_6 Sig(amp{\times}y_5 + C_3 y_0) - 2by_{10} - b^2 y_4 \\
y_5' &= y_5 + 2\pi{\times}freq{\times}y_{11} - y_5(y_5^2 + y_{11}^2) \\
y_{11}' &= y_{11} - 2\pi{\times}freq{\times}y_5 - y_{11}(y_5^2 + y_{11}^2)
\end{aligned}
\tag{3.1}
$$

This set of differential equations is equivalent to the set presented by Wendling (Wendling et al., 2002b), plus the two differential equations represent electrical stimulation, which were derived by using a simple change of variable. This representation provides direct access to the LFP value presented by the variable X. These equations depend on 14 parameters $(A, a, B, b, \dots)$ plus the stimulation amplitude and frequency, denoted by amp and $freq$, respectively. Regarding the system initial conditions, all were fixed equal to 0, except $y_{11}(0)$ which was equal to the stimulation amplitude. In this set of differential equations, $y_5(t)$ represents the sinusoidal stimulation of a frequency equal to $freq$ and a given amplitude.

Table 2 summarizes the interpretation of model parameters along with their values. By tuning model parameters, these five different types of activity can be simulated (background activity, sporadic spikes, rhythmic spikes, fast onset activity and theta-alpha seizure-like activity). Since we aimed at describing the changes caused by electrical stimulation as seizure starts, we selected model parameters producing rhythmic spikes, as presented in Figure 3.9-a.

For this particular parameter setting (sustained spiking activity), the model can be viewed as a dynamical system composed of coupled oscillators. The solution, presented in Figure 3.9-a, corresponds to a stable periodic orbit repeating itself over

time. This orbit, represented in a two-dimensional manifold, is a limit cycle, as disclosed by the plotting of the phase portrait of the model under the “no stimulation” condition (Figure 3.9-b,c).

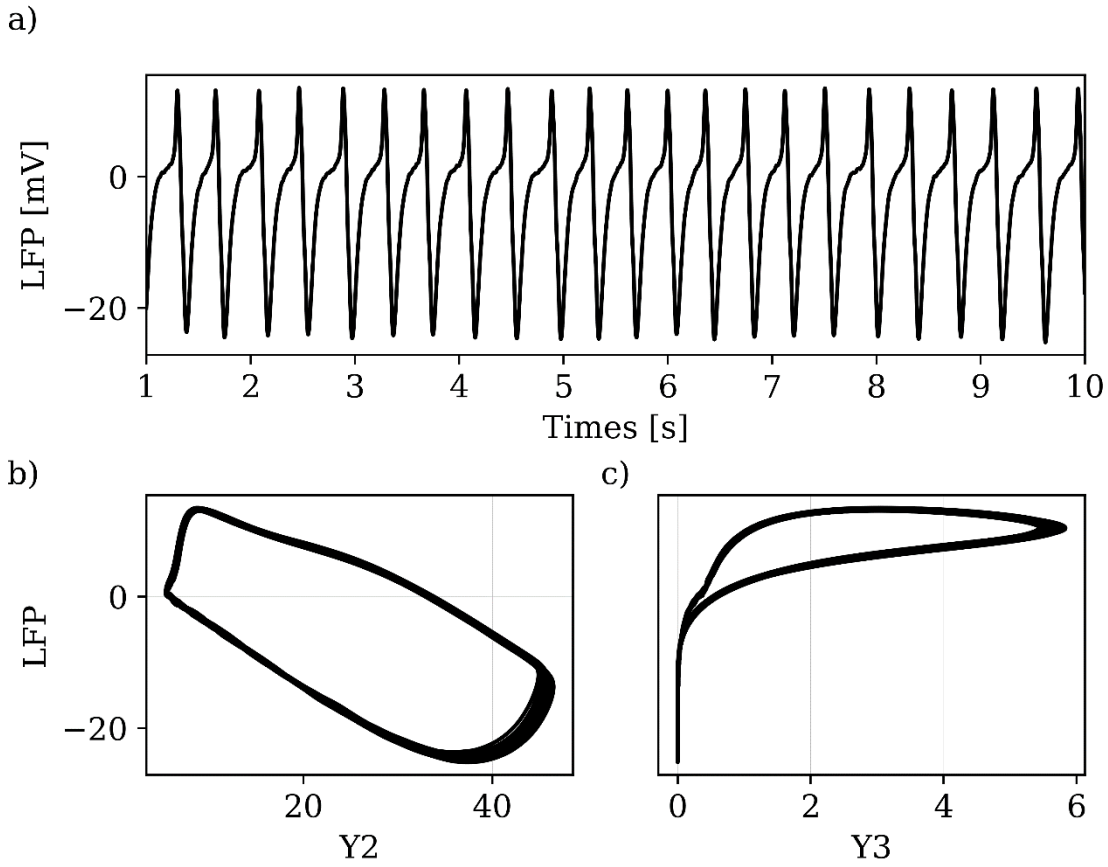

Figure 3.9. a) LFP generated by Wendling’s NMM in the absence of stimulation $(amp, freq) = (0, 0)$. b, c) LFP with respect to slow and fast inhibitory synaptic potentials. This closed solution correspond to a cycle or periodic orbit of (2.6). The excitatory and slow inhibitory synaptic gains were equal to (5.5, 25) mV, respectively. All other parameters were kept equal to values presented in Table 2.

Bifurcation analysis

This section is organized as follows. First, the bifurcation diagram when varying the stimulation amplitude is presented. Second, the bifurcation diagram obtained when varying the stimulation frequency is reported for a fixed amplitude.

Amplitude variation

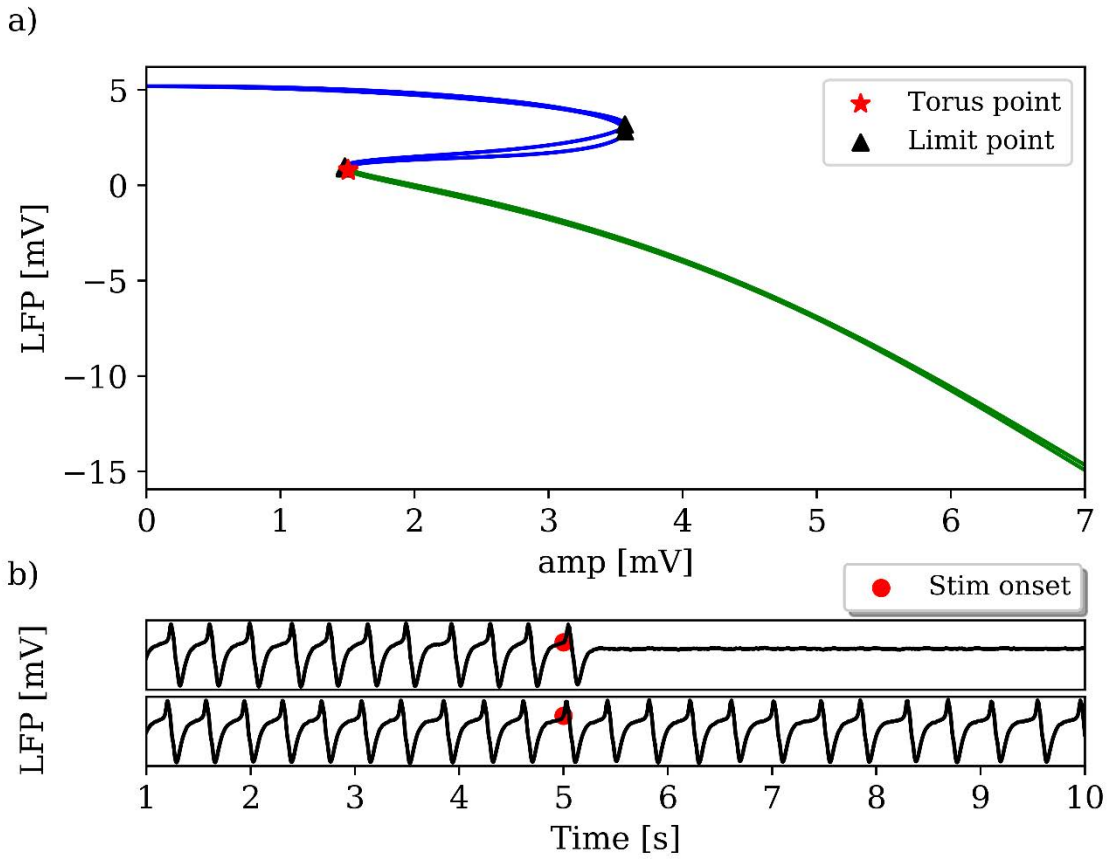

Figure 3.10. a) LFP bifurcation diagram with respect the input amplitude. The green lines correspond to stable limit cycles, while the blue lines represent unstable ones. The red star denotes a Torus bifurcation, and black triangles represent limit points. b) Time series while applying sinusoidal stimulation of a frequency equal to 90 Hz and an amplitude equal to 3 mV and 1 mV, respectively. The stimulation is applied at $t = 5s$.

The bifurcation analysis was started from the periodic orbit when the stimulation amplitude was equal to 7 mV and the frequency equal to 90 Hz. The initial step for bifurcation calculation was chosen equal to -10^{-2}. For $amp = 1{,}479\ mV$, the system undergoes a limit point accompanied by a change of stability, pointing out that two periodic solutions collide and disappear when the amplitude passes this critical value. Another limit point was detected when amp was equal to 3.56 mV, only indicating a turning point of the branch and not involving a change in stability.

Figure 3.10-a illustrates that the system continued to generate rhythmic activity when the stimulation amplitude was changed. For every amp value, we observed a cycle. However, the LFP amplitude differed from the one presented in Figure 3.9-a for the studied system without stimulation. In fact, the rhythmic activity generated without stimulation had an amplitude equal to 37.8 mV, while applying a sinusoidal stimulation of a frequency equal to 90 Hz and an amplitude higher than 1.5 mV reduced this value, as presented in Figure 3.10-b. For instance, applying a sinusoidal stimulation of an amplitude equal to 3 mV and a frequency of 90 Hz resulted in an LFP of amplitude 0.13 mV. Therefore, we can conclude that this specific stimulation suppressed epileptiform activity.

Frequency variation

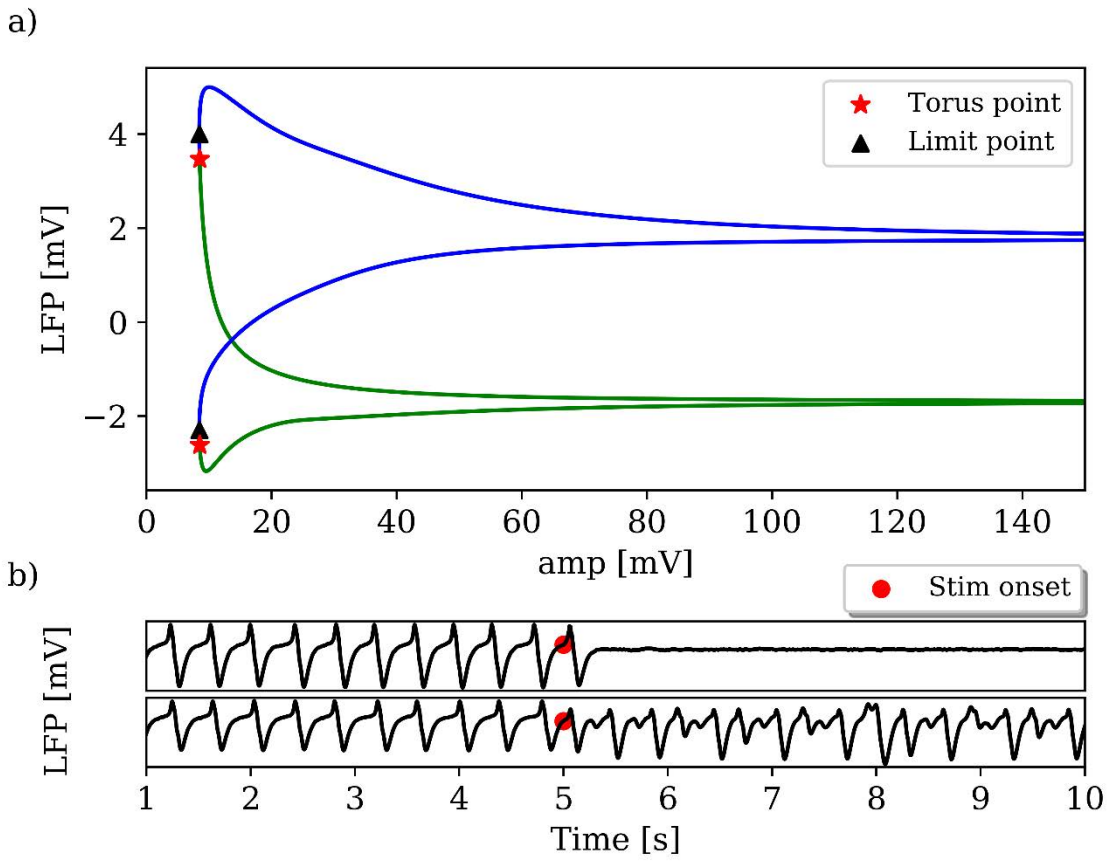

Figure 3.11. a) LFP bifurcation diagram with respect to the input frequency. The green lines correspond to stable limit cycles while the blue lines represent instable ones. The red star denotes a Torus bifurcation and black triangles represent limit points. b) Time

series while applying sinusoidal stimulation of an amplitude equal to 3 mV and a frequency equal to 5 Hz and 90 Hz, respectively. The stimulation is applied at $t = 5\ s$.

The bifurcation diagram presented in Figure 3.11-a shows two types of limit cycles: stable limit cycles (green), and unstable limit cycles (blue). The limit point that separates those two types was detected when the stimulation frequency was equal to 8.45 Hz. We concluded that increasing the stimulation frequency decreases LFP amplitude.

For stimulation frequencies lower than 8.45 Hz, the system generates rhythmic activity of higher amplitude, presumably since the stimulation frequency was close to the system's intrinsic frequency. Therefore, this confirms that stimulation efficacy of stimulation depends both on amplitude and frequency. The optimal (amplitude, frequency) couple able to suppress epileptic activity are in the sub-region of the parameter space where the frequency is higher than 90 Hz, and the amplitude greater than 1.5 mV.

Understanding how the variation of stimulation parameters impacts neuronal dynamics is key for the design of rationale-based stimulation protocol, and providing such bifurcation diagrams for a realistic model of neuronal activity is a step in that direction. These diagrams provided results consistent with previous works related to the identification of effective stimulation parameters capable of aborting epileptic seizures (Beurrier et al., 2001; Filali et al., 2004; Shen et al., 2003). Results also confirmed that the use of high frequencies (over 90 Hz) along with a specific amplitude (2 mV in the model) has the potential to suppress low-frequency epileptiform activity. Future work will validate this prediction *in vivo*.

Finally, our model-guided approach reinforces the rationale for the design of neuromodulation therapies, which classically involves an empirical, sub-optimal "trial-and-error" approach. Using the tools presented here, it appears at reach to design optimal waveforms (frequency, amplitude), that drive a dynamical system (here, a neural mass model) from one attractor (here, a limit cycle corresponding to pathological low-frequency oscillations) onto a fixed point (here, background activity).

3.3 Particular case: weak perturbations

In this section, an explicit mathematical expression of the transfer function relating the input (applied stimulation) to the output (simulated LFP under stimulation) is provided. The motivation for following this approach is the potential to classify effective stimulation parameters by quantifying the stimulation impact on neuronal activity patterns. The major roadblock to derive such transfer function is that neural mass models feature a non-linearity, preventing the analytical derivation of the system's transfer function. Generally, non-linear functions are replaced by linear ones, or a linearization around equilibrium point is performed. In the following, we followed a different approach enabling the derivation of an analytical expression of the transfer function for a non-linear system.

Here, we propose to tackle this issue by using a different mathematical approach inspired from non-commutative rings theory, enabling the identification of a transfer function for a non-linear system. First, the algebraic formalism and the proposed approach that enables the derivation of the transfer function for a non-linear system without the linearization assumption are introduced. Second, the resulting function is validated by comparing with numerical simulations of the model. These results provide further understanding of frequency-dependent effects of the applied stimulation and resonance phenomena.

The response of a system to a specific stimulation is in general possible through the transfer function, which is a compact description of the input/output relationship. The transfer function is a powerful method for dealing with complex systems, since it provides knowledge of the system's response for any input signal, and on resonance frequencies where the response amplitude is a relative maximum. The identification of such resonance frequencies is especially relevant to ends of therapy. In the case of linear systems, the Laplace transform can be used to compute the transfer function. For instance, it is used in the design controllers to switch between different types of system representations; mainly between a state-space representation and an input-output description. However, the system of differential equations governing a simple neural mass model, namely the Jansen-Rit model, involves non-linear functions.

Therefore, the use of the Laplace transform is not possible, since associativity is not valid. To explain this further, let us consider two simple non-linear systems:

$$\begin{aligned} y_1 &= g_1(u_1) \\ y_2 &= g_2(u_2) \end{aligned} \tag{3.1}$$

where $u_1, u_2, y_1, y_2 \in \mathbb{R}$ represent the inputs and outputs, respectively, and g_1, g_2 are differentiable functions from $\mathbb{R}$ to $\mathbb{R}$. The system output depends on the order in which these systems are combined together. For instance, the system $y = g_2\big(g_1(u)\big)$ is not equivalent to the system $y = g_1\big(g_2(u)\big)$. To tackle this issue, differentiating is used, since the derivative of a composite function is simply a product of derivatives of its components. However, this requires an appropriate algebraic framework, which is presented below.

In the following, the algebraic point of view in non-linear control systems and methods of pseudo-linear algebra are presented. For more technical constructions and further details, the reader can refer to (Conte et al., 1999).

Meromorphic functions and differential forms

Our aforementioned non-linear dynamic system (2.5) can be written under the following form:

$$\begin{aligned} \dot{Y} &= f(Y, Stim) \\ X &= g(Y, Stim) \end{aligned} \tag{3.2}$$

where $Y \in R^n$, $Stim \in R^m$ and $X \in R^p$ denote the state vector, input and output of the system, respectively. Moreover, f and g are meromorphic functions, which are elements of the quotient field of the ring of holomorphic functions. This dynamic system is called control system or non-linear control system, to stress the fact that f and g are non-linear. Let K denote the field of meromorphic functions of Y and $Stim$. Therefore, the system (3.2) belongs to K. A derivative operator δ acting on K is defined as follows:

$$\delta Y_i = \dot{Y}_i = f_i(Y, Stim)$$
$$\delta f(Y, Stim) = \sum_{i=1}^{n} \frac{\partial f}{\partial Y_i} \delta Y_i + \sum_{j=1}^{m} \frac{\partial f}{\partial Stim_j} \delta Stim_j \qquad \forall i \in \{1, \dots, n\} \tag{3.3}$$

To handle the theoretical properties of the non-linear system (3.2), we define a vector space spanned over K by differentials of elements of K, namely:

$$\varepsilon = span_{\mathcal{K}}\{d\xi;\ \xi \in \mathcal{K}\} \tag{3.4}$$

Elements of ε are called one-forms, or more generally differential forms. Any element in ε is a vector of the form:

$$\omega = \sum_i \alpha_i\, d\xi_i \tag{3.5}$$

where all $\alpha_i \in K$. We define a differential operator, denoted by d, from K to ε, as:

$$d: \mathcal{K} \longrightarrow \varepsilon\ ; df = \sum_{i=1}^{n} \frac{\partial f}{\partial Y_i} dY_i + \sum_{j=1}^{m} \frac{\partial f}{\partial Stim_j} dStim_j \tag{3.6}$$

Thus, df is usually referred to the differential of f. Finally, the vector space ε can be endowed with a differential structure by defining a derivative operator:

$$\delta\omega = \dot{\omega} = \sum_i [\delta(\alpha_i) d\xi_i + \alpha_i d(\delta\xi_i)] \tag{3.7}$$

This algebraic point of view enables treating non-linear control problems of the form (3.2). However, we still need to introduce some algebraic objects to ensure analytical computation of a non-linear transfer function.

Pseudo-derivations, skew polynomials and pseudo-linear operators

In this section, we present skew polynomials, which act as differential operators on the vector space ε. Quotients of such polynomials can be considered as the transfer function of the considered non-linear system. This function completely characterizes non-linear dynamics of a given system at any operating point, which prevents approximations such as linearizing around a fixed operating point. For more theoretical

details, the reader is referred to (Bronstein and Petkovšek, 1996; Halás et al., 2008; Zheng et al., 2001). In the following, all fields are commutative and all rings are non-commutative.

1) **Pseudo derivation**. Let $\mathcal{K}$ be a field and $\sigma: \mathcal{K} \longrightarrow \mathcal{K}$ an injective endomorphism, it satisfies:

$$\begin{aligned} \sigma(a+b) &= \sigma(a) + \sigma(b) \\ \sigma(ab) &= \sigma(a)\sigma(b) \qquad \forall a, b \in \mathcal{K} \end{aligned} \tag{3.8}$$

A map $\delta: \mathcal{K} \longrightarrow \mathcal{K}$ which satisfies:

$$\begin{aligned} \delta(a+b) &= \delta(a) + \delta(b) \\ \delta(ab) &= \sigma(a)\delta(b) + \delta(a)b \end{aligned} \tag{3.9}$$

is called a pseudo-derivation.

2) **Skew polynomials.** The left skew polynomial ring given by σ, and δ is the ring $(\mathcal{K}[x]; +, .)$ of polynomials in the indeterminate x over $\mathcal{K}$ with the usual addition, and the non-commutative multiplication given by the commutation rule:

$$xa = \sigma(a)x + \delta(a) \ , \forall a \in \mathcal{K} \tag{3.10}$$

We denote the left skew polynomial ring $\mathcal{K}[x; \sigma, \delta]$. Elements of this ring are called skew polynomials, or non-commutative polynomials.

3) **Pseudo-linear operators.** Let $\mathcal{V}$ be a vector space over $\mathcal{K}$. A map $\theta: \mathcal{V} \longrightarrow \mathcal{V}$ is called pseudo-linear if:

$$\begin{aligned} \theta(u+v) &= \theta(u) + \theta(v) \\ \theta(au) &= \sigma(a)\theta(u) + \delta(a)u \\ \forall a \in \mathcal{K}, \forall u, v \in \mathcal{V} \end{aligned} \tag{3.11}$$

If $\sigma = 1$, then (3.11) is similar to a derivation on $\mathcal{V}$. Skew polynomials can act on the vector space $\mathcal{V}$ and thus represent operators. Any pseudo-linear map $\theta: \mathcal{V} \longrightarrow \mathcal{V}$ induces an action:

$$.: \mathcal{K}[x;\sigma,\delta]\times\mathcal{V} \longrightarrow \mathcal{V};\ \left(\sum_{i=0}^{n} a_i x^i\right).u = \sum_{i=0}^{n} a_i \theta^i(u) \qquad \forall u \in \mathcal{V} \qquad (3.12)$$

Quotients of skew polynomials

One of the most important properties of the left skew polynomial ring $\mathcal{K}[x;\sigma,\delta]$ is the non-containment of zero divisors. Such property is used in the following section to compute the inverse of a matrix and determine the transfer function, and is summarized in the following condition.

Ore condition. For all non-zero $a, b \in \mathcal{K}[x;\sigma,\delta]$, there exists a non-zero $c, d \in \mathcal{K}[x;\sigma,\delta]$ such that

$$cb = da \qquad (3.13)$$

In other words, each two elements of $\mathcal{K}[x;\sigma,\delta]$ have a common left multiple. $\mathcal{K}[x;\sigma,\delta]$ can thus be embedded into a non-commutative quotient field by defining quotients as

$$\frac{a}{b} = b^{-1}.a \qquad \forall a, b \in \mathcal{K}[x;\sigma,\delta], b \neq 0 \qquad (3.14)$$

We denote the quotient field of skew polynomials by $\mathcal{K} < x;\ \sigma,\delta >$. In the following, the transfer function of a non-linear system will be written as a fraction of two skew polynomials.

Calculation of the Jansen and Rit model transfer function

Using the pseudo-linear algebra presented above, the transfer function of the Jansen and Rit model can be computed. The non-linear system **(3.1)** can be written as follows:

$$\dot{Y} = \begin{pmatrix} \dot{y}_0(t) \\ \dot{y}_1(t) \\ \dot{y}_2(t) \\ \dot{y}_3(t) \\ \dot{y}_4(t) \\ \dot{y}_5(t) \end{pmatrix} = f(Y, Stim) = \begin{pmatrix} y_3(t) \\ y_4(t) \\ y_5(t) \\ AaSig\big(Stim(t)\big) - 2ay_3(t) - a^2 y_0(t) \\ AaC_2 Sig\big(C_1 y_0(t)\big) - 2ay_4(t) - a^2 y_1(t) \\ BbC_4 Sig\big(C_3 y_0(t)\big) - 2by_5(t) - b^2 y_2(t) \end{pmatrix} \tag{3.15}$$

$$X = g(Y, Stim) = (0 \quad 1 \quad -1 \quad 0 \quad 0 \quad 0) \begin{pmatrix} y_0(t) \\ y_1(t) \\ y_2(t) \\ y_3(t) \\ y_4(t) \\ y_5(t) \end{pmatrix}$$

where X is the system output, and is equal to the difference between the post-synaptic potential at the level of pyramidal cells. We differentiate (17) and apply the following Lemma:

For any $f \in \mathcal{K}$,

$$\delta(df) = d(\delta f) \tag{3.16}$$

Proof: using equation (3.7), we obtain

$$\begin{aligned} \delta(df) &= \delta\left(\sum_{i=1}^{n} \frac{\partial f}{\partial \xi_i} d\xi_i\right) = \sum_{i=1}^{n} \delta\left(\frac{\partial f}{\partial \xi_i}\right) d\xi_i + \sum_{i=1}^{n} \frac{\partial f}{\partial \xi_i} d(\delta \xi_i) \\ &= \sum_{i,j=1}^{n} \frac{\partial^2 f}{\partial \xi_j \partial \xi_i} \delta\xi_j d\xi_i + \sum_{i=1}^{n} \frac{\partial f}{\partial \xi_i} d(\delta \xi_i) \end{aligned} \tag{3.17}$$

$$\begin{aligned} d(\delta f) &= d\left(\sum_{i=1}^{n} \frac{\partial f}{\partial \xi_i} \delta\xi_i\right) = \sum_{i=1}^{n} d\left(\frac{\partial f}{\partial \xi_i}\right) \delta\xi_i + \sum_{i=1}^{n} \frac{\partial f}{\partial \xi_i} d(\delta \xi_i) \\ &= \sum_{i,j=1}^{n} \frac{\partial^2 f}{\partial \xi_j \partial \xi_i} d\xi_j \delta\xi_i + \sum_{i=1}^{n} \frac{\partial f}{\partial \xi_i} d(\delta \xi_i) \end{aligned} \tag{3.18}$$

After considering the fact that for any $f \in \mathcal{K}$, $\partial^2 f/\partial\xi_j\partial\xi_i = \partial^2 f/\partial\xi_i\partial\xi_j$ we obtain $\delta(df) = d(\delta f)$. As a result of (3.16), a state representation (3.15) can be written after differentiating as follows:

$$\begin{aligned} d\dot{Y} &= AdY + BdStim \\ dX &= CdY \end{aligned} \tag{3.19}$$

where:

$$A = \frac{\partial f}{\partial Y} = \begin{pmatrix} 0 & 0 & 0 & 1 & 0 & 0 \\ 0 & 0 & 0 & 0 & 1 & 0 \\ 0 & 0 & 0 & 0 & 0 & 1 \\ -a^2 & 0 & 0 & -2a & 0 & 0 \\ AaC_2C_1Sig'\big(C_1y_0(t)\big) & -a^2 & 0 & 0 & -2a & 0 \\ BbC_4C_3Sig'\big(C_3y_0(t)\big) & 0 & -b^2 & 0 & 0 & -2b \end{pmatrix}$$

$$B = \frac{\partial f}{\partial Stim} = \begin{pmatrix} 0 \\ 0 \\ 0 \\ AaSig'(Stim) \\ 0 \\ 0 \end{pmatrix} \tag{3.20}$$

$$C = \frac{\partial g}{\partial Y} = \begin{pmatrix} 0 \\ 1 \\ -1 \\ 0 \\ 0 \\ 0 \end{pmatrix}$$

In light of the above, we notice that the derivative operator δ acting on $\mathcal{K}$ (3.3) is a pseudo-derivation (3.9) with respect to $\sigma = 1_{\mathcal{K}}$. Therefore, the derivative operator acting on ε (3.7) is a pseudo-linear map (3.11), with respect to $\sigma = 1_{\mathcal{K}}$ also. This leads to the following action:

$$.: \mathcal{K}[x; 1_{\mathcal{K}}, \delta] \times \varepsilon \longrightarrow \varepsilon;\ \left(\sum_{i=0}^{n} a_i s^i\right).u = \sum_{i=0}^{n} a_i \delta^i(u) \tag{3.21}$$

Moreover, the commutation rule (3.10) is transformed into $sf = fs + \dot{f}$ on $\mathcal{K}[x; 1_{\mathcal{K}}, \delta]$.

Thus, the polynomials may not only act on one-forms, but it is also possible to extract from one-forms corresponding polynomials. For instance, a one-form $d\dot{y}$ can be written as sdy.

By using (3.21), we obtain:

$$\begin{aligned}(sI_6 - A)dY &= BdStim \\ dX &= CdY\end{aligned} \tag{3.22}$$

where I_6 is the identity matrix. Consequently, $dX = C(sI_6 - A)^{-1}BdStim$. As a result, the transfer function of our system is:

$$F(s) = C(sI_6 - A)^{-1}B \tag{3.23}$$

To compute the transfer function (25), we have to compute the left-hand inverse of the matrix $(sI_6 - A)$, which is not trivial since multiplication is not commutative and the entries of our matrix are skew polynomials. In order to solve linear equations in non-commutative fields, the Ore condition (Ore, 1933) is used. It guarantees that each two elements of the skew polynomial ring $\mathcal{K}[s; \sigma, \delta]$ have a common left multiple. Let's denote $(sI_6 - A)^{-1}$ as follows:

$$(sI_6 - A)^{-1} = \begin{pmatrix} \boldsymbol{a_{11}} & \cdots & \boldsymbol{a_{16}} \\ \vdots & \ddots & \vdots \\ \boldsymbol{a_{61}} & \cdots & \boldsymbol{a_{66}} \end{pmatrix} \tag{3.24}$$

By considering the values of vectors B and C, the transfer function is related to identifying the terms a_{24} and a_{34}. We first decompose $(sI_6 - A)$ into four blocks:

$$(sI_6 - A) = \begin{pmatrix} A_{11} & A_{12} \\ A_{21} & A_{22} \end{pmatrix} \tag{3.25}$$

Due to the Ore condition, matrices C_{11},C_{12}, C_{21} and C_{22} of appropriate dimensions could be found such that $C_{22}A_{12} = C_{12}A_{22}$ and $C_{21}A_{11} = C_{11}A_{21}$. Then,

$$(sI_6 - A)^{-1} = \begin{pmatrix} (C_{22}A_{11} - C_{12}A_{21})^{-1}C_{22} & -(C_{22}A_{11} - C_{12}A_{21})^{-1}C_{12} \\ -(C_{11}A_{22} - C_{21}A_{12})^{-1}C_{21} & (C_{11}A_{22} - C_{21}A_{12})^{-1}C_{11} \end{pmatrix} \tag{3.26}$$

represents the left-hand inverse. Since we are interested in terms a_{24} and a_{34}, we only need to compute the matrix $-(C_{22}A_{11} - C_{12}A_{21})^{-1}C_{12}$. By using the Ore condition, we obtain:

$$-(C_{22}A_{11} - C_{12}A_{21})^{-1}C_{12} = \begin{pmatrix} \frac{1}{(s+a)^2} & 0 & 0 \\ \frac{AaC_1C_2Sig'(C_1y_0(t))}{(s+a)^4} & \frac{1}{(s+a)^2} & 0 \\ \frac{BbC_3C_4Sig'(C_3y_0(t))}{(s+a)^2(s+b)^2} & 0 & \frac{1}{(s+b)^2} \end{pmatrix} \quad (3.27)$$

Hence, the transfer function of non-linear system (3.15) is equal to:

$$F(s) = \left(\frac{AaC_1C_2Sig'(C_1y_0)}{(s+a)^4} - \frac{BbC_3C_4Sig'(C_3y_0)}{(s+a)^2(s+b)^2}\right) \times AaSig'(Stim) \quad (3.28)$$

Let us mention that this analytical expression of the transfer function features the variable $y_0(t)$, corresponding to the output firing rate of the pyramidal population, and also the applied stimulation $Stim(t)$. Therefore, this implies that the obtained transfer function is time-dependent, i.e., for each frequency, equation (3.28) is a function of time, which is challenge since this implies a numerical resolution that we aimed at avoiding by the use of an analytical transfer function.

In order to overcome this difficulty, we approximated the function mean value within the frequency response. For instance, we assumed that the mean value of y_0 is small and close to zero, and changes slightly while varying the frequency. More precisely, at low frequencies, the mean value of the postsynaptic potential of pyramidal cells y_0 fluctuates slightly around a given value, noted here by $\overline{y_0}$, before converging towards it while increasing the frequency.

Using this approximation, equation (3.28) becomes independent of y_0 variations, and becomes

$$\tilde{F}(s) = \left(\frac{AaC_1C_2Sig'(C_1\overline{y_0})}{(s+a)^4} - \frac{BbC_3C_4Sig'(C_3\overline{y_0})}{(s+a)^2(s+b)^2}\right) \times AaSig'(Stim) \quad (3.29)$$

In Figure 3.12 below, we present the frequency responses obtained either by using equation (3.28), or just by simply approximating y_0 as its mean value when the stimulation frequency is equal to $100\ Hz$.

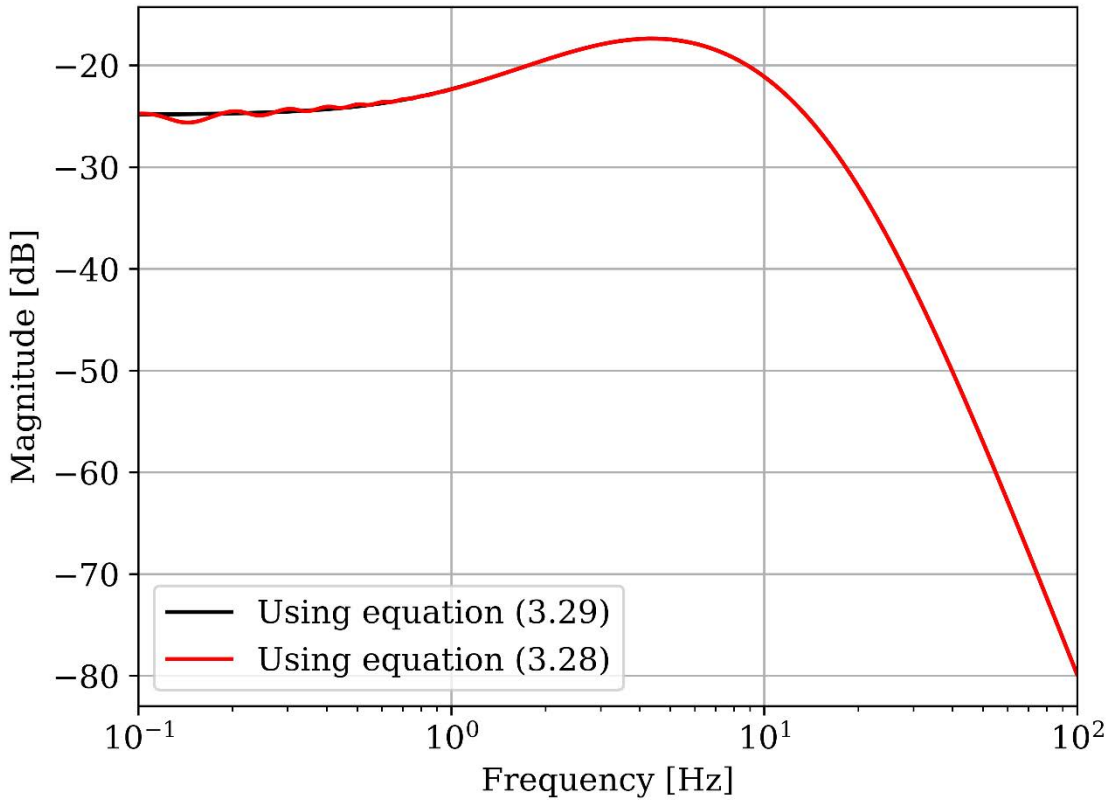

Figure 3.12. Frequency responses calculated using either equation (3.28) or equation (3.29). For the first equation, the mean value of postsynaptic potential of pyramidal cells y_0 for each frequency was computed. However, for equation (3.29), only the mean value of y_0 for stimulation frequency equal to 100 Hz is required.

To verify the validity of the aforementioned analytical transfer function, we compared it to the transfer function computed numerically. Indeed, system (2.5) provides the necessary information to compute the numerical transfer function. For several stimulation frequencies, and by keeping the parameters values used originally by Jansen and Rit, the set of non-linear differential equations was solved. For these LFPs, the numerical frequency response was extracted:

$$NTF = 20log_{10}(V_s/V_e) \tag{3.30}$$

where $V_s = \frac{\max(LFP) - \min(LFP)}{2}$, and $V_e = 1$ since the stimulation amplitude is equal to 1mV.

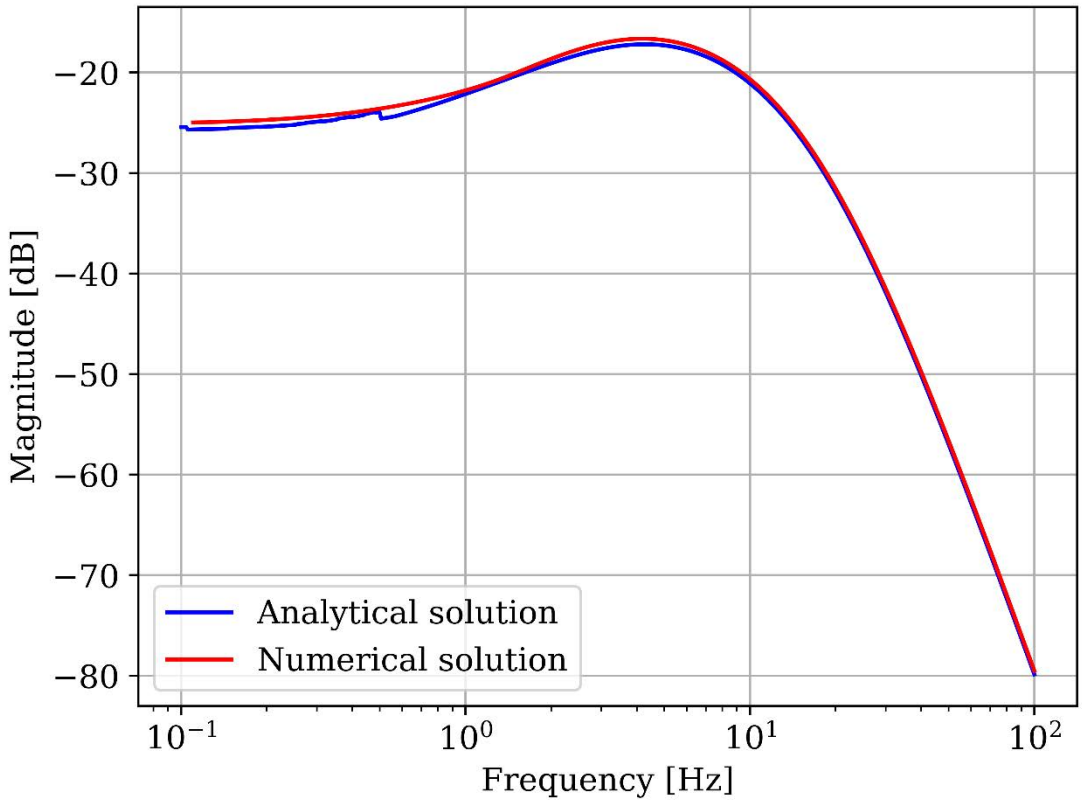

Figure 3.13. Comparison of analytical and numerical transfer functions. The blue curve represents the frequency response obtained from equation (3.29), while the red curve represents the frequency response obtained numerically. For each frequency, we computed the output of the system (LFP), the numerical frequency response being described by equation (3.30).

The comparison between the analytical and numerical solutions presented in Figure 3.13 illustrates the effectiveness of our analytical transfer function calculated by using non-commutative field theory. The curves are extremely similar up to $100\ Hz$, even if minor differences are present due to the solving method used for simulations and the simplifications suggested to remove the time-dependency. However, the resonance frequency is identical for both, which is one of the major characteristics provided by the non-linear transfer function.

This analytical expression, linking an external electrical stimulation to neural activity, illustrate how model parameters impact the characteristics of the local field potential. Moreover, it gives insights into the subset of parameters that control the level of excitability. Second, using this expression resulted in a considerably lower computation time. For example, for a frequency vector composed of 500 points, 48 seconds were required to calculate all frequency responses, while our approximation led to a computation time of less than 3 seconds (factor 16).

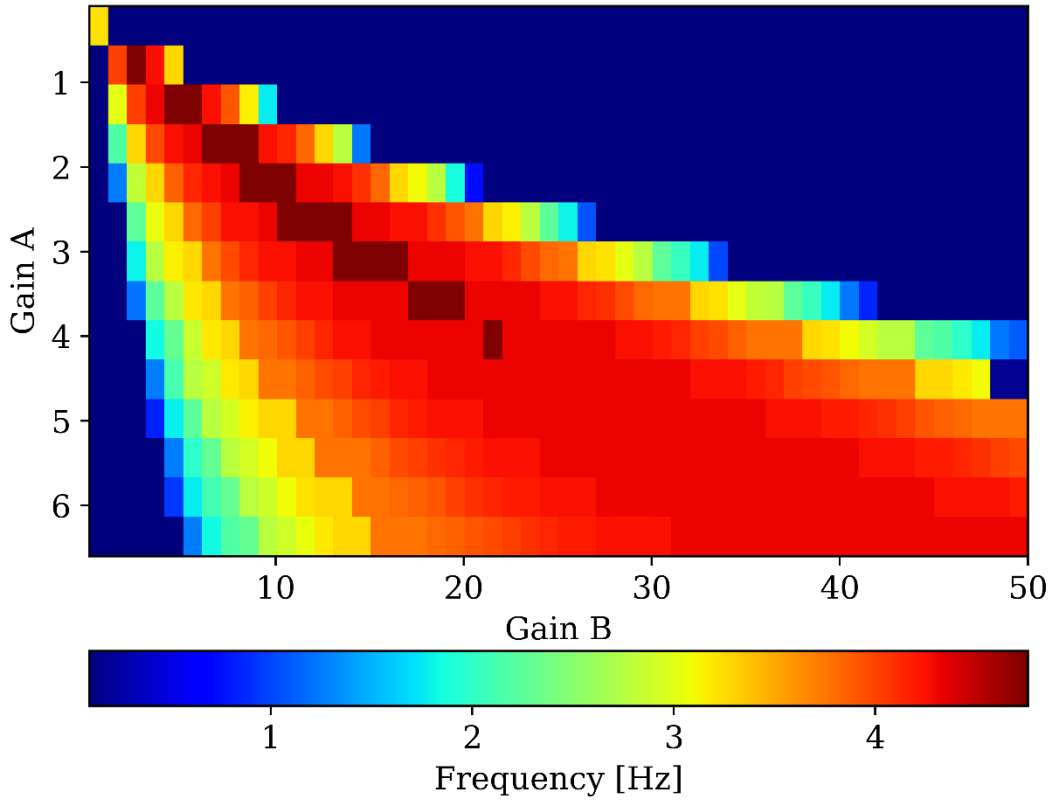

Figure 3.14. Resonance frequencies for different gain values. The excitatory synaptic gain $A \in [0.1, 7]$ mV and the inhibitory synaptic gain $B \in [0.1, 50]$ mV.

First, the highest frequencies are located along a line corresponding to a specific excitability ratio A/B and evolve smoothly. Second, when this ratio decreases or increases, the resonance frequency decreases or vanishes. More specifically, the blue regions represent the frequency responses diagrams with a starting magnitude approximately equal to the maximum value. In such cases, a change in stimulation frequency does not alter the system's dynamics.

As aforementioned, the resonance frequency could have a greater impact on neural activity, since it favors the generation of high amplitude oscillations. Therefore, if the objective is to replace epileptiform activity by a more “physiological” activity, it is then reasonable to avoid the use of this frequency as a stimulation frequency. We evaluate the validity of this hypothesis below. Previously, we computed the frequency response for different excitatory and inhibitory synaptic gains, which are associated with distinct neural dynamics. For instance, if the excitatory synaptic gain A is equal to $4\ mV$ and the inhibitory synaptic gain B is equal to $28\ mV$, the gain diagram presented in Figure 3.15 is obtained.

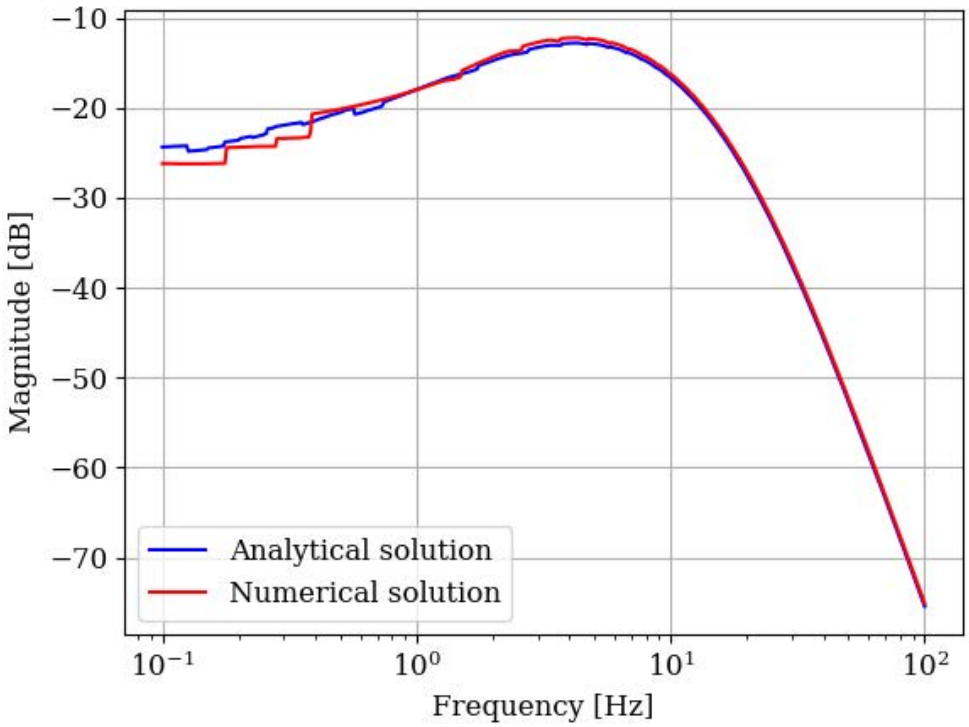

Figure 3.15. Analytically- and numerically-derived transfer function. Here, the excitatory synaptic gain is equal to 4 mV and the inhibitory synaptic gain B is equal to 28 mV.

First, there is a good agreement between the analytical and numerical frequency responses, and the analytical transfer function remains valid for a wide range of synaptic gain values. Furthermore, the maximal magnitude is reached for a frequency of approximately 5 Hz, which can be considered as the resonance frequency. Then, using the parameters from Table 1, we changed the stimulation frequency only.

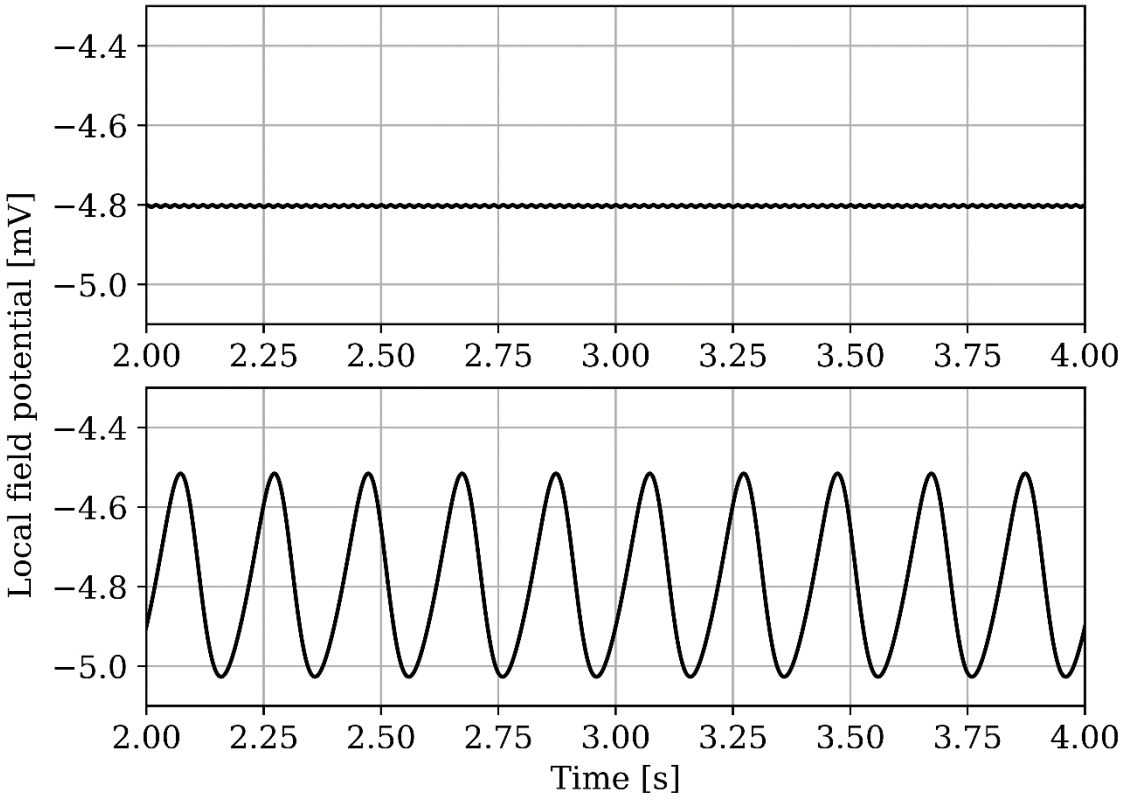

Figure 3.16. Simulated LFP generated with the model (3.15) during 50 Hz (upper panel) and 5 Hz (lower panel) stimulation. The simulated LFP represents the summed average post-synaptic potentials on pyramidal cells. The LFP during 5 Hz stimulation is drastically different than for 50 Hz stimulation, with significantly higher-amplitude oscillations induced at the stimulation frequency.

The results presented in Figure 3.16 demonstrate that the amplitude of LFP oscillations induced by stimulation are drastically different depending on the stimulation frequency. By choosing a stimulation frequency close to the resonance frequency, it is possible to alter LFP dynamics and induce oscillations, highlighting the key role of the stimulation frequency. For example, if the objective is to abort epileptic seizures, which involve low-frequency activity during the beginning of the seizure itself (< 10 Hz), it is first required to determine the appropriate stimulation parameters that could reverse/abort pathological dynamics and not exacerbating those.

Here, we provided an analytical expression of the transfer function for a non-linear system, namely the Jansen and Rit neural mass model. The motivation for this work is the generic nature of this model, which is widely used in neuroscience and can

be used as a basis for large-scale models of brain activity. Furthermore, neural mass models have the advantage to provide signals that are directly comparable with experimental LFPs. Therefore, the perspective of identifying transfer functions avoiding inappropriate stimulation parameters and estimating optimal ones to alter neural dynamics in a predetermined way is especially appealing. This would indeed save a considerable computation time as compared to running an extensive number of numerical simulations.

Since the system described by equations (3.15) involves non-linear asymmetric functions, we first attempted at replacing them by linear ones. We proceeded to a linearization around a special point v_0 describing the PSP for which a 50 % firing rate is achieved. The resulting system was an approximation of the original system for which it was much simpler to compute the transfer function through the Laplace transform. This procedure has been followed earlier to design a closed-loop proportional-integral controller for the Jansen and Rit neural mass model (Wang et al., 2016). Although it provides an approximation of the system dynamics, the frequency responses were unreliable due to the loss of linearity, and were different from those obtained numerically.

Over the last decades, mathematicians developed sophisticated theories to develop further non-linear approaches. Here, we applied the theory of non-commutative rings to overcome the non-associativity problem accompanying non-linear systems, which impedes the determination of an analytical expression linking the system input to its output. Hence, following this method, we provided a unique description of the stimulation/LFP relationship for the non-linear Jansen and Rit neural mass model, which is not achievable using conventional methods. However, this approach has some limitations. In addition to the difficulty of calculating the left-hand inverse of a matrix $(sI_n - A), n \in \mathbb{N}$, due to both the non-commutative multiplication and the dimension of our system, it should also be stressed that the analytical expression of the transfer function may contain a state space variable (which is our case) as opposed to linear systems.

In conclusion, we presented a method solving the non-associativity problem, and computed the transfer function of the Jansen and Rit model without any linearization of the system. This analytical expression was used to study the frequency

response. In addition to determining the range of optimal frequencies able to alter neural dynamics as measured using the LFP, it indicates which frequencies to avoid (resonant frequencies). In terms of future work, one possibility would be to derive the transfer function of a coupled Jansen and Rit neural mass model, paving the way to study and optimize the stimulation of large-scale neural networks involving a generator of epileptic activity. Since we derived an analytical expression involving frequency, this would provide a better control of the high-dimensional system. The extension of this work to more biologically comprehensive neural mass models could also provide a unique view on the mechanisms of physiological and pathophysiological activity in realistic large-scale networks.

Closed-loop Jansen and Rit model:

Below, we extracted an analytical transfer function for the open-loop Jansen and Rit model. Here, we use the same method to extract the transfer function for a closed loop Jansen and Rit model receiving an external electrical stimulation at the level of pyramidal cells. This system depends on the past in contrast the previous one, which challenges the derivation of an analytical expression of its transfer function.

$$\dot{Y} = \begin{pmatrix} \dot{y}_0(t) \\ \dot{y}_1(t) \\ \dot{y}_2(t) \\ \dot{y}_3(t) \\ \dot{y}_4(t) \\ \dot{y}_5(t) \end{pmatrix} = f(Y, Stim)$$

$$\dot{Y} = \begin{pmatrix} y_3(t) \\ y_4(t) \\ y_5(t) \\ AaSig(Stim(t) + y_1(t) - y_2(t)) - 2ay_3(t) - a^2 y_0(t) \\ AaC_2 Sig\big(C_1 y_0(t)\big) - 2ay_4(t) - a^2 y_1(t) \\ BbC_4 Sig\big(C_3 y_0(t)\big) - 2by_5(t) - b^2 y_2(t) \end{pmatrix} \tag{3.31}$$

$$X = g(Y, Stim) = (0 \quad 1 \quad -1 \quad 0 \quad 0 \quad 0) \begin{pmatrix} y_0(t) \\ y_1(t) \\ y_2(t) \\ y_3(t) \\ y_4(t) \\ y_5(t) \end{pmatrix}$$

The model can be represented as follows:

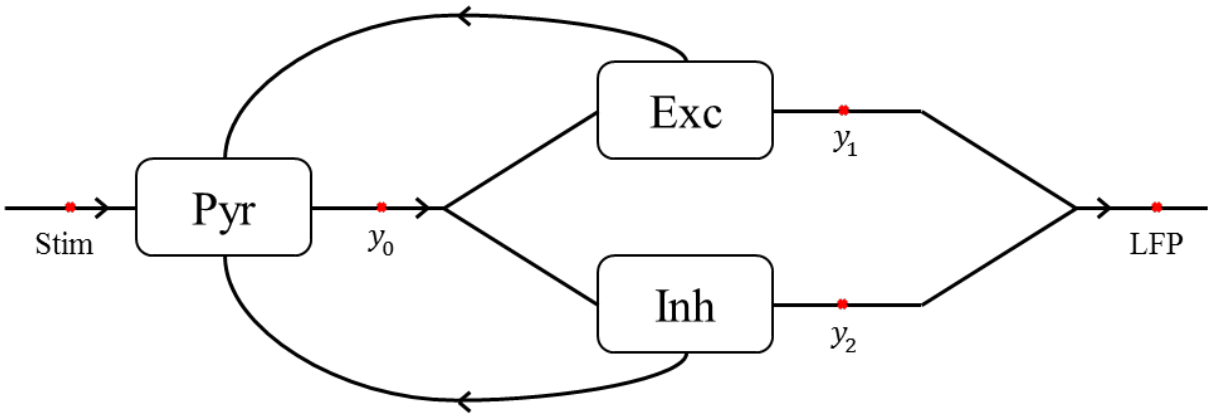

Instead of studying the whole system, we decomposed it into several connected transfer functions representing each neuronal subpopulation:

$$\begin{aligned} dLFP &= dy_1 - dy_2 \\ dLFP &= Exc\ dy_0 - Inh\ dy_0 \\ dLFP &= Exc\ Pyr\ dStim + Exc\ Pyr\ dy_1 - Exc\ Pyr\ dy_2 \\ &\quad - Inh\ Pyr\ dStim - Inh\ Pyr\ dy_1 + Inh\ Pyr\ dy_2 \end{aligned} \tag{3.32}$$

$$dLFP = \frac{Exc\ Pyr - Inh\ Pyr}{1 - Exc\ Pyr + Inh\ Pyr} dStim$$

Exc, Pyr and Inh represent transfer function for pyramidal cells, excitatory and inhibitory interneurons and are equal to:

$$Exc = \frac{AaC_1C_2}{(s+a)^2} Sig'(C_1 y_0)$$

$$Inh = \frac{BbC_3C_4}{(s+b)^2} Sig'(C_3 y_0)$$

$$Pyr = \frac{Aa}{(s+a)^2} Sig'(Stim + y_1 - y_2)$$

Therefore, we obtain the following transfer function for the closed-loop Jansen and Rit model:

$$TF(s) = \frac{\left(\frac{AaC_1C_2Sig'(C_1y_0)}{(s+a)^4} - \frac{BbC_3C_4Sig'(C_3y_0)}{(s+b)^2(s+a)^2}\right) AaSig'(Stim + y_1 - y_2)}{1 - \left(\frac{AaC_1C_2Sig'(C_1y_0)}{(s+a)^4} - \frac{BbC_3C_4Sig'(C_3y_0)}{(s+b)^2(s+a)^2}\right) AaSig'(Stim + y_1 - y_2)}$$

(3.33)

As presented above, this technique led to an analytical expression linking the input (electrical stimulation) to the model response represented by the LFP. It should be noted that even the transfer function of coupled models is possible using this approach (already calculated but not presented here). However, the use this expression remains limited since it depends on state variables such as the post-synaptic potential of excitatory and inhibitory interneurons (y_1, y_2). Therefore, an approximation of this system is needed to envision further developments and applications.

3.4 Perturbed condition: dynamics of a local neuronal region receiving afferents from another region

In this section, we investigate the impact on dynamics caused by incoming afferents from another region as a perturbation, instead of an applied electrical stimulation. We consider two unidirectionally coupled WNMMs, each representing a neuronal region (region 1 and region 2), given in eq. (2.12). Then, we investigate how epileptogenic discharges spread from one region to the other showing a healthy activity. In particular, we consider projections from pyramidal cells of the first region to (i) pyramidal cells, (ii) slow GABAergic interneurons, and (iii) fast GABAergic interneurons of the second region.

Parameter values of both regions are equal to those presented in Table 2, except excitatory and slow inhibitory synaptic gain of regions 1; $(A, B) = (5.5, 25)$ mV.

3.4.1 Variation of connectivity strength between the pyramidal cells of two neuronal regions

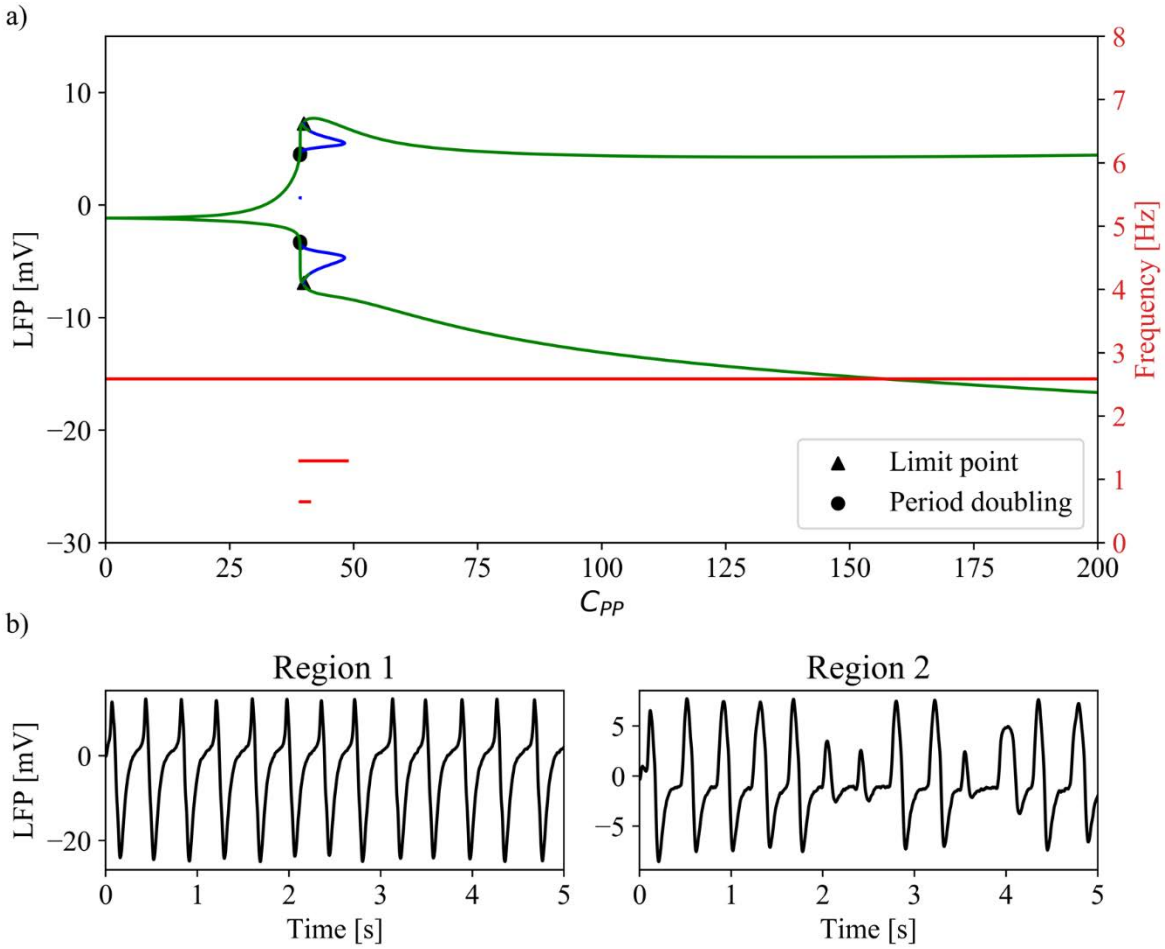

Figure 3.17. a) LFP of region 2 as function of C_{PP} and the frequency of periodic oscillations. b) LFPs of the both regions when $C_{PP} = 40$. The green and blue curves represent stable and unstable limit cycles, respectively. Red curves represent the frequency of limit cycles.

In the absence of synaptic interaction between the pyramidal cells of the two regions, region 2 generates background activity. As the coupling strength C_{PP} increases, region 1 modulates the activity of region 2. The latter begins to generate periodic oscillations at a frequency equal to those generated by the region 1. The amplitude of the LFP signal slightly increases until $C_{PP} \approx 39.15$, where we observe a sharp increase from 5 mV to 15 mV. The system undergoes a period doubling (PD) bifurcation around $C_{PP} \approx 39.15$ again that is followed by a cascade of PD bifurcations.

The right axis of Figure 3.17-a shows the frequency of periodic oscillations. For $C_{PP} \in [39.15, 50]$, the LFP is a mix of rhythmic activities of different amplitudes, as presented in Figure 3.17-b.

As C_{PP} continues to increase, the LFP amplitude of region 2 increases while maintaining the same frequency with region 1. The LFP maximal amplitude of region 2 depends on the maximal values of the average post-synaptic membrane potentials of the neuronal subpopulations of region 2, which are influenced by the corresponding synaptic gains. For higher values of C_{PP}, region 2 becomes fully synchronized with region 1.

3.4.2 Variation of connectivity strength between pyramidal cells of region 1 and slow or fast inhibitory interneurons of region 2

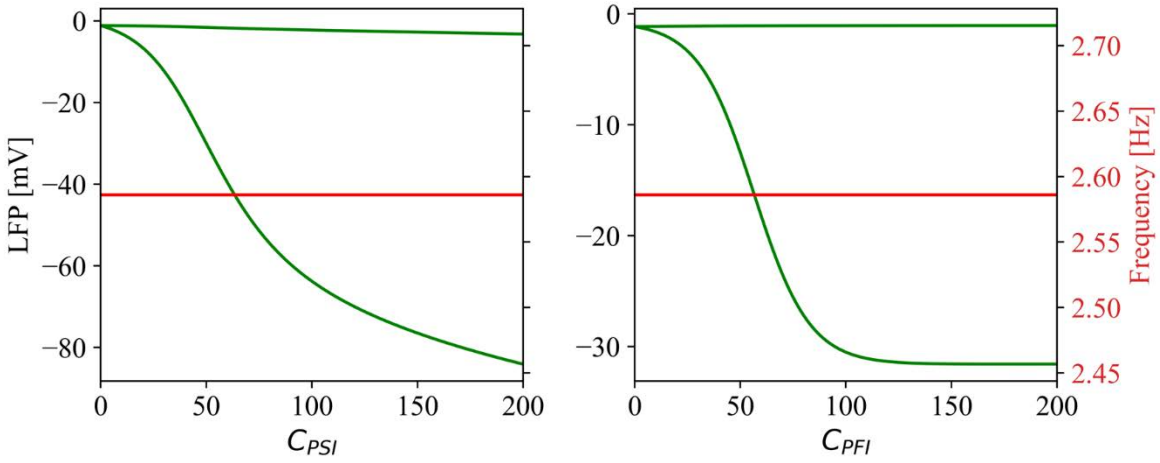

Figure 3.18. LFP of region 2 and frequency of periodic oscillations as a function of C_{PSI} and C_{PFI}. The green curves represent the minima and maxima of the stable limit cycles. Red curves represent the frequency of the cycles.

Introducing an interaction between the pyramidal cells of region 1 and the $GABA_{A,slow}$ interneurons of region 2 by taking $C_{PSI} \neq 0$ yields a rhythmic activity in the region 2 at a frequency equal to that of the LFP of the region 1. Excitation of $GABA_{A,slow}$ interneurons impacts the activity of the $GABA_{A,fast}$ interneurons due to the inhibitory relation between them. Furthermore, exciting $GABA_{A,slow}$ interneurons prevents

pyramidal cells from firing, hence, influences indirectly the activity of excitatory interneurons. The maximum value of the LFP generated decreases for $C_{PSI} > 35$ and approaches 0, indicating the saturation of $GABA_{A,slow}$ interneurons.

When an interaction between the pyramidal cells of region 1 and the $GABA_{A,fast}$ interneurons of region 2 is introduced by taking $C_{PFI} \neq 0$, the LFP of region 2 evolves similarly to the one for $C_{PSI} \neq 0$. The difference we observe while C_{PFI} and C_{PSI} are being increased is the amplitude of the resulting LFPs, which is due to the difference in synaptic gains B and G.

Finally, differently than the case where we vary the fast inhibitory synaptic gain in section 3.1, when a region receives an excitatory post-synaptic potential in the pre-ictal regime from highly-connected region, it oscillates at a frequency equal to that of the master (Figure 3.18, right y-axis) instead of producing its own frequency.

3.4.3 Dynamic repertoire of region 2 under a unidirectional influence of region 1

It is experimentally evidenced that the intrinsic properties (connectivity, synaptic gains, excitability...) of neural regions receiving epileptic activity varies. Therefore, strategies for preventing pathological activity at a certain region can depend on the network structure, mainly to the connectivity strength. In Section 3.1, we have provided a repertoire of the dynamics for a single WNMM as a function of the synaptic gains. Here, we perform a similar analysis, where we vary the synaptic gains of region 2 while it receives pre-ictal rhythmic activity from region 1. We reconsider the three different network structures presented in Section 3.4.2. In all cases, the connectivity strengths are set to 60.

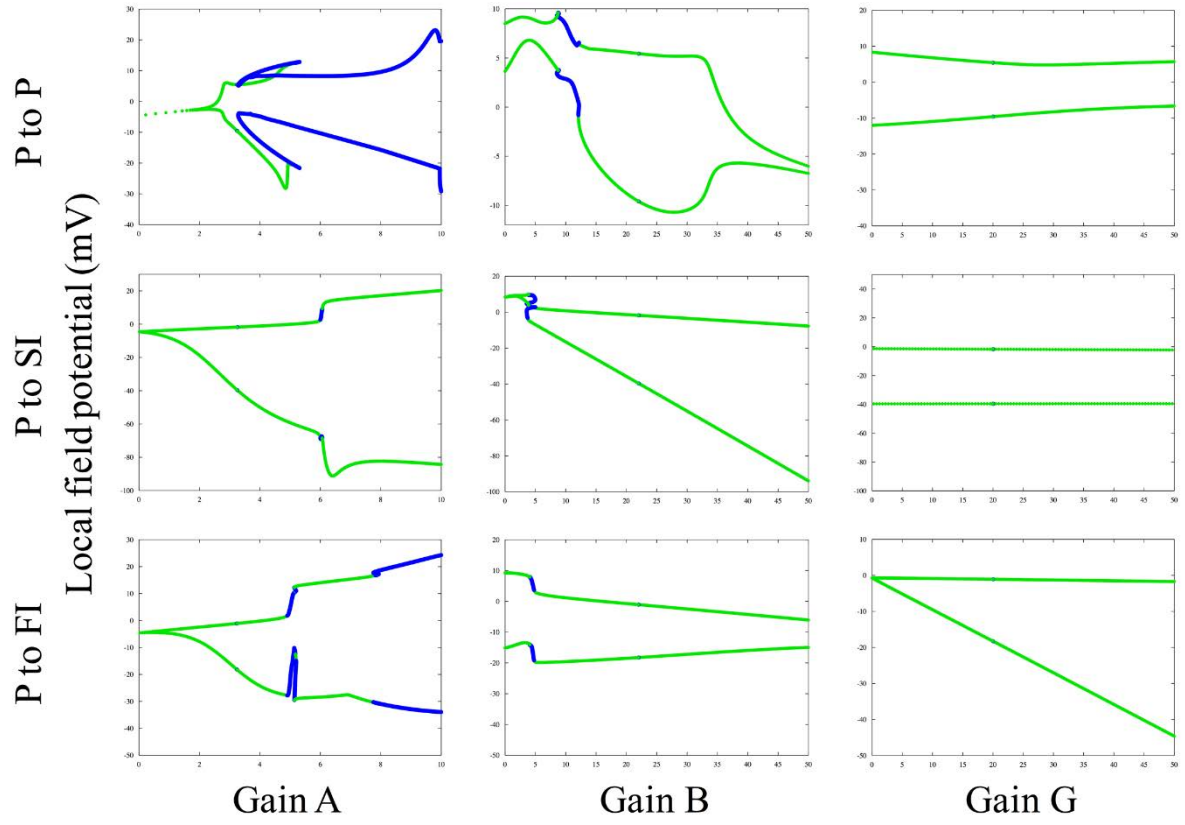

Figure 3.19. Bifurcation diagrams as a function of the excitatory, slow inhibitory and fast inhibitory synaptic gains for unidirectional single projection from the pyramidal cells of the region 1 to the different subpopulations of the region 2. Along row 1 $(C_{PP}, C_{PSI}, C_{PFI}) = (60, 0, 0)$, row 2 $(C_{PP}, C_{PSI}, C_{PFI}) = (0, 60, 0)$, and row 3 $(C_{PP}, C_{PSI}, C_{PFI}) = (0, 0, 60)$. The green and blue curves denote the maxima and minima of the stable and unstable limit cycles, respectively.

The first column of Figure 3.19 shows that increasing the excitatory synaptic gain A increases the amplitude of the periodic oscillations in region 2. In all cases, over-excitation preserves the rhythmic activity, as opposed to the single WNMM in Figure 3.2 where the over-excitation stops the rhythmic activity. Moreover, the over-excitation pushes the system towards non-periodic chaotic oscillations.

For a connection between pyramidal cells of both regions, the bifurcation diagram when varying the excitatory synaptic gain A shows a sudden transition, separating periodic oscillations of large amplitudes from a small amplitude ones. A similar transition was observed while varying the connectivity strength C_{PP} (Figure 3.17-a). Even if these neurophysiological factors (C_{PP} and A) impact different neuro-

electrical signals; the first one impacts postsynaptic potential while the second one impacts action potentials, they cause similar variations in activity.

The second column of Figure 3.19 shows that increasing the slow inhibitory synaptic gain B inhibits the whole system for $C_{PSI} = 0$. The LFP amplitude become smaller for bigger values of B. These appearing low-amplitude oscillations could be considered closer to background activity, which is in line with results shown in Figure 3.3. However, when the $GABA_{A,slow}$ subpopulation receives an oscillatory afferent, its post-synaptic potential increases. Combined with the increase of the synaptic gain B, they cause an imbalance between the post-synaptic potentials and the system continues to generate periodic oscillations at higher amplitudes than the other network structures would yield.

In neither of the coupling strategies increasing the fast inhibitory synaptic gain G decreases the LFP amplitude, nor aborts a seizure. The same remark was inferred previously in Section 3.1. However, the system generates an oscillatory behavior even for small values of G, unlike what was shown in Figure 3.2-c.

We studied the impact of an epileptic afferent, or in other words seizure propagation, as a function of both the coupling strength and network structure. We have observed that a synchronization of neural activity, hence both regions oscillate at the same frequency, with the amplitude depending on the projected neuronal subpopulation. For instance, the pyramidal cells show more “resistance” to afferent than somatic or dendritic projecting inhibitory interneurons as indicated by higher levels of connectivity strength required to transmit region 1 activity. These results are in line with previous experimental work that highlighted a higher activation threshold of pyramidal cells than as compared to interneurons (Kann, 2016).

Although new dynamics emerge comparing to results presented in section 3.1, the slow inhibitory interneuron subpopulation remains as the subpopulation able to inhibit epileptiform patterns. Moreover, our results underline an important difference between increasing the average post-synaptic potential of slow inhibitory interneurons and increasing the average pre-synaptic potential on the same population. The first inhibits the neuronal region and then stops epileptic activity, while the second yields high-amplitude oscillations in the system.

Chapter 4

Optimization of multi-site stimulation

There is experimental evidence that stimulating multiple brain regions could be more effective than stimulating a single one (Sobayo and Mogul, 2016). In this chapter, we present models of functionally connected epileptogenic regions by coupling modified Jansen and Rit NMMs (presented in Chapter 2), enabling the study of network effects in response to stimulation-like perturbations. This approach is used to determine relevant regions driving and controlling epileptiform activity. In addition, single-site stimulation is compared with multi-site stimulation, and designed optimal strategies are proposed to desynchronize neuronal activity and abort epileptiform activity at the network scale. The impact of the number of targets is studied, and a strategy to select potential stimulation targets from patient electrophysiological signals is suggested.

Network architecture

The constructed network consisted in seven regions denoted by NM_i, $i \in \{1, \dots, 7\}$ (as presented in Figure 4.1-c). Each region was modelled using the modified

Jansen and Rit NMM presented below (Figure 4.1-d). Parameter values were equal to those in Table 1, except excitatory and inhibitory synaptic gains that were modified to 3.85 mV and 16.7 mV, respectively, to generate interictal discharges. White Gaussian noise was added to the firing rate of incoming excitatory input onto pyramidal cells in each NMM, with a mean m and a standard deviation σ equal to 90 Hz and 1.2, respectively. We used the Euler-Maruyama method to solve the set of equations (Maruyama, 1955). The network was fully connected, in that each NMM received afferents from all other NMMs; action potentials of pyramidal cells of all $NM_j,\ j \in \{1, \dots, 7\},\ j \neq i$ were added at the level of pyramidal cells of NM_i (Figure 4.1-d). These afferents were modulated through a NMM-dependent connectivity constants $C_{i,j}, i, j \in \{1, \dots, 7\}$ and a propagation delay arbitrarily chosen as 30 ms. The connectivity matrix was a hollow matrix with dimensionless components chosen uniformly within the interval [0, 1.7]. Those randomly chosen values were kept fixed for all simulations.

Stimulation

The stimulation waveform is another key parameter in determining the impact of neuromodulation on brain tissue (Warren M. Grill, 2015). We used a square bi-phasic waveform to mimic the charge-balanced biphasic pulse stimulation used in clinical practice. Compared to monophasic pulse stimulation or direct current stimulation, bi-phasic stimulation limits irreversible damage caused by charge accumulation in the tissue (Merrill et al., 2005; Butson et al., 2005). The stimulation of network nodes was altered *via* population-dependent coupling coefficients $k_i \in \{0, 1\}, \forall i \in \{1, \dots, 7\}$, as presented in Figure 4.1-c.

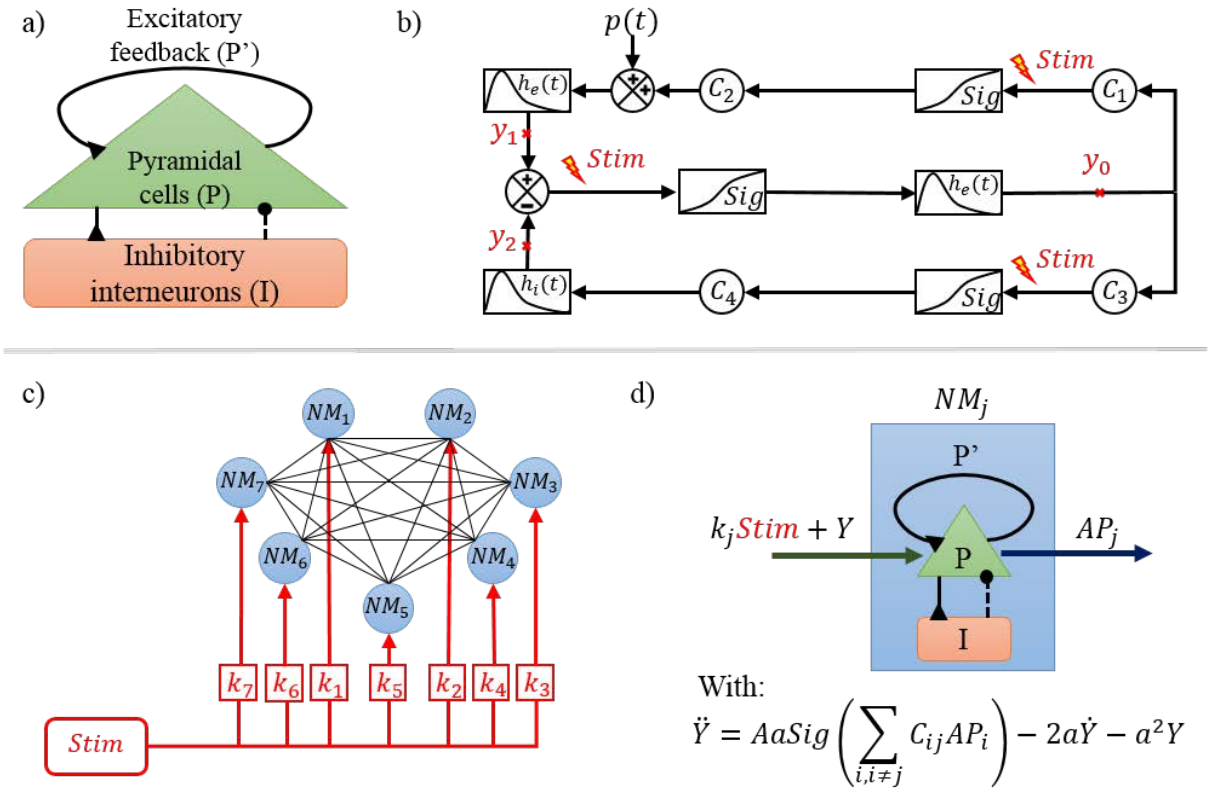

Figure 4.1. a) Structure and b) Block diagram of the modified Jansen and Rit NMM accounting for stimulation. c) Diagram of the complete network allowing for single-site and multi-site stimulation, and d) block diagram of each node with its input and output. a) Population of pyramidal cells (green triangle) interacts with an inhibitory population of interneurons (orange rectangle). Solid-lines arrows represent excitatory connections, while dashed-lines represent inhibitory ones. b) $y_i(t)$, $i \in \{0, 1, 2\}$ correspond to the output of pyramidal cells, excitatory and inhibitory interneurons, respectively. $p(t)$ is a white Gaussian noise representing excitatory inputs from neighboring areas. The "Stim" symbol represents a modification with respect as compared to the original Jansen and Rit model, where electrical stimulation is applied in the model. c and d) The network is composed of 7 fully connected NMMs. Each node receives stimulation (bi-phasic waveform) with population-dependent coupling coefficients k_i, $i \in \{1, \dots, 7\}$, in addition to afferents from other NMMs. The afferents received by a given NMM *j* from a given NMM *i* with $i \in \{1, \dots, 7\}$ and $i \neq j$ are converted into a post-synaptic potential before being added as an input to pyramidal cells. The $C_{i,j}$, $i, j \in \{1, \dots, 7\}$ coefficients represent connectivity constants between network populations.

Before passing to the network scale, we first analyzed stimulation effects on a single population. We tuned the synaptic gains (Table 1) of the NMM to generate interictal discharges, as shown in Figure 4.2-a. We then evaluated the impact of sinusoidal stimulation parameters (amplitude, frequency) on the neuronal population activity. Results are summarized in the bifurcation diagram of Figure 4.2, which shows the changes in dynamics under stimulation.

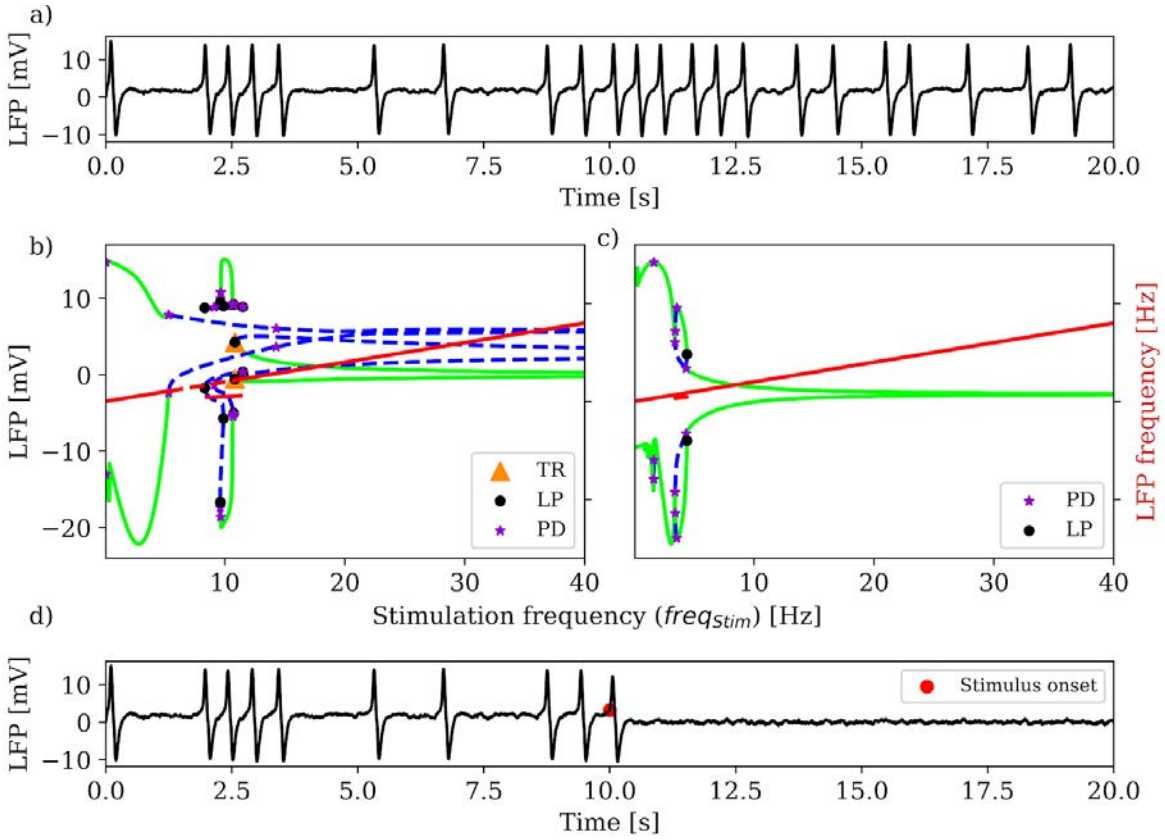

Figure 4.2. Analysis of stimulation effects on a single population. a) Simulated interictal discharges under “no stimulation” condition. b) Sinusoidal stimulation (amplitude 3 mV, frequency ranging from 0 to 150 Hz) applied to all neuronal subpopulations. c) Sinusoidal stimulation (amplitude 3 mV, frequency ranging from 0 to 150 Hz) applied only to inhibitory interneurons. b,c) In both cases, system dynamics depend on stimulation parameters as depicted by LFP amplitudes (blue and green curves) and frequencies (red curves). Stable and unstable limit cycles are represented by solid green and dashed blue lines, while their frequencies are represented by solid and dashed red lines, respectively. d) LFP signal observed for optimal stimulation

parameters (amplitude 3 mV, frequency 90 Hz). To generate sporadic discharges, average excitatory (A) and inhibitory (B) synaptic gains were fixed at 3.85 mV and 15 mV, respectively. For the sake of readability, results are shown for stimulation frequencies within the [0, 40] Hz range. Abbreviations; LP: limit points, PD: period doubling, TR: Torus bifurcations.

Figures 4.2-b,c illustrate all the dynamics that the system presented in Figure 4.1-b can generate while varying the frequency of a sinusoidal stimulation applied either on all neuronal subpopulations (left panel), or only to inhibitory interneurons (right panel). It is then possible to distinguish between stimulation frequencies for which the system generates high-amplitude oscillations, and those for which the system is attracted by a small, stable limit cycle that can be considered as a stable limit point. In addition, it highlights the sensitivity of neurostimulation parameters and reveals the effects of neuronal selectivity.

The bifurcation diagram presented in Figure 4.2-b can be divided into three regions. In the first region where $freq_{Stim} \in [0, 5.18[$ Hz, the system is attracted by stable limit cycles and generates rhythmic activities of increasing frequencies and modulated amplitudes. In the second region where $freq_{Stim} \in [5.18, 10.83[$ Hz, population activity is altered and unsteady. We detect closed trajectories of limit cycles with different amplitude ranges and numerous period doublings where oscillations of double the period of original ones are induced. Throughout this interval, the LFP consists in an oscillatory activity involving a mix of frequencies and amplitudes. Third, for $freq_{Stim} \in [10.83, 150]$ Hz, we detect a saddle-node bifurcation for periodic orbits coupled to a subcritical Neimark-Sacker bifurcation for $freq_{Stim} = 10.83$ Hz. Beyond these bifurcation points, a pair of limit cycles, stable and unstable (solid-green and dashed-blue lines), are created and the system is attracted by stable limit cycles of decreasing amplitudes. Increasing stimulation frequency (typically > 50 Hz) leads to periodic oscillations of frequency identical to the stimulation frequency, and of amplitude close to zero.

The bifurcation diagram presented in Figure 4.2-c exhibits similar dynamics, since global activity is still altered until reaching a separation stimulation frequency

from which the amplitude of the oscillating activity decreases. Interestingly, unstable cycles (dashed blue lines) disappear while stimulating only inhibitory interneurons. This highlights the differential effects of stimulation depending on specific neuronal subtypes that are impacted. The stimulation frequency required to abort epileptiform activity is lower when targeting GABAergic interneurons, as compared to all subpopulations.

Those results provide indication of the potential parameters able to locally abort epileptiform activity, and promote instead an electrophysiological pattern closer to physiological activity (Figure 4.2-d). In the following, we take advantage of the knowledge at the single population level to attempt controlling epileptic activity in networks of neuronal populations.

Resonance phenomena

Another important point to investigate is the impact of stimulation on a “healthy” neuronal region. Therefore, we studied the effects of stimulation frequency while a single unconnected NMM was generating background activity. Average excitatory and inhibitory synaptic gains were fixed to 6 mV and 7 mV, respectively. All other model parameters were equal to the values presented in Table 1.

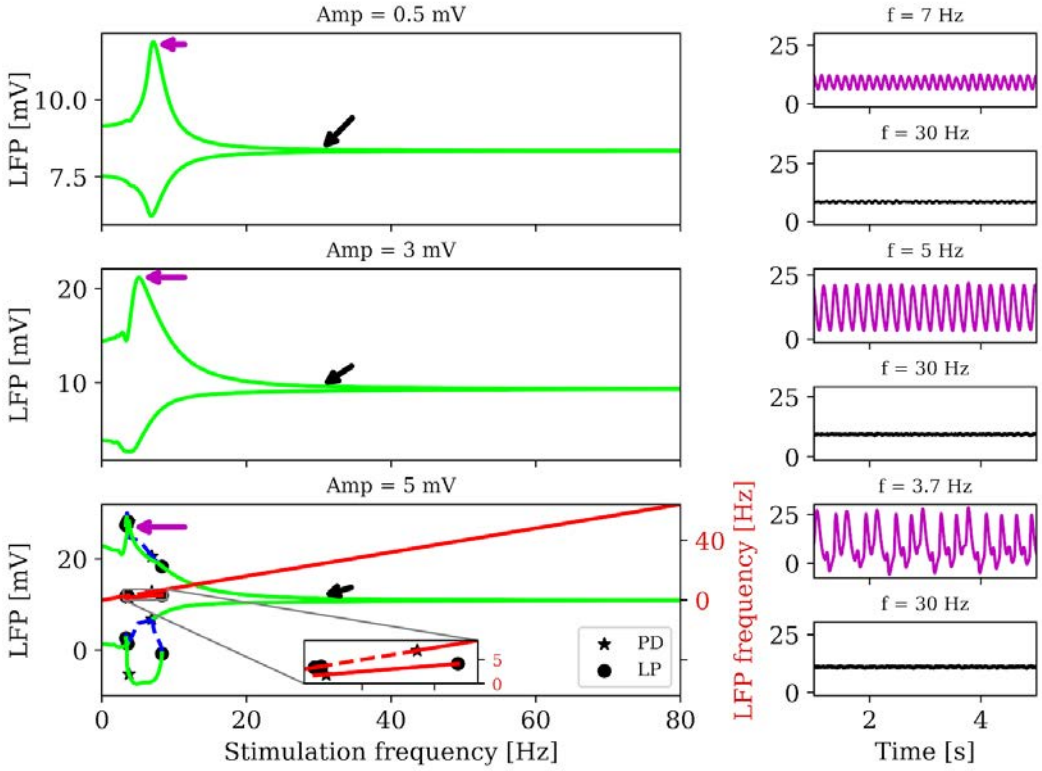

Figure 4.3. (*Left panels*) LFP amplitude and frequency as a function of stimulation frequency. (*Right panels)* Corresponding resonant and non-resonant time series. The same sinusoidal stimulation was added to the post-synaptic potential for all model subpopulations, $(k_e, k_i) = (1, 1)$. Stable and unstable limit cycles are represented by solid green and dashed blue lines, while their frequencies are represented by solid and dashed red lines, respectively. The stars and circles denote period-doublings (PD) and limit points (LP), respectively.

Figure 4.3 shows LFP amplitude as a function of the stimulation frequency and for fixed stimulation amplitudes. Depending on the stimulation amplitude, the system had a different resonance frequency for which high-amplitude oscillations appear. By increasing the stimulation amplitude, the model had a smaller resonance frequency, and generated oscillations of larger amplitude. For a stimulation amplitude equal to 0.5 mV *(upper panel)*, the resonance frequency was 7 Hz. However, by increasing the stimulation amplitude to 5 mV (lower panel), the resonance frequency decreased to 3.5 Hz and bifurcation points, impacting the LFP frequency domain, were detected unlike upper and middle panels.

For $freq_{Stim}$ = *6.9 Hz,* a period doubling bifurcation was detected, and the following limit cycles lost stability. Moreover, their frequency was changed and became equal to half the frequency of stable cycles. Then, another period doubling bifurcation point was detected for $freq_{Stim}$ = *3.58 Hz* preceded by a limit point for $freq_{Stim}$ = *3.35 Hz.* This period doubling point led to another change in stability and a doubling of the frequency of limit cycles. For $freq_{Stim} \in]3.35, 8.3[$ Hz, the system was attracted by stable and unstable attractors, and the LFP frequency domain included other frequencies in addition to the stimulation frequency.

4.1 Optimal stimulation strategy: Single- vs multi-site stimulation and identification of stimulation targets

From the single-site stimulation study, we retained the following stimulation parameters for multi-site stimulation: amplitude equal to 3 mV and a frequency equal to 90 Hz. In order to mimic stimulation protocols routinely performed in clinical epileptology, biphasic pulse stimulation was used. Pulse stimulation (amp=3mV, $freq_{Stim}$=90 Hz, pulse width=5 ms per phase) was applied to pyramidal cells and interneurons subpopulations as soon as epileptic spiking activity was detected in at least one network node. Stimulation duration was set to 1s, and was delivered only during time intervals showing epileptic activity for more than 1s. Spiking periods of shorter durations were not considered (no stimulation delivered).

In simulated networks, nodes were represented by NMMs in which parameters were set to generate interictal spikes. In the presence of connections, these epileptic spikes showed a higher degree of synchronization, as depicted in Figure 4.4-a for a network of 7 nodes. Epochs of epileptic activity and background activity are reflected in the summation of LFPs (denoted by Σ) generated at each node (Figure 4.4-b). Therefore, Σ was used to determine multi-site stimulation onset times. As depicted in Figure 4.4-b, stimulation times (red dots) could be correctly determined, i.e. as soon as at least one node of the network generated epileptiform activity. Figure 4.4-c presents the impact of stimulation delivered at these stimulation times when one node was stimulated, while Figure 4.4-d shows this impact when stimulation was applied on

all nodes at the exact same times. Interestingly, multi-site stimulation leads to shorter epochs of epileptic activity and longer epochs of background activity.

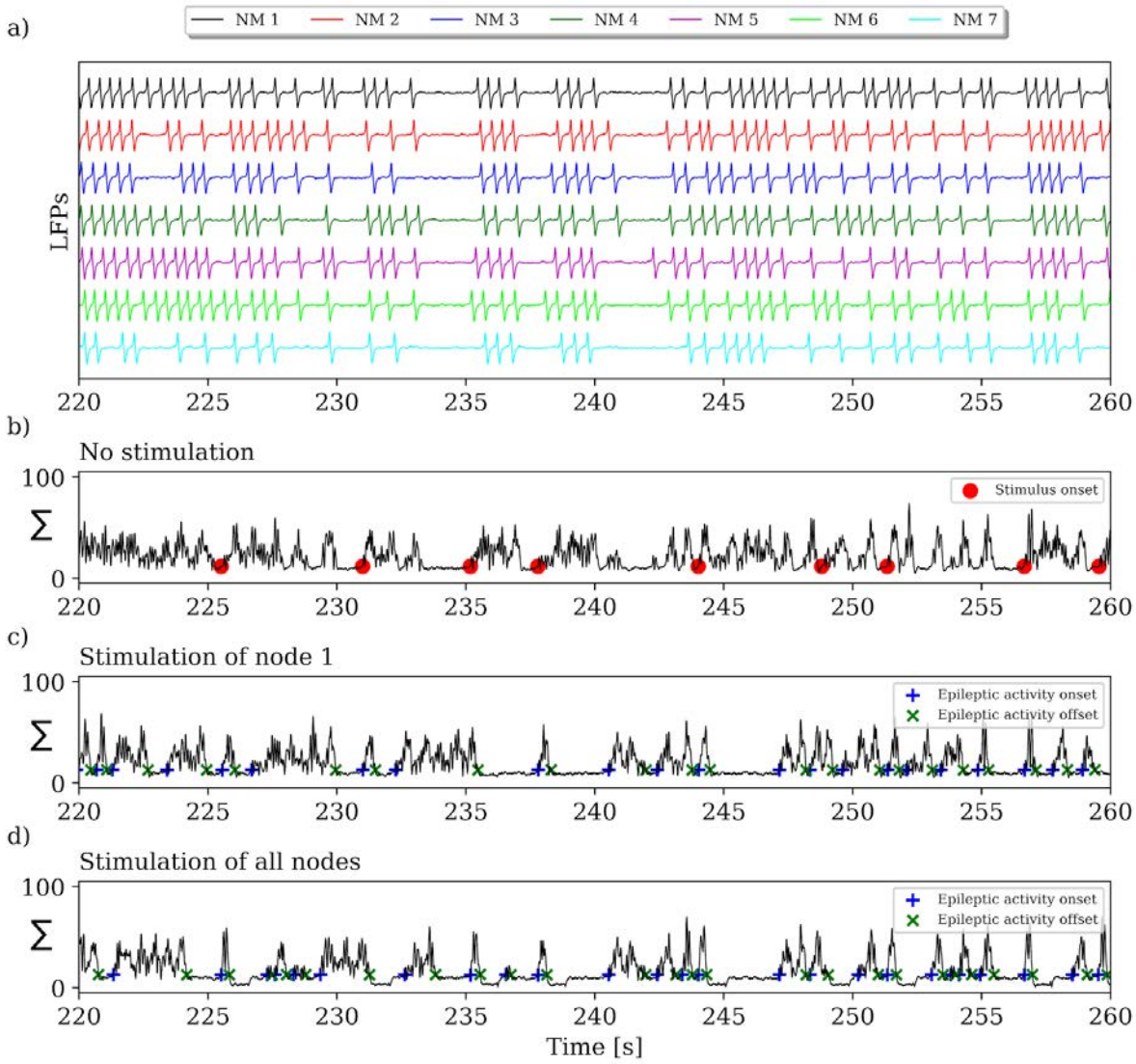

Figure 4.4. a) LFPs of each network NMMs in the absence of electrical stimulation, and b) their summation. c, d) LFP summation after applying a charge-balanced biphasic stimulation of amplitude, frequency and pulse width of 3 mV, 90 Hz and 5 ms, on NMM 1 and all NMMs; respectively. Red circles indicate stimulus onsets, while blue and green markers indicate respectively the beginning and end of epileptic activity epochs.

Quantification of stimulation efficiency

In order to quantify the efficiency of stimulation in terms of suppressing epileptic discharges, we proposed a new index based on their occurrence. It is referred to as the amount of epileptic discharges index (*AEDI*) and defined as follows:

$$AEDI = \sum_i N_i \Delta_i^4 \quad (4.1)$$

Where N_i represents the occurrence of an interval of a duration Δ_i during which epileptic activity is observed. The duration exponent emphasizes the duration of interictal discharges. This index quantifies the number and duration of time intervals exhibiting epileptic discharges. In the following, any stimulation protocol leading to the reduction of the *AEDI* computed under control condition (no stimulation) is considered to have a therapeutic effect. The issue is to identify stimulation parameters (amplitude, frequency, nodes to stimulate) which maximize this reduction (i.e. minimize *AEDI*). In practice, therapeutic effect is marked by an increase/decrease of short/long Δ_i on the histogram. Thus, once stimulation was delivered, we delimited non-silent intervals (i.e. exhibiting epileptic activity) on the summation of all network LFP signals in absolute value, by setting a threshold and applying a forward and backward filter to smooth the signal. Then, histograms showing their occurrence with respect to their duration were generated and *AEDI* values were computed.

How many nodes and which ones?

We simulated LFP signals for 1000 networks of 7 coupled neuronal populations (Figure 4.1-c). For each network, we investigated the impact of stimulation and constructed the histograms of epileptic discharges occurrence for all 127 possible ways to stimulate the network when the number *n* of nodes varies from 1 to 7, and when all combinations of the *n* stimulated nodes are being tested. The 7-NMMs had the same parameters values, and only the connectivity matrix and random excitatory inputs describing the influence of neighboring NMMs were generated each time. Then, *AEDI* values were computed as a function of the number of stimulated NMMs on a total of 127,000 simulations.

To classify network nodes according to their impact on network-level activity, we used a graph theory measure known as eigenvector centrality (EVC), which was used to score the influence of each node. Computed on functional connectivity matrices, a high EVC value means that a considered node is connected to have preferential connections to other nodes in the network and drives their activity. In practice, we used LFP signals to compute EVC. To determine connectivity matrices, we computed the degree of coupling between network nodes, while considering the directionality of coupling. Connectivity matrices were computed from the non-linear correlation coefficient h^2 (Lopes da Silva et al., 1989; Pijn and Lopes da Silva, 1993) which is given by:

$$h^2 = \frac{\sum_{i=1}^{N}(y_i - \bar{y})^2 - \sum_{i=1}^{N}\left(y_i - f(x_i)\right)^2}{\sum_{i=1}^{N}(y_i - \bar{y})^2} \qquad (4.2)$$

Where $y_i, x_i,\ \forall i \in [1, N]$ represent samples of two LFP signals generated by two nodes x, y. f is a piecewise function passing from midpoints $(\bar{x}, \bar{y})$ after presenting the amplitude signal y with respect to that of signal x and dividing the x-axis into equal sized bins. These linear line segments form a linear approximation of the nonlinear regression curve. The correlation value varies between 0 (no association between signals) and 1 (one signal is fully predictable based on the other).

Finally, results were compared to ground-truth connectivity matrices explicitly known for each network model.

Results

Using Σ, we first determined the number of nodes to stimulate to obtain the highest therapeutic effect as denoted by minimal *AEDI* values. To proceed, we first evaluated the stimulation impact on the network using Σ as a function of the number of NMMs stimulated. For this purpose, we simulated LFPs while applying all the 127 possible combinations for the stimulation and compared *AEDI*s (number and choice of nodes to stimulate). Then, we focused on how to identify the optimal NMM to be stimulated from LFP signals. In our investigation, we used the nonlinear correlation

coefficient h^2 to estimate connectivity links between network NMMs, and computed EVC values to determine the stimulation targets. Ground truth connectivity matrices were used to validate model-based predictions.

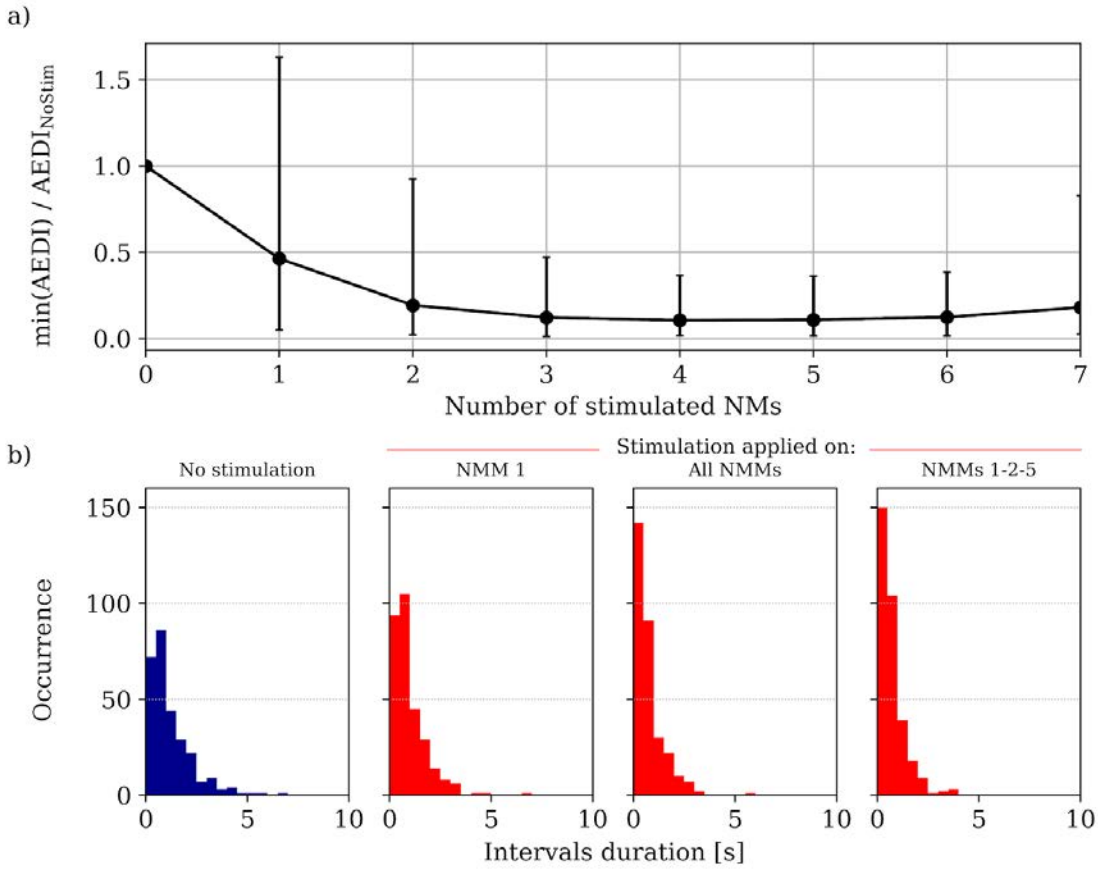

Figure 4.5. a) Normalized *AEDI* as a function of the number of stimulated NMMs in the network. b) Histograms of epileptic discharges occurrence with respect to their duration. The same charge-balanced biphasic stimulation (amplitude 3 mV, frequency 90 Hz, pulse width 5 ms) was used for all simulations.

Figure 4.5 confirms the effectiveness of multi-site stimulation as compared to single-site stimulation. Furthermore, it shows that stimulating a network subset is sufficient and efficient, in terms of *AEDI*, than stimulating the whole network (optimality while stimulating four NMMs). For each network simulation, 127 stimulation possibilities were tested, and the minimal *AEDI* obtained while stimulating the same number of NMMs was retained, and an average value over all simulations was plotted.

We identified the optimal number of NMMs to stimulate as equal to four. However, starting from 3 and up to 6 NMMs, the difference in *AEDI*s was minimal.

Targeted network nodes. For each simulation, we compared the first three dominant NMMs showing higher EVC scores to those possessing a higher number of outgoing connections. Interestingly, EVC values predicted correctly 2 out of 3 optimal stimulation targets 862 times (89.2% of simulations), the exact same three NMMs 375 times (38.8%), and at least two NMMs 487 times (50.4%).

Regarding the simulation presented in Figure 4.4-a, the reconstructed connectivity matrix identified NMMs 1, 2 and 5 as the most involved in epileptiform activity propagation. Interestingly, the same NMMs were detected by the EVC calculation, suggesting that the level of induced network synchrony was a key factor in stimulation efficacy. While testing all the 35 possible combinations for a multi-site stimulation targeting three NMMs, the minimal AEDI was obtained while targeting these NMMs and was equal after normalization with respect to infinity norm (max) to 0.15. Again, this value was lower than when all network nodes were stimulated. Figure 4.5-b presents the resulting histograms in the absence of stimulation and while stimulating NMM 1, the whole network and the set {1, 2, 5} of NMMs, respectively.

4.2 Optimal stimulation strategy: Open- vs closed-loop and impact of stimulation timing with respect to epileptic discharge onset

In addition to emphasizing the effectiveness of multi-site stimulation, Figure 4.6 (below) enables the comparison between closed- and open-loop stimulation protocols, and illustrates the impact of stimulation timing. Figures 4.6-a and 4.6-b present the proportion of epileptic activity in the absence of stimulation, after applying a stimulation regardless of oscillation onsets (OL), once oscillations begin (CL_1) and a 0.25 second before oscillations' onsets (CL_2). This metric is defined by the ratio of the multiplication of the occurrence of interictal discharges by their duration and the signal duration.

Using a charge-balanced biphasic stimulation of amplitude 3 mV and a frequency of 90 Hz upon all network NMMs, and for a total of 500 simulations in the case of one or group of networks (single or different individuals) (as the connectivity coefficients are fixed or not), we found that OL stimulation reduced the proportion of epileptic activity by 30 % and provided similar results as compared to (CL_1) stimulation. However, (CL_2) was more efficient than both previous forms of neuromodulation. These differences were related to the stimulation triggering moments. In order to illustrate this difference, we projected the y3-nullcline and the system's response to stimulation (black curves) on the (y_2, y_0)-plane in panels c and d of Figure 4.6. The green arrows in panel 4.6-c show the flow direction. The y_3-nullcline is given by the following function driven from system (1) by taking its right hand side to 0:

$$func(y_0) = \left(\frac{A}{a}\right) \times \{p + C_2 Sig(C_1 y_0)\} - Sig^{-1}(\left(\frac{a}{A}\right) y_0) \qquad (4.3)$$

Notice that the function (3) yields a hysteresis curve, along which the large amplitude oscillations take place by jumping between the upper and lower branches and passing close to the fold points. A closed-loop stimulation algorithm based on oscillations detection would be inefficient to prevent the system from oscillating, since such stimulation would be applied when the flow takes off after passing close to the left hand side fold point. In order to prevent large amplitude oscillations and maintain background activity, the stimulation should be applied before the system reaches the left hand side fold point (Figure 4.6-d). Otherwise, once a spike is triggered, it is not possible to stop it until it approaches this point.

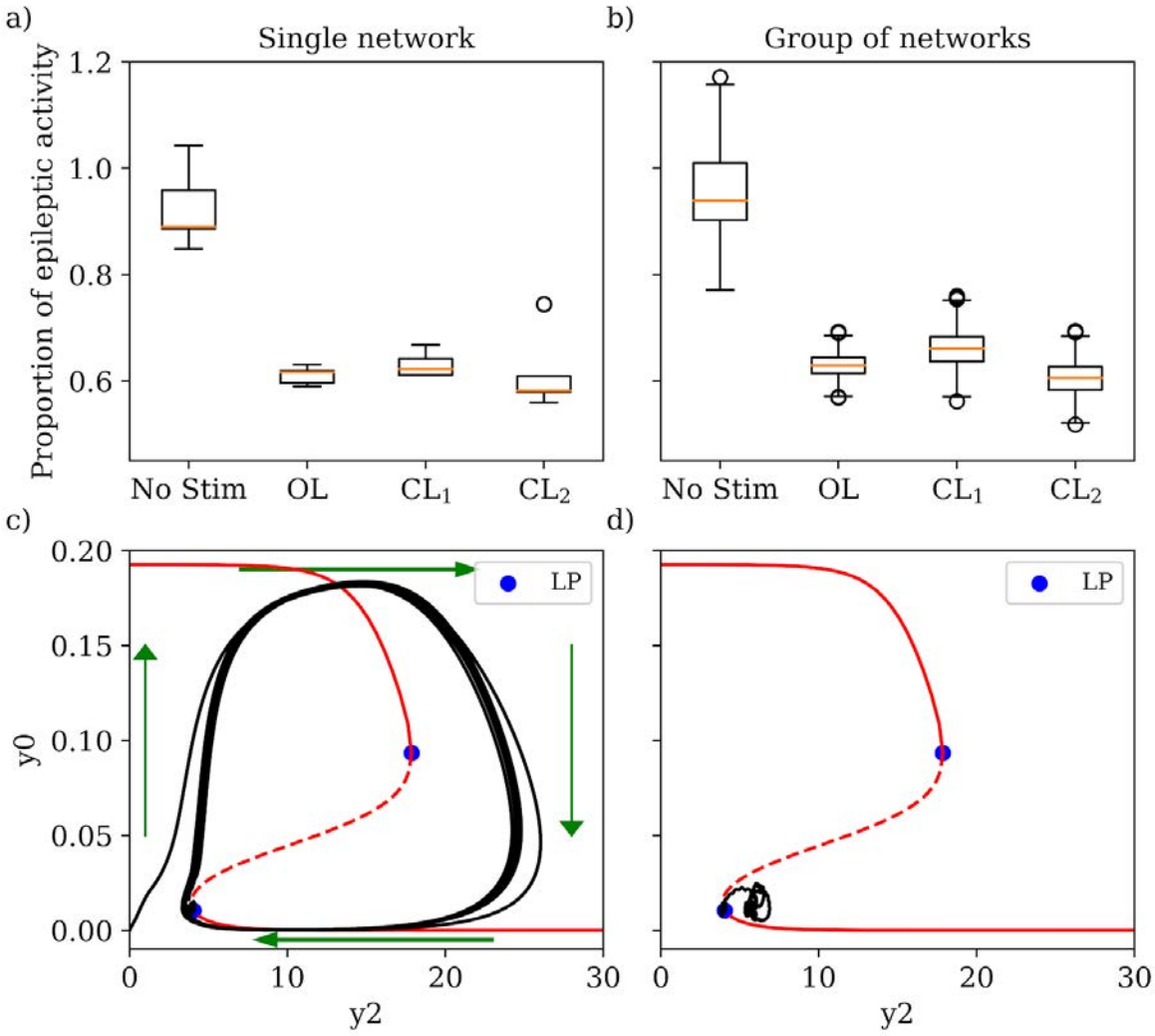

Figure 4.6. a,b) Boxes showing normalized *AEDI* while stimulating randomly (OL) or at oscillation onsets (CL_1), or 0.25 s before oscillation onsets (CL_2). c,d) the projection y_3-nullcline and trajectories of the Jansen-Rit NMM in the plane (y_2, y_0), while synaptic gains were fixed to generate spiking activity, in the absence and presence of a charge-balanced biphasic pulses stimulation (amp=3 mV, $freq_{Stim}$=90 Hz) applied one second before spiking onset, respectively. In b) both connectivity coefficients and noise are modified (multiple networks), as opposed to a) where only the noise is modified (same network). The boxes mean values from left to right are [(a: {0.92, 0.61, 0.63, 0.60}), (b: {0.94, 0.63, 0.66, 0.60})]. Continuous and dashed parts of the red curve represent stable and unstable branches of the y3-nullcline, respectively, where the blue points represent the folds of the curve. The green arrows represent the flow direction.

To summarize, we developed biologically-inspired models of brain activity receiving stimulation at two levels of description (single- and multi-population epileptogenic networks). First, bifurcation analysis was used to determine optimal parameters able to abort epileptiform patterns. Second, a graph-theory based method based on EVC was presented to classify network nodes in an epileptogenic network based on their contribution to seizure generation and propagation. The best therapeutic effects (i.e., reduction of epileptiform discharges duration and occurrence rate) were obtained by the specific targeting of nodes with the highest eigenvector centrality values. The timing of stimulation was also found to be critical in seizure abortion impact. Overall, these results provide a proof-of concept that using network neuroscience combined with physiology-based computational models of brain activity can provide an effective method for the rational design of brain stimulation protocols in epilepsy.

General discussion and Future perspectives

Neurostimulation has long been identified as a promising approach to decrease the occurrence of seizures, which dramatically impair the quality of life of patients suffering from epilepsy. However, despite recognized applicability, safety and encouraging results, brain stimulation still cannot be routinely indicated as a treatment for focal epilepsies. From a clinical viewpoint, stimulation parameters are chosen empirically and a rational definition and design of stimulation protocols is still missing. From a theoretical viewpoint, understanding the factors underlying the generation of epileptiform activity is still challenging. Furthermore, predicting and understanding the brain network response to specific electrical stimulation patterns is a delicate and open problem.

One of the main objectives of this thesis was to study and design a multi-site electrical stimulation able to abort epileptic seizures. To achieve this, we opted for a gradual approach. First, we studied the qualitative changes in dynamics caused by quantitative changes in excitability. After providing the whole dynamical repertoire of a neuronal region while altering its excitability, we moved to the study of its dynamics under stimulation. EEG signals were analyzed to identify qualitative changes in dynamics caused by specific stimulations, as well as the types of bifurcations involved in these changes, and the impact of electrical stimulation parameter space on the model behavior was explored in order to understand the effects of stimulations on activity patterns. The findings and observations were used as a basis for studying the

stimulation impact on a whole neuronal network composed of different connected neuronal populations.

Impact of neighboring neuronal regions and the activity of specific types of neurons on its dynamics

We have used a generic modeling approach representing neuronal networks across the cortex as “neural masses” consisting in a few thousands of neurons, and describing their averaged activity. This approach is widely used and accepted in neuroscience, and can be used as a basis for a large-scale models of brain activity. Furthermore, neural mass models have the advantage to simulate signals that are directly comparable with experimental LFPs, since both simulated and recorded signals originate from phenomena at a comparable spatial scale.

After introducing the bio-inspired computational models allowing the simulation of the activity of a neuronal population, we conducted bifurcation analyzes. The results provided an exhaustive characterization of changes in population activity with respect to the variation of synaptic gains and an external input from neighboring neuronal populations. Furthermore, the excitation/ inhibition ratio was presented as an index underlying the dysfunction and stability of a neuronal circuit. However, the use of Wendling’s neural mass model, which includes an additional type of inhibitory interneurons (fast somatic-projecting inhibitory interneurons), had shown that this index might not be optimal to quantify the epileptogenicity of a neuronal population. In fact, the conducted bifurcation analysis while varying the synaptic gain of fast inhibitory interneurons has demonstrated the involvement of these inhibitory interneurons in the generation of the epileptic activity, challenging the notion that promoting the appearance of epileptiform activity requires necessarily a high excitation/ inhibition ratio. Besides, the bifurcation diagrams while varying either the excitatory input p or the excitatory synaptic gain A show that an over-excitation triggers the compensatory inhibitory role of slow inhibitory interneurons, and then counteracts over-excitation, stops the pathological oscillatory activity and imposes background activity.

Design of optimal stimulation protocols able to abort epileptiform activity in a single neuronal population

Significant research efforts have been made over the last decades to identify effective stimulation parameters in specific therapeutic applications. Some studies have argued for the efficacy of high stimulation frequencies (typically around 100 Hz) (Filali et al., 2004; Kim et al., 2012; Shen et al., 2003; Beurrier et al., 2001), while others provided evidence that low frequency stimulation (frequency lower than 5Hz) is an effective perturbation able to reduce seizures frequency (Albensi et al., 2004; Jerger and Schiff, 1995). A common conclusion from those studies is that the most effective stimulation parameters to control epileptiform activity remain unknown to date.

In this thesis, the response of neuronal populations to electrical stimulation applied during seizure onset was explored. EEG signals were analyzed to identify qualitative changes in dynamics caused by stimulation, as well as the types of bifurcations involved in these changes. Our results support previous studies promoting the use of high stimulation frequencies to abort seizures (Bikson et al., 2001; Lian et al., 2003). However, our results highlight the dependence of stimulation efficacy on both stimulation intensity and frequency. Stimulations with an amplitude lower than 2 mV were identified as non-effective irrespective of frequency. Moreover, resonance stimuli that can lead to an exacerbation of epileptiform activity have been found. It is worth mentioning that, in our investigations, the stimulation amplitude represents an alteration of the post-synaptic potential caused by applying an electrical stimulation at a specific intensity. An additional step relating these two measures (i.e., voltage and intensity) would be required before conducting experimental studies. Let us note that additional biophysical factors related to the tissue properties (e.g., conductivity) and the electrode/electrolyte interface influence this conversion.

Then, we attempted to determine an analytical expression of the transfer function for a non-linear system, namely Jansen and Rit model, as another strategy to estimate optimal stimulation parameters to alter specific properties of neural dynamics and avoid resonance effects. As in the case of bifurcation analysis, the use of a transfer

function would save a considerable computational time, as compared to running an extensive number of numerical simulations.

Since the neural mass model represented by equations (3.15), involves non-linear asymmetric functions, we first attempted at replacing them by linear ones. We proceeded to a linearization around a special point describing the PSP for which a 50% firing rate is achieved. The resulting system was an approximation of the original system for which it was much simpler to compute the transfer function through the Laplace transform. This procedure has been followed previously to design a closed-loop proportional-integral controller for the Jansen and Rit neural mass model (Wang, Niebur et al., 2016). Although it provides some information and approximates the system behavior, the frequency responses were unreliable due to the loss of linearity and were different from those obtained numerically. This motivated the investigation of other non-linear approaches allowing the control of non-linear system without performing a linearization.

Over the last decades, mathematicians have developed sophisticated theories that have paved the path for the development of non-linear approaches. Here, we applied the theory of non-commutative rings to overcome the non-associativity problem which is characteristic of non-linear systems, and prevents the derivation of an analytical expression linking the system input to its output. Hence, following this method, we provided a unique description of the simulation/LFP relationship for the non-linear Jansen and Rit neural mass model, which is not achievable using conventional methods. However, this approach has some limitations, including the fact that the analytical expression of the transfer function may contain a state space variable as opposed to linear systems.

Design of a multi-site stimulation to abort epileptic seizures at the network level

The investigations conducted at the level of one single neuronal population were extended to optimize multi-site neurostimulation and generate experimentally testable hypotheses. The perspective to perform multi-site stimulation in epilepsy is in part motivated by reported effects of multi-site stimulation in humans, for example in working memory enhancement (Alagapan et al., 2019). In our investigation, we

developed a computational model of an epileptogenic neuronal network and studied the impact of multi-site stimulation on connected neuronal regions generating interictal discharges; an activity recognized as an electrophysiological marker of epileptogenic neuronal systems (Wendling et al., 2002). Our results confirmed the effectiveness of multi-site stimulation in reducing the frequency of epileptic discharges, and have shown that it is possible to guide the choice of stimulation targets based on a graph theory metric (namely eigenvector centrality). We also presented a method for selecting and limiting the number of target regions based on “recorded” LFPs, which should be achievable experimentally based on recorded LFPs. These chosen connectivity hubs are characterized by a high output functional connectivity, and stimulating those regions strongly impacts network dynamics, as opposed to other locations. Moreover, it is worth mentioning that multi-site stimulation of a few regions was identified as optimal, and outperformed stimulation of the entire network or of a single region.

We have shown that closed-loop stimulation based on the detection of low-frequency epileptiform activity is able to suppress interictal discharges. However, the difference as compared to open-loop stimulation, while the system is in an epileptogenic state, was minimal. Despite this similar performance, a closed-loop paradigm should be preferred since stimulation is only delivered if and when needed, minimizing the injection of current within brain tissue. Our results also suggest that a closed-loop protocol could be efficient to determine the seizure onset, and deliver stimulation for a fixed period of time that would be equivalent to the duration of a seizure (Jenssen et al., 2006).

Furthermore, our study provides new insights on the role that GABAergic inhibitory neurons play in regulating the activity of glutamatergic neurons (Ingram et al., 2019; Komarov et al., 2019). We conclude that the capability to selectively activate specific neuronal types will greatly enhance the efficiency of brain stimulation by reducing the termination time and minimizing seizure spread within the cortical network. We propose that this model prediction could be tested experimentally using optogenetics, which is an experimental neuromodulation technique that enables the selective activation of specific neuronal types. In addition, we identified a resonant frequency to avoid in brain stimulation protocols for epilepsy, since stimulation delivered at this frequency can enhance the generation of epileptiform patterns and

favor the generation of high-amplitude oscillations, which is in addition amplified by network effects. Therefore, in order to replace epileptiform activity by a more “physiological” activity, it would be appropriate to avoid using such resonant frequencies as stimulation frequencies.

In terms of limitations, avenues for improvement could consist in adopting more realistic models, such as the Wendling neural mass model (Wendling et al., 2002). This model comprises somatic-projecting interneurons with faster synaptic kinetics, and has the ability to generate more diverse activities (e.g., fast onset activity). In the presence of these fast components, the circuit structure could be reconsidered by including feedforward inhibition to the feedforward excitation adopted here (Chen et al., 2017; Womelsdorf et al., 2014). Finally, the biophysics layer of the model describing the impact of the electrical stimulation onto neuronal types could be improved by using experimental data linking the levels of *in situ* electric fields with the corresponding depolarization at the level of neuron membranes (Bikson et al., 2004). Other interaction mechanisms between the induced electric field and brain tissue could also be investigated, such as the possible modulation of neurotransmitter release probability by the induced electric field (Denoyer et al., 2020).

List of Figures

List of Publications

International journal article

M. Arrais, J. Modolo, D. Mogul and F. Wendling. Designing optimal multi-site brain stimulation protocols for epilepsy using neuro-inspired modeling, Journal of Neural Engineering (Under revision).

International conferences

M. Arrais, F. Wendling and J. Modolo. Identification of effective stimulation parameters to abort epileptic seizures in a neural mass model, Engineering in Medicine and Biology Conference 2019.

M. Arrais, F. Wendling and J. Modolo. Bifurcation analysis of a stimulated Wendling's neural mass model, BioEM Conference 2019.

M. Arrais, D. Mogul, F. Wendling and J. Modolo. Identification of sinusoidal electrical stimulation parameters able to abort epileptic activity based on co-dimension 2 bifurcation analysis, International Conference for Technology and Analysis of Seizures (ICTALS) 2019.

References

Akhtar, H., Bukhari, F., Nazir, M., Anwar, M.N., Shahzad, A., 2016. Therapeutic Efficacy of Neurostimulation for Depression: Techniques, Current Modalities, and Future Challenges. Neurosci Bull 32, 115–126. https://doi.org/10.1007/s12264-015-0009-2

Alagapan, S., Riddle, J., Huang, W.A., Hadar, E., Shin, H.W., Fröhlich, F., 2019. Network-Targeted, Multi-site Direct Cortical Stimulation Enhances Working Memory by Modulating Phase Lag of Low-Frequency Oscillations. Cell Reports 29, 2590-2598.e4. https://doi.org/10.1016/j.celrep.2019.10.072

Allen, P.J., Fish, D.R., Smith, S.J., 1992. Very high-frequency rhythmic activity during SEEG suppression in frontal lobe epilepsy. Electroencephalogr Clin Neurophysiol 82, 155–159.

Badawy, R. a. B., Freestone, D.R., Lai, A., Cook, M.J., 2012. Epilepsy: Ever-changing states of cortical excitability. Neuroscience 222, 89–99. https://doi.org/10.1016/j.neuroscience.2012.07.015

Bailey, P., Bremer, F., 1938. A sensory cortical representation of the vagus nerve: with a note on the effects of low blood pressure on the cortical electrogram. Journal of Neurophysiology 1, 405–412. https://doi.org/10.1152/jn.1938.1.5.405

Banks, M.I., White, J.A., Pearce, R.A., 2000. Interactions between distinct GABA(A) circuits in hippocampus. Neuron 25, 449–457.

Barrio, R., Shilnikov, A., 2011. Parameter-sweeping techniques for temporal dynamics of neuronal systems: case study of Hindmarsh-Rose model. J Math Neurosci 1, 6. https://doi.org/10.1186/2190-8567-1-6

Benabid, A.L., Pollak, P., Louveau, A., Henry, S., Rougemont, J. de, 1987. Combined (Thalamotomy and Stimulation) Stereotactic Surgery of the VIM Thalamic Nucleus for Bilateral Parkinson Disease. SFN 50, 344–346. https://doi.org/10.1159/000100803

Ben-Menachem, E., Mañon-Espaillat, R., Ristanovic, R., Wilder, B.J., Stefan, H., Mirza, W., Tarver, W.B., Wernicke, J.F., 1994. Vagus Nerve Stimulation for Treatment of Partial Seizures: 1. A Controlled Study of Effect on Seizures. Epilepsia 35, 616–626. https://doi.org/10.1111/j.1528-1157.1994.tb02482.x

Bernhardt, B.C., Kim, H., Bernasconi, N., 2013. Patterns of subregional mesiotemporal disease progression in temporal lobe epilepsy. Neurology 81, 1840–1847. https://doi.org/10.1212/01.wnl.0000436069.20513.92

Beurrier, C., Bioulac, B., Audin, J., Hammond, C., 2001. High-frequency stimulation produces a transient blockade of voltage-gated currents in subthalamic neurons. J. Neurophysiol. 85, 1351–1356. https://doi.org/10.1152/jn.2001.85.4.1351

Bikson, M., Inoue, M., Akiyama, H., Deans, J.K., Fox, J.E., Miyakawa, H., Jefferys, J.G.R., 2004. Effects of uniform extracellular DC electric fields on excitability in rat hippocampal slices in vitro. The Journal of Physiology 557, 175–190. https://doi.org/10.1113/jphysiol.2003.055772

Boyer, K., 2016. Not Necessarily Benign: Rolandic Epilepsy. Epilepsy Curr 16, 254–255. https://doi.org/10.5698/1535-7511-16.4.254

Bronstein, M., Petkovšek, M., 1996. An introduction to pseudo-linear algebra. Theoretical Computer Science 157, 3–33. https://doi.org/10.1016/0304-3975(95)00173-5

Butson, C.R., Cooper, S.E., Henderson, J.M., McIntyre, C.C., 2006. Predicting the effects of deep brain stimulation with diffusion tensor based electric field models. Med Image Comput Comput Assist Interv 9, 429–437. https://doi.org/10.1007/11866763_53

Buzsáki, G., 2002. Theta Oscillations in the Hippocampus. Neuron 33, 325–340. https://doi.org/10.1016/S0896-6273(02)00586-X

Buzsáki, G., Silva, F.L. da, 2012. High frequency oscillations in the intact brain. Prog. Neurobiol. 98, 241–249. https://doi.org/10.1016/j.pneurobio.2012.02.004
Campisi, P., La Rocca, D., Scarano, G., 2012. EEG for Automatic Person Recognition. Computer 45, 87–89. https://doi.org/10.1109/MC.2012.233
Cavanagh, J.F., Frank, M.J., 2014. Frontal theta as a mechanism for cognitive control. Trends Cogn Sci 18, 414–421. https://doi.org/10.1016/j.tics.2014.04.012
Cendes, F., 2004. Febrile seizures and mesial temporal sclerosis. Current Opinion in Neurology 17, 161–164.
Chen, G., Zhang, Y., Li, X., Zhao, X., Ye, Q., Lin, Y., Tao, H.W., Rasch, M.J., Zhang, X., 2017. Distinct Inhibitory Circuits Orchestrate Cortical beta and gamma Band Oscillations. Neuron 96, 1403-1418.e6. https://doi.org/10.1016/j.neuron.2017.11.033
Chrysafides, S.M., Bordes, S., Sharma, S., 2020. Physiology, Resting Potential, in: StatPearls. StatPearls Publishing, Treasure Island (FL).
Conte, G., Moog, C.H., Perdon, A.M., 1999. Nonlinear Control Systems: An Algebraic Setting, Lecture Notes in Control and Information Sciences. Springer-Verlag, London.
Cooper, I.S., Upton, A.R., Amin, I., 1980. Reversibility of chronic neurologic deficits. Some effects of electrical stimulation of the thalamus and internal capsule in man. Appl Neurophysiol 43, 244–258. https://doi.org/10.1159/000102263
Dalton, B., Bartholdy, S., Campbell, I.C., Schmidt, U., 2018. Neurostimulation in Clinical and Sub-clinical Eating Disorders: A Systematic Update of the Literature. Curr Neuropharmacol 16, 1174–1192. https://doi.org/10.2174/1570159X16666180108111532
Das, S., Holland, P., Frens, M.A., Donchin, O., 2016. Impact of Transcranial Direct Current Stimulation (tDCS) on Neuronal Functions. Front Neurosci 10. https://doi.org/10.3389/fnins.2016.00550
Davies, J.E., 2007. The pharmacological basis of therapeutics. Occup Environ Med 64, e2. https://doi.org/10.1136/oem.2007.033902
Davis, R., Engle, H., Kudzma, J., Gray, E., Ryan, T., Dusnak, A., 1982. Update of chronic cerebellar stimulation for spasticity and epilepsy. Appl Neurophysiol 45, 44–50.
Delgado, J.M.R., Hamlin, H., Chapman, W.P., 1952. Technique of intracranial electrode implacement for recording and stimulation and its possible therapeutic value in psychotic patients. Confin Neurol 12, 315–319. https://doi.org/10.1159/000105792
Denoyer, Y., Merlet, I., Wendling, F., Benquet, P., 2020. Modelling acute and lasting effects of tDCS on epileptic activity. J Comput Neurosci 48, 161–176. https://doi.org/10.1007/s10827-020-00745-6
Deuschl, G., Schade-Brittinger, C., Krack, P., Volkmann, J., Schäfer, H., Bötzel, K., Daniels, C., Deutschländer, A., Dillmann, U., Eisner, W., Gruber, D., Hamel, W., Herzog, J., Hilker, R., Klebe, S., Kloss, M., Koy, J., Krause, M., Kupsch, A., Lorenz, D., Lorenzl, S., Mehdorn, H.M., Moringlane, J.R., Oertel, W., Pinsker, M.O., Reichmann, H., Reuss, A., Schneider, G.-H., Schnitzler, A., Steude, U., Sturm, V., Timmermann, L., Tronnier, V., Trottenberg, T., Wojtecki, L., Wolf, E., Poewe, W., Voges, J., German Parkinson Study Group, Neurostimulation Section, 2006. A randomized trial of deep-brain stimulation for Parkinson's disease. N. Engl. J. Med. 355, 896–908. https://doi.org/10.1056/NEJMoa060281
Dhooge, A., Govaerts, W., Kuznetsov, Yu.A., 2003. MATCONT: A MATLAB Package for Numerical Bifurcation Analysis of ODEs. ACM Trans. Math. Softw. 29, 141–164. https://doi.org/10.1145/779359.779362
Doedel, E.J., Champneys, A.R., Fairgrieve, T.F., Kuznetsov, Y.A., Sandstede, B., Wang, X., 1997. AUTO 97: Continuation And Bifurcation Software For Ordinary Differential Equations (with HomCont).
Dossi, R.C., Nuñez, A., Steriade, M., 1992. Electrophysiology of a slow (0.5-4 Hz) intrinsic oscillation of cat thalamocortical neurones in vivo. J Physiol 447, 215–234.
Dostrovsky, J.O., Lozano, A.M., 2002. Mechanisms of deep brain stimulation. Mov. Disord. 17 Suppl 3, S63-68. https://doi.org/10.1002/mds.10143

Dubey, D., Alqallaf, A., Hays, R., Freeman, M., Chen, K., Ding, K., Agostini, M., Vernino, S., 2017. Neurological Autoantibody Prevalence in Epilepsy of Unknown Etiology. JAMA Neurol 74, 397–402. https://doi.org/10.1001/jamaneurol.2016.5429

Ebersole, J.S., Ebersole, S.M., 2010. Combining MEG and EEG source modeling in epilepsy evaluations. J Clin Neurophysiol 27, 360–371. https://doi.org/10.1097/WNP.0b013e318201ffc4

Edwards, C.A., Kouzani, A., Lee, K.H., Ross, E.K., 2017. Neurostimulation Devices for the Treatment of Neurologic Disorders. Mayo Clinic Proceedings 92, 1427–1444. https://doi.org/10.1016/j.mayocp.2017.05.005

Ermentrout, B., n.d. XPPAUT5.0 – the differential equations tool 99.

Ertl, M., Hildebrandt, M., Ourina, K., Leicht, G., Mulert, C., 2013. Emotion regulation by cognitive reappraisal — The role of frontal theta oscillations. NeuroImage 81, 412–421. https://doi.org/10.1016/j.neuroimage.2013.05.044

Fedele, T., van 't Klooster, M., Burnos, S., Zweiphenning, W., van Klink, N., Leijten, F., Zijlmans, M., Sarnthein, J., 2016. Automatic detection of high frequency oscillations during epilepsy surgery predicts seizure outcome. Clin Neurophysiol 127, 3066–3074. https://doi.org/10.1016/j.clinph.2016.06.009

Filali, M., Hutchison, W.D., Palter, V.N., Lozano, A.M., Dostrovsky, J.O., 2004. Stimulation-induced inhibition of neuronal firing in human subthalamic nucleus. Exp Brain Res 156, 274–281. https://doi.org/10.1007/s00221-003-1784-y

Fisher, R., Salanova, V., Witt, T., Worth, R., Henry, T., Gross, R., Oommen, K., Osorio, I., Nazzaro, J., Labar, D., Kaplitt, M., Sperling, M., Sandok, E., Neal, J., Handforth, A., Stern, J., DeSalles, A., Chung, S., Shetter, A., Bergen, D., Bakay, R., Henderson, J., French, J., Baltuch, G., Rosenfeld, W., Youkilis, A., Marks, W., Garcia, P., Barbaro, N., Fountain, N., Bazil, C., Goodman, R., McKhann, G., Babu Krishnamurthy, K., Papavassiliou, S., Epstein, C., Pollard, J., Tonder, L., Grebin, J., Coffey, R., Graves, N., SANTE Study Group, 2010. Electrical stimulation of the anterior nucleus of thalamus for treatment of refractory epilepsy. Epilepsia 51, 899–908. https://doi.org/10.1111/j.1528-1167.2010.02536.x

Fisher, R.S., Acevedo, C., Arzimanoglou, A., Bogacz, A., Cross, J.H., Elger, C.E., Engel, J., Forsgren, L., French, J.A., Glynn, M., Hesdorffer, D.C., Lee, B.I., Mathern, G.W., Moshé, S.L., Perucca, E., Scheffer, I.E., Tomson, T., Watanabe, M., Wiebe, S., 2014. ILAE official report: a practical clinical definition of epilepsy. Epilepsia 55, 475–482. https://doi.org/10.1111/epi.12550

Fisher, R.S., van Emde Boas, W., Blume, W., Elger, C., Genton, P., Lee, P., Engel, J., 2005. Epileptic seizures and epilepsy: definitions proposed by the International League Against Epilepsy (ILAE) and the International Bureau for Epilepsy (IBE). Epilepsia 46, 470–472. https://doi.org/10.1111/j.0013-9580.2005.66104.x

FitzHugh, R., 1961. Impulses and Physiological States in Theoretical Models of Nerve Membrane. Biophys J 1, 445–466.

Freeman, W.J., 1975. Mass Action in the Nervous System: Examination of the Neurophysiological Basis of Adaptive Behavior Through the EEG. Academic Press.

Grimbert, F., Faugeras, O., 2006. Bifurcation analysis of Jansen's neural mass model. Neural Comput 18, 3052–3068. https://doi.org/10.1162/neco.2006.18.12.3052

Guerrini, R., Pellacani, S., 2012. Benign childhood focal epilepsies. Epilepsia 53, 9–18. https://doi.org/10.1111/j.1528-1167.2012.03609.x

Halás, M., Kotta, Ü., Moog, C.H., 2008. Transfer Function Approach to the Model Matching Problem of Nonlinear Systems. IFAC Proceedings Volumes, 17th IFAC World Congress 41, 15197–15202. https://doi.org/10.3182/20080706-5-KR-1001.02570

Hamid, P., Malik, B.H., Hussain, M.L., 2019. Noninvasive Transcranial Magnetic Stimulation (TMS) in Chronic Refractory Pain: A Systematic Review. Cureus 11, e6019. https://doi.org/10.7759/cureus.6019

Handforth, A., DeGiorgio, C.M., Schachter, S.C., Uthman, B.M., Naritoku, D.K., Tecoma, E.S., Henry, T.R., Collins, S.D., Vaughn, B.V., Gilmartin, R.C., Labar, D.R., Morris, G.L.,

Salinsky, M.C., Osorio, I., Ristanovic, R.K., Labiner, D.M., Jones, J.C., Murphy, J.V., Ney, G.C., Wheless, J.W., 1998. Vagus nerve stimulation therapy for partial-onset seizures: a randomized active-control trial. Neurology 51, 48–55. https://doi.org/10.1212/wnl.51.1.48

Heck, C.N., King-Stephens, D., Massey, A.D., Nair, D.R., Jobst, B.C., Barkley, G.L., Salanova, V., Cole, A.J., Smith, M.C., Gwinn, R.P., Skidmore, C., Van Ness, P.C., Bergey, G.K., Park, Y.D., Miller, I., Geller, E., Rutecki, P.A., Zimmerman, R., Spencer, D.C., Goldman, A., Edwards, J.C., Leiphart, J.W., Wharen, R.E., Fessler, J., Fountain, N.B., Worrell, G.A., Gross, R.E., Eisenschenk, S., Duckrow, R.B., Hirsch, L.J., Bazil, C., O'Donovan, C.A., Sun, F.T., Courtney, T.A., Seale, C.G., Morrell, M.J., 2014. Two-year seizure reduction in adults with medically intractable partial onset epilepsy treated with responsive neurostimulation: final results of the RNS System Pivotal trial. Epilepsia 55, 432–441. https://doi.org/10.1111/epi.12534

Hoang, K.B., Cassar, I.R., Grill, W.M., Turner, D.A., 2017. Biomarkers and Stimulation Algorithms for Adaptive Brain Stimulation. Front Neurosci 11. https://doi.org/10.3389/fnins.2017.00564

Hodgkin, A.L., Huxley, A.F., 1952. A quantitative description of membrane current and its application to conduction and excitation in nerve. J Physiol 117, 500–544.

Höller, Y., Kutil, R., Klaffenböck, L., Thomschewski, A., Höller, P.M., Bathke, A.C., Jacobs, J., Taylor, A.C., Nardone, R., Trinka, E., 2015. High-frequency oscillations in epilepsy and surgical outcome. A meta-analysis. Frontiers in Human Neuroscience 9, 574. https://doi.org/10.3389/fnhum.2015.00574

Hyman, S.E., 2005. Neurotransmitters. Curr. Biol. 15, R154-158. https://doi.org/10.1016/j.cub.2005.02.037

Jacobs, J., LeVan, P., Chander, R., Hall, J., Dubeau, F., Gotman, J., 2008. Interictal high-frequency oscillations (80-500 Hz) are an indicator of seizure onset areas independent of spikes in the human epileptic brain. Epilepsia 49, 1893–1907. https://doi.org/10.1111/j.1528-1167.2008.01656.x

Jacobs, J., Levan, P., Châtillon, C.-E., Olivier, A., Dubeau, F., Gotman, J., 2009. High frequency oscillations in intracranial EEGs mark epileptogenicity rather than lesion type. Brain 132, 1022–1037. https://doi.org/10.1093/brain/awn351

Jacobs, J., Staba, R., Asano, E., Otsubo, H., Wu, J.Y., Zijlmans, M., Mohamed, I., Kahane, P., Dubeau, F., Navarro, V., Gotman, J., 2012. High-frequency oscillations (HFOs) in clinical epilepsy. Prog Neurobiol 98, 302–315. https://doi.org/10.1016/j.pneurobio.2012.03.001

Jacobs, J., Zijlmans, M., Zelmann, R., Chatillon, C.-E., Hall, J., Olivier, A., Dubeau, F., Gotman, J., 2010. High-frequency electroencephalographic oscillations correlate with outcome of epilepsy surgery. Ann. Neurol. 67, 209–220. https://doi.org/10.1002/ana.21847

Jansen, B.H., Rit, V.G., 1995. Electroencephalogram and visual evoked potential generation in a mathematical model of coupled cortical columns. Biol. Cybern. 73, 357–366. https://doi.org/10.1007/BF00199471

Jefferys, J.G., Traub, R.D., Whittington, M.A., 1996. Neuronal networks for induced "40 Hz" rhythms. Trends Neurosci. 19, 202–208.

Jefferys, J.G.R., Menendez de la Prida, L., Wendling, F., Bragin, A., Avoli, M., Timofeev, I., Lopes da Silva, F.H., 2012. Mechanisms of physiological and epileptic HFO generation. Prog. Neurobiol. 98, 250–264. https://doi.org/10.1016/j.pneurobio.2012.02.005

Jirsa, V.K., Stacey, W.C., Quilichini, P.P., Ivanov, A.I., Bernard, C., 2014. On the nature of seizure dynamics. Brain 137, 2210–2230. https://doi.org/10.1093/brain/awu133

Jobst, B.C., Darcey, T.M., Thadani, V.M., Roberts, D.W., 2010. Brain stimulation for the treatment of epilepsy. Epilepsia 51, 88–92. https://doi.org/10.1111/j.1528-1167.2010.02618.x

Jobst, B.C., Kapur, R., Barkley, G.L., Bazil, C.W., Berg, M.J., Bergey, G.K., Boggs, J.G., Cash, S.S., Cole, A.J., Duchowny, M.S., Duckrow, R.B., Edwards, J.C., Eisenschenk, S., Fessler, A.J., Fountain, N.B., Geller, E.B., Goldman, A.M., Goodman, R.R., Gross,

R.E., Gwinn, R.P., Heck, C., Herekar, A.A., Hirsch, L.J., King-Stephens, D., Labar, D.R., Marsh, W.R., Meador, K.J., Miller, I., Mizrahi, E.M., Murro, A.M., Nair, D.R., Noe, K.H., Olejniczak, P.W., Park, Y.D., Rutecki, P., Salanova, V., Sheth, R.D., Skidmore, C., Smith, M.C., Spencer, D.C., Srinivasan, S., Tatum, W., Van Ness, P., Vossler, D.G., Wharen, R.E., Worrell, G.A., Yoshor, D., Zimmerman, R.S., Skarpaas, T.L., Morrell, M.J., 2017. Brain-responsive neurostimulation in patients with medically intractable seizures arising from eloquent and other neocortical areas. Epilepsia 58, 1005–1014. https://doi.org/10.1111/epi.13739

Kandel, E., 2000. Principles of Neural Science, Fourth Edition. McGraw-Hill Companies,Incorporated.

Katchanov, J., Birbeck, G.L., 2012. Epilepsy care guidelines for low- and middle- income countries: From WHO mental health GAP to national programs. BMC Med 10, 107. https://doi.org/10.1186/1741-7015-10-107

Kobau, R., Zahran, H., Thurman, D.J., Zack, M.M., Henry, T.R., Schachter, S.C., Price, P.H., Centers for Disease Control and Prevention (CDC), 2008. Epilepsy surveillance among adults--19 States, Behavioral Risk Factor Surveillance System, 2005. MMWR Surveill Summ 57, 1–20.

Koppert, M., Kalitzin, S., Velis, D., Lopes Da Silva, F., Viergever, M.A., 2016. Preventive and Abortive Strategies for Stimulation Based Control of Epilepsy: A Computational Model Study. Int J Neural Syst 26, 1650028. https://doi.org/10.1142/S0129065716500283

Kucewicz, M.T., Cimbalnik, J., Matsumoto, J.Y., Brinkmann, B.H., Bower, M.R., Vasoli, V., Sulc, V., Meyer, F., Marsh, W.R., Stead, S.M., Worrell, G.A., 2014. High frequency oscillations are associated with cognitive processing in human recognition memory. Brain 137, 2231–2244. https://doi.org/10.1093/brain/awu149

Kumar, K., North, R., Taylor, R., Sculpher, M., Van den Abeele, C., Gehring, M., Jacques, L., Eldabe, S., Meglio, M., Molet, J., Thomson, S., O'Callaghan, J., Eisenberg, E., Milbouw, G., Fortini, G., Richardson, J., Buchser, E., Tracey, S., Reny, P., Brookes, M., Sabene, S., Cano, P., Banks, C., Pengelly, L., Adler, R., Leruth, S., Kelly, C., Jacobs, M., 2005. Spinal Cord Stimulation vs. Conventional Medical Management: A Prospective, Randomized, Controlled, Multicenter Study of Patients with Failed Back Surgery Syndrome (PROCESS Study). Neuromodulation 8, 213–218. https://doi.org/10.1111/j.1525-1403.2005.00027.x

Kumar, K., Taylor, R.S., Jacques, L., Eldabe, S., Meglio, M., Molet, J., Thomson, S., O'Callaghan, J., Eisenberg, E., Milbouw, G., Buchser, E., Fortini, G., Richardson, J., North, R.B., 2008. The effects of spinal cord stimulation in neuropathic pain are sustained: a 24-month follow-up of the prospective randomized controlled multicenter trial of the effectiveness of spinal cord stimulation. Neurosurgery 63, 762–770; discussion 770. https://doi.org/10.1227/01.NEU.0000325731.46702.D9

Kuznetsov, Y.A., 1998. Elements of Applied Bifurcation Theory, Second Edition 614.

Kwan, P., Arzimanoglou, A., Berg, A.T., Brodie, M.J., Allen Hauser, W., Mathern, G., Moshé, S.L., Perucca, E., Wiebe, S., French, J., 2010. Definition of drug resistant epilepsy: consensus proposal by the ad hoc Task Force of the ILAE Commission on Therapeutic Strategies. Epilepsia 51, 1069–1077. https://doi.org/10.1111/j.1528-1167.2009.02397.x

Kwan, P., Brodie, M.J., 2000. Early identification of refractory epilepsy. N. Engl. J. Med. 342, 314–319. https://doi.org/10.1056/NEJM200002033420503

Lainscsek, C., Hernandez, M.E., Weyhenmeyer, J., Sejnowski, T.J., Poizner, H., 2013. Non-Linear Dynamical Analysis of EEG Time Series Distinguishes Patients with Parkinson's Disease from Healthy Individuals. Front Neurol 4. https://doi.org/10.3389/fneur.2013.00200

Laxpati, N.G., Kasoff, W.S., Gross, R.E., 2014. Deep Brain Stimulation for the Treatment of Epilepsy: Circuits, Targets, and Trials. Neurotherapeutics 11, 508–526. https://doi.org/10.1007/s13311-014-0279-9

Lega, B.C., Jacobs, J., Kahana, M., 2012. Human hippocampal theta oscillations and the formation of episodic memories. Hippocampus 22, 748–761. https://doi.org/10.1002/hipo.20937
Li, M.C.H., Cook, M.J., 2018. Deep brain stimulation for drug-resistant epilepsy. Epilepsia 59, 273–290. https://doi.org/10.1111/epi.13964
Lodish, H., Berk, A., Zipursky, S.L., Matsudaira, P., Baltimore, D., Darnell, J., 2000. The Action Potential and Conduction of Electric Impulses. Molecular Cell Biology. 4th edition.
Lopez, L., Chan, C.Y., Okada, Y.C., Nicholson, C., 1991. Multimodal characterization of population responses evoked by applied electric field in vitro: extracellular potential, magnetic evoked field, transmembrane potential, and current-source density analysis. J. Neurosci. 11, 1998–2010. https://doi.org/10.1523/JNEUROSCI.11-07-01998.1991
Lovinger, D.M., 2008. Communication networks in the brain: neurons, receptors, neurotransmitters, and alcohol. Alcohol Res Health 31, 196–214.
Lundstrom, B.N., Van Gompel, J., Britton, J., Nickels, K., Wetjen, N., Worrell, G., Stead, M., 2016. Chronic Subthreshold Cortical Stimulation to Treat Focal Epilepsy. JAMA Neurol 73, 1370–1372. https://doi.org/10.1001/jamaneurol.2016.2857
Lundstrom, B.N., Worrell, G.A., Stead, M., Gompel, J.J.V., 2017. Chronic subthreshold cortical stimulation: a therapeutic and potentially restorative therapy for focal epilepsy. Expert review of neurotherapeutics 17, 661–666. https://doi.org/10.1080/14737175.2017.1331129
Mackay, W.A., 1997. Synchronized neuronal oscillations and their role in motor processes. Trends Cogn. Sci. (Regul. Ed.) 1, 176–183. https://doi.org/10.1016/S1364-6613(97)01059-0
Maruyama, G., 1955. Continuous Markov processes and stochastic equations. Rend. Circ. Mat. Palermo 4, 48. https://doi.org/10.1007/BF02846028
McKnight, K., Jiang, Y., Hart, Y., Cavey, A., Wroe, S., Blank, M., Shoenfeld, Y., Vincent, A., Palace, J., Lang, B., 2005. Serum antibodies in epilepsy and seizure-associated disorders. Neurology 65, 1730–1736. https://doi.org/10.1212/01.wnl.0000187129.66353.13
Meisenhelter, S., Jobst, B.C., 2018. Neurostimulation for Memory Enhancement in Epilepsy. Curr Neurol Neurosci Rep 18, 30. https://doi.org/10.1007/s11910-018-0837-3
Miranda, P.C., Lomarev, M., Hallett, M., 2006. Modeling the current distribution during transcranial direct current stimulation. Clin Neurophysiol 117, 1623–1629. https://doi.org/10.1016/j.clinph.2006.04.009
Morrell, M.J., Halpern, C., 2016. Responsive Direct Brain Stimulation for Epilepsy. Neurosurg. Clin. N. Am. 27, 111–121. https://doi.org/10.1016/j.nec.2015.08.012
Morris, C., Lecar, H., 1981. Voltage oscillations in the barnacle giant muscle fiber. Biophys. J. 35, 193–213. https://doi.org/10.1016/S0006-3495(81)84782-0
Ngugi, A.K., Kariuki, S.M., Bottomley, C., Kleinschmidt, I., Sander, J.W., Newton, C.R., 2011. Incidence of epilepsy: a systematic review and meta-analysis. Neurology 77, 1005–1012. https://doi.org/10.1212/WNL.0b013e31822cfc90
Niedermeyer's Electroencephalography: Basic Principles, Clinical Applications, and Related Fields, n.d. , Niedermeyer's Electroencephalography. Oxford University Press.
Nunez, P.L., Cutillo, B.A., 1995. Neocortical Dynamics and Human EEG Rhythms. Oxford University Press.
Nunez, P.L., Srinivasan, R., n.d. Electric Fields of the Brain: The neurophysics of EEG, Electric Fields of the Brain. Oxford University Press.
Ore, O., 1933. Theory of Non-Commutative Polynomials. Annals of Mathematics 34, 480–508. https://doi.org/10.2307/1968173
Ovsepian, S.V., 2017. The birth of the synapse. Brain Struct Funct 222, 3369–3374. https://doi.org/10.1007/s00429-017-1459-2
Pack, A.M., 2019. Epilepsy Overview and Revised Classification of Seizures and Epilepsies. CONTINUUM: Lifelong Learning in Neurology 25, 306. https://doi.org/10.1212/CON.0000000000000707

Peltola, J.T., Haapala, A.-M., Isojärvi, J.I., Auvinen, A., Palmio, J., Latvala, K., Kulmala, P., Laine, S., Vaarala, O., Keränen, T., 2000. Antiphospholipid and antinuclear antibodies in patients with epilepsy or new-onset seizure disorders. The American Journal of Medicine 109, 712–717. https://doi.org/10.1016/S0002-9343(00)00617-3

Penry, J.K., Dean, J.C., 1990. Prevention of intractable partial seizures by intermittent vagal stimulation in humans: preliminary results. Epilepsia 31 Suppl 2, S40-43. https://doi.org/10.1111/j.1528-1157.1990.tb05848.x

Perko, L., 2001. Differential Equations and Dynamical Systems, 3rd ed, Texts in Applied Mathematics. Springer-Verlag, New York.

Pohlmann-Eden, B., Newton, M., 2008. First seizure: EEG and neuroimaging following an epileptic seizure. Epilepsia 49 Suppl 1, 19–25. https://doi.org/10.1111/j.1528-1167.2008.01445.x

Pollo, C., Villemure, J.G., 2007. Rationale, mechanisms of efficacy, anatomical targets and future prospects of electrical deep brain stimulation for epilepsy. Acta Neurochir. Suppl. 97, 311–320. https://doi.org/10.1007/978-3-211-33081-4_34

Radman, T., Ramos, R.L., Brumberg, J.C., Bikson, M., 2009. Role of Cortical Cell Type and Morphology in Sub- and Suprathreshold Uniform Electric Field Stimulation. Brain Stimul 2, 215–228. https://doi.org/10.1016/j.brs.2009.03.007

Rahman, M., Abd-El-Barr, M.M., Vedam-Mai, V., Foote, K.D., Murad, G.J.A., Okun, M.S., Roper, S.N., 2010. Disrupting abnormal electrical activity with deep brain stimulation: is epilepsy the next frontier? Neurosurg Focus 29, E7. https://doi.org/10.3171/2010.4.FOCUS10104

Ramanathan, S., Bleasel, A., Parratt, J., Orr, C., Dale, R.C., Vincent, A., Fung, V.S.C., 2014. Characterisation of a syndrome of autoimmune adult onset focal epilepsy and encephalitis. Journal of Clinical Neuroscience 21, 1169–1175. https://doi.org/10.1016/j.jocn.2013.09.024

Ranck, J.B., 1975. Which elements are excited in electrical stimulation of mammalian central nervous system: a review. Brain Res. 98, 417–440. https://doi.org/10.1016/0006-8993(75)90364-9

Rattay, F., 1989. Analysis of models for extracellular fiber stimulation. IEEE Trans Biomed Eng 36, 676–682. https://doi.org/10.1109/10.32099

Reddy, M.S., Vijay, M.S., 2017. Repetitive Transcranial Magnetic Stimulation for Depression: State of the Art. Indian Journal of Psychological Medicine 39, 1–3. https://doi.org/10.4103/0253-7176.198951

Rizvi, S., Khan, A.M., n.d. Use of Transcranial Magnetic Stimulation for Depression. Cureus 11. https://doi.org/10.7759/cureus.4736

Roehri, N., Pizzo, F., Lagarde, S., Lambert, I., Nica, A., McGonigal, A., Giusiano, B., Bartolomei, F., Bénar, C.-G., 2018. High-frequency oscillations are not better biomarkers of epileptogenic tissues than spikes. Annals of Neurology 83, 84–97. https://doi.org/10.1002/ana.25124

Sankaraneni, R., Lachhwani, D., 2015. Antiepileptic drugs--a review. Pediatr Ann 44, e36-42. https://doi.org/10.3928/00904481-20150203-10

Scheffer, I.E., Berkovic, S., Capovilla, G., Connolly, M.B., French, J., Guilhoto, L., Hirsch, E., Jain, S., Mathern, G.W., Moshé, S.L., Nordli, D.R., Perucca, E., Tomson, T., Wiebe, S., Zhang, Y.-H., Zuberi, S.M., 2017. ILAE classification of the epilepsies: Position paper of the ILAE Commission for Classification and Terminology. Epilepsia 58, 512–521. https://doi.org/10.1111/epi.13709

Shen, K.-Z., Zhu, Z.-T., Munhall, A., Johnson, S.W., 2003. Synaptic plasticity in rat subthalamic nucleus induced by high-frequency stimulation. Synapse 50, 314–319. https://doi.org/10.1002/syn.10274

Shorvon, S., 1994. Status Epilepticus: Its Clinical Features and Treatment in Children and Adults. Cambridge University Press, Cambridge. https://doi.org/10.1017/CBO9780511526930

Skarpaas, T.L., Jarosiewicz, B., Morrell, M.J., 2019. Brain-responsive neurostimulation for epilepsy (RNS® System). Epilepsy Res. 153, 68–70. https://doi.org/10.1016/j.eplepsyres.2019.02.003

Sobayo, T., Mogul, D.J., 2016. Should stimulation parameters be individualized to stop seizures: Evidence in support of this approach. Epilepsia 57, 131–140. https://doi.org/10.1111/epi.13259

Spiegler, A., Jirsa, V., 2013. Systematic approximations of neural fields through networks of neural masses in the virtual brain. Neuroimage 83, 704–725. https://doi.org/10.1016/j.neuroimage.2013.06.018

Steriade, M., McCormick, D.A., Sejnowski, T.J., 1993. Thalamocortical oscillations in the sleeping and aroused brain. Science 262, 679–685. https://doi.org/10.1126/science.8235588

Sun, F.T., Morrell, M.J., Wharen, R.E., 2008. Responsive Cortical Stimulation for the Treatment of Epilepsy. Neurotherapeutics : the journal of the American Society for Experimental NeuroTherapeutics 5, 68–74. https://doi.org/10.1016/j.nurt.2007.10.069

Tatum, W.O., 2012. Mesial temporal lobe epilepsy. J Clin Neurophysiol 29, 356–365. https://doi.org/10.1097/WNP.0b013e31826b3ab7

Tawfik, V.L., Chang, S.-Y., Hitti, F.L., Roberts, D.W., Leiter, J.C., Jovanovic, S., Lee, K.H., 2010. Deep Brain Stimulation Results in Local Glutamate and Adenosine Release: Investigation Into the Role of Astrocytes. Neurosurgery 67, 367–375. https://doi.org/10.1227/01.NEU.0000371988.73620.4C

Taylor, P.N., Wang, Y., Goodfellow, M., Dauwels, J., Moeller, F., Stephani, U., Baier, G., 2014. A Computational Study of Stimulus Driven Epileptic Seizure Abatement. PLoS One 9. https://doi.org/10.1371/journal.pone.0114316

The Brain's Alpha Rhythms and the Mind - 1st Edition [WWW Document], n.d. URL https://www.elsevier.com/books/the-brains-alpha-rhythms-and-the-mind/shaw/978-0-444-51397-7 (accessed 9.23.20).

Thom, M., Liagkouras, I., Elliot, K.J., Martinian, L., Harkness, W., McEvoy, A., Caboclo, L.O., Sisodiya, S.M., 2010. Reliability of patterns of hippocampal sclerosis as predictors of postsurgical outcome. Epilepsia 51, 1801–1808. https://doi.org/10.1111/j.1528-1167.2010.02681.x

Upton, A.R., Cooper, I.S., 1976. Some neurophysiological effects of cerebellar stimulation in man. Can J Neurol Sci 3, 237–254.

van Drongelen, W., Lee, H.C., Stevens, R.L., Hereld, M., 2007. Propagation of Seizure-like Activity in a Model of Neocortex. Journal of Clinical Neurophysiology 24, 182–188. https://doi.org/10.1097/WNP.0b013e318039b4de

Veit, J., Hakim, R., Jadi, M.P., Sejnowski, T.J., Adesnik, H., 2017. Cortical gamma band synchronization through somatostatin interneurons. Nat Neurosci 20, 951–959. https://doi.org/10.1038/nn.4562

Vezzani, A., Fujinami, R.S., White, H.S., Preux, P.-M., Blümcke, I., Sander, J.W., Löscher, W., 2016. Infections, inflammation and epilepsy. Acta Neuropathol. 131, 211–234. https://doi.org/10.1007/s00401-015-1481-5

Wang, J., Niebur, E., Hu, J., Li, X., 2016. Suppressing epileptic activity in a neural mass model using a closed-loop proportional-integral controller. Scientific Reports 6, 27344. https://doi.org/10.1038/srep27344

Weaver, F.M., Follett, K., Stern, M., Hur, K., Harris, C., Marks, W.J., Rothlind, J., Sagher, O., Reda, D., Moy, C.S., Pahwa, R., Burchiel, K., Hogarth, P., Lai, E.C., Duda, J.E., Holloway, K., Samii, A., Horn, S., Bronstein, J., Stoner, G., Heemskerk, J., Huang, G.D., CSP 468 Study Group, 2009. Bilateral deep brain stimulation vs best medical therapy for patients with advanced Parkinson disease: a randomized controlled trial. JAMA 301, 63–73. https://doi.org/10.1001/jama.2008.929

Wendling, F., Bartolomei, F., Bellanger, J.J., Chauvel, P., 2002a. Epileptic fast activity can be explained by a model of impaired GABAergic dendritic inhibition. European Journal of Neuroscience 15, 1499–1508. https://doi.org/10.1046/j.1460-9568.2002.01985.x

Wendling, F., Bellanger, J.J., Bartolomei, F., Chauvel, P., 2000. Relevance of nonlinear lumped-parameter models in the analysis of depth-EEG epileptic signals. Biol Cybern 83, 367–378. https://doi.org/10.1007/s004220000160

Wendling, Fabrice, Benquet, P., Bartolomei, F., Jirsa, V., 2016. Computational models of epileptiform activity. Journal of Neuroscience Methods, Methods and Models in Epilepsy Research 260, 233–251. https://doi.org/10.1016/j.jneumeth.2015.03.027

Wendling, F., Gerber, U., Cosandier-Rimele, D., Nica, A., De Montigny, J., Raineteau, O., Kalitzin, S., Lopes da Silva, F., Benquet, P., 2016. Brain (Hyper)Excitability Revealed by Optimal Electrical Stimulation of GABAergic Interneurons. Brain Stimul 9, 919–932. https://doi.org/10.1016/j.brs.2016.07.001

Whittington, M.A., Traub, R.D., Kopell, N., Ermentrout, B., Buhl, E.H., 2000. Inhibition-based rhythms: experimental and mathematical observations on network dynamics. Int J Psychophysiol 38, 315–336.

Wilson, H.R., Cowan, J.D., 1973. A mathematical theory of the functional dynamics of cortical and thalamic nervous tissue. Kybernetik 13, 55–80. https://doi.org/10.1007/BF00288786

Womelsdorf, T., Valiante, T.A., Sahin, N.T., Miller, K.J., Tiesinga, P., 2014. Dynamic circuit motifs underlying rhythmic gain control, gating and integration. Nature Neuroscience 17, 1031–1039. https://doi.org/10.1038/nn.3764

Worrell, G.A., Gardner, A.B., Stead, S.M., Hu, S., Goerss, S., Cascino, G.J., Meyer, F.B., Marsh, R., Litt, B., 2008. High-frequency oscillations in human temporal lobe: simultaneous microwire and clinical macroelectrode recordings. Brain 131, 928–937. https://doi.org/10.1093/brain/awn006

Wright, G.D., Weller, R.O., 1983. Biopsy and post-mortem findings in a patient receiving cerebellar stimulation for epilepsy. J. Neurol. Neurosurg. Psychiatry 46, 266–273.

Zangiabadi, N., Ladino, L.D., Sina, F., Orozco-Hernández, J.P., Carter, A., Téllez-Zenteno, J.F., 2019. Deep Brain Stimulation and Drug-Resistant Epilepsy: A Review of the Literature. Front. Neurol. 10. https://doi.org/10.3389/fneur.2019.00601

Zewdie, E., Ciechanski, P., Kuo, H.C., Giuffre, A., Kahl, C., King, R., Cole, L., Godfrey, H., Seeger, T., Swansburg, R., Damji, O., Rajapakse, T., Hodge, J., Nelson, S., Selby, B., Gan, L., Jadavji, Z., Larson, J.R., MacMaster, F., Yang, J.F., Barlow, K., Gorassini, M., Brunton, K., Kirton, A., 2020. Safety and tolerability of transcranial magnetic and direct current stimulation in children: Prospective single center evidence from 3.5 million stimulations. Brain Stimulation: Basic, Translational, and Clinical Research in Neuromodulation 13, 565–575. https://doi.org/10.1016/j.brs.2019.12.025

Zheng, Y., Willems, J.C., Zhang, C., 2001. A polynomial approach to nonlinear system controllability. IEEE Transactions on Automatic Control 46, 1782–1788. https://doi.org/10.1109/9.964691